약학박사 학위논문

Chitosan-based hybrid nanocomplex for siRNA delivery and its application for cancer therapy

Chitosan을 이용한 siRNA 전달용 융합 나노복합체와 항암치료로의 활용

2014년 8월

서울대학교 대학원

제약학과 약제과학

기 민 효

Chitosan-based hybrid nanocomplex for siRNA delivery and its application for cancer therapy

Chitosan을 이용한 siRNA 전달용 융합 나노복합체와 항암치료로의 활용

지도교수 김 대 덕

이 논문을 약학박사 학위논문으로 제출함

2013년 11월

서울대학교 대학원

제약학과 약제과학

기 민 효

기민효의 박사 학위논문을 인준함

2013년 12월

위 원 장 _____ (인)

부 위 원 장 _____ (인)

위 원 _____ (인)

위 원 _____ (인)

위 원 _____ (인)

CONTENTS

ABSTRACT

Chitosan, a natural and biocompatible cationic polymer, is an attractive carrier for siRNA delivery. The purpose of this study is to develop a chitosan-based hybrid nanocomplex that exhibits enhanced stability in the blood stream compared to conventional chitosan nanoparticles. Hybrid nanocomplexes composed of chitosan, protamine, lecithin, and thiamine pyrophosphate (TPP) were prepared for the systemic delivery of survivin (SVN) siRNA and evaluated for their *in vitro* and *in vivo* therapeutic efficacies. Physicochemical properties of the nanoparticles were investigated, which included particle size measurements in distilled water, cell culture media, and 50% fetal bovine serum conditions. Cellular uptake and target gene silencing efficiencies of the siRNAnanocomplexes in prostate cancer cells (PC-3 cells) were measured. *In vivo* tumor targetability and anti-tumor efficacy were assessed in PC-3 tumor xenografted mouse model by near-infrared fluorescence (NIRF) imaging and tumor growth monitoring, respectively. The SVN siRNA-loaded hybrid nanocomplex (GP-L-CT) showed of < 200 nm mean diameter with positive zeta potential value in water and maintained the diameter

without aggregation even in serum. Mean SVN expression rate in PC-3 cells was reduced to 21.8% after treating with GP-L-CT. The fluorescence intensity in the tumor region and the tumor growth inhibitory effect of the new nanocomplex were indicative of the cancer theranostic efficacy in the prostate cancer mouse model. In conclusion, a chitosan-based hybrid nanocomplex was successfully developed for the systemic delivery of SVN siRNA, which could serve as an alternative to the cationic polymeric nanoparticles that are unstable in serum.

Keywords:chitosan, lecithin, nanocomplex, protamine, survivinsiRNA, thiamine pyrophosphate

List of Tables

List of Figures

1. Introduction

Various preclinical and clinical studies have been attempted for the development of siRNA therapeutics based on RNA interference technology. According to these reports on gene therapeutics, overcoming the low cellular permeability of nucleic acids as well as the low stability against serum proteins and degradative enzymes was considered a prerequisite for therapeutic applications [1-3].One of primary approaches to solve these difficulties is the development of highly efficient nucleic acid delivery systems which endow the protection of siRNA as a drug substancefrom nucleases presented in the body fluids, the improvement of low cellular membrane permeability and the amelioration of endosomolysis [4].

Many strategies were developed using non-viral vehicles for nucleic acid delivery [5]. Endowing cationic and lipophilic properties to overcome the limited cellular permeability of anionic and hydrophilic nucleic acids has been considered as themain approach. Among these, nucleic acid delivery systems based on cationic polymershave gained much attention with cationic lipids [6]. Typical cationic polymers could be

classified into synthetic polymers (*i.e.*, polyethyleneimine, poly-L-lysine, poly-L-arginine) and natural polymers (*i.e.*, chitosan) [7,8]. Particularly, chitosan as a natural polymer has been widely used in the development of nucleic acid delivery systems as it is known to have low cytotoxicity, high biocompatibility and high cellular permeability [9].In addition, its nucleic acid binding and delivering capacity can be influenced by its molecular weight, the degree of deacetylation and its salt form [10,11]. Moreover, chitosan conjugated with cationic polymer, peptide, and hydrophilic or hydrophobic residue is reported to exhibit an improved gene transfection efficiency [12-15]. Polyethylene glycol can be also introduced into chitosan for increasing its hydrophilicity and stability in biological fluids [16].

However, chitosan conjugates can encounter barriers (*i.e.*, problems in reproducibility in manufacturing and toxicity of the delivery vehicle itself) for clinical application and commercialization, and thus natural chitosan-based gene delivery system is more preferable.It also should be noted that cationic nanoparticle based on polyethylenimine as well as chitosan can induce plasma protein binding and aggregation with platelet resulting in hemolysis and thrombosis, as the surface charge increases[17-19]. These phenomena can influence the delivery accuracy and efficiency of therapeutics

[20]. Moreover, it is reported that, although chitosan may exhibit high binding affinity with siRNA due to high cationic charge density in acidic pH, siRNA/chitosan complex tends to be unstable in neutral and basic pH condition [21]. To maintain the stability of siRNA/chitosan complex in physiological pH, thiamine pyrophosphate (TPP) could be added.The delivery efficiency of chitosan could be highly kept at physiological pH due to the positively charged amine group of thiazolium included in TPP [22].

Survivin (SVN) belongs to the member of the inhibitor of apoptosis family protein and is known to be a promising target for cancer therapy. Its expression has been shown to be up-regulated in many cancers including prostate cancer while minimally expressed in normal tissues [23]. Thus, SVN could be a good target protein for siRNAnanocomplex studies. Studies have shown that protamine, which binds to the nucleic acids to form a stable nanocomplex*via* ionic and hydrophobic interactions, could be used for the pre-complex preparation in the development of a SVN siRNA-loaded hybrid nanocomplex[24-26]. Herein, we report on the preparation, physicochemical properties and delivery efficiencies of a SVN siRNA-loaded hybrid nanocomplex (Fig. 1). Pre-complex in this study was prepared to havenegative net chargefor the binding with cationic chitosan in the next step, by combination of a limited amount of protamine.

Phospholipid including lipid moiety was then introduced into siRNA/protamine pre-complex for the enhancement of nanocomplexstability in the blood stream. Until this step, the complex hadno transfection efficacy because of the lack of cationic charge in anentire particle. Finally, chitosan and TPP were added to induce the enhanced siRNA delivery which was caused by the stabilized positive surface charge achieved from chitosan and TPP. Then, the physicochemical properties and siRNA delivery efficiency of developed hybrid nanocomplex were assessed *in vitro* and *in vivo*.

2.Materials and methods

2.1. Materials

Survivin (SVN)siRNA, luciferase siRNA, and cy5.5-SVN siRNA (cy5.5-siRNA) wereprovided by BioneerCo. (Daejeon, Korea). Their sequences were as follows: SVNsiRNA (sense: 5'-AAG GAG AUC AAC AUU UUC A(dTdT)-3', anti-sense: 5'-UGA AAA UGU UGA UCU CCU U(dTdT)-3'), luciferase siRNA (sense: 5'-UUG UUU UGG AGC ACG GAA A(dTdT)-3', anti-sense: 5'-UUU CCG UGC UCC AAA ACA A(dTdT)-3'). Chitosan acetate and chitosan hydrochloride (HCl) were purchased from Heppe Medical Chitosan (Halle, Germany) and FMCBioPolymer (Philadelphia, PA, USA), respectively. BLOCK-iT fluorescent oligo and Lipofectamine 2000 (L2K) was obtained from Invitrogen (Carlsbad, CA, USA) and GelRed was acquired from Biotium, Inc. (Hayward, CA, USA). Lecithin, protamine andthiamine pyrophosphate (TPP) werepurchased from Alps Pharmaceutical (Hida, Japan), Lipoid (Ludwigshafen, Germany), and Sigma-Aldrich (St. Louis, MO, USA), respectively. Human SurvivinQuantikine ELISA kit was obtained from R&D systems (Minneapolis, MN,

USA) and Matrigel was acquired from BD Biosciences (Bedford, MA, USA). Fetal bovine serum (FBS), penicillin, streptomycin, RPMI 1640 (developed at Roswell Park Memorial Institute), phosphate buffered saline (PBS), tris-borate-EDTA, and trypsin-EDTA were obtained from GibcoLife Technologies, Inc. (Grand Island, NY, USA). All other chemicals were of analytical grade.

2.2. Gel retardation assays

The influences of molecular weight (MW) and the kind of salt form of chitosan on complex formation with SVN siRNA were investigated by gel retardation assayas reported in the literature [27].In this investigation, chitosan acetate or hydrochloride which has 50~400 kDa MW and 83~95% deacetylation degree were selected (Table 1). The weight ratios between chitosan and siRNA were 1, 10, 20, 30, 40, 50, 75, 100, and 150 (w/w).Each sample was electrophoresed in 2.5% agarose gel,including 0.01% GelRedwith tris-borate-EDTAbuffer at50V for 15 min. After electrophoresis, the complex formation was evaluated by scanning with MiniBIS Pro (DNR Bio-imaging

Systems, USA).

2.3. In vitro transfection efficiency according to the chitosan type

PC-3 cell, as a human prostate cancer cell, was purchased fromKorea Cell Line Bank (KCLB; Seoul, Korea). Cells were cultured with RPMI 1640 containing 10% FBS,100 U/ml penicillin, and 100 μg/ml streptomycin, in a 5% CO_2 atmosphere with 95% relative humidity at 37℃. To evaluate gene silencing efficiency according to the chitosan type and weight ratio between chitosan and siRNA, SVN expression (%) was measured by Human SurvivinQuantikineELISA kit.In brief, PC-3 cells were seeded into 6-well plate at a density of 1×10^5cells per well and cultured for 48 h. Before loading SVN siRNA/chitosan complex, cells were stabilized for 2 h with fresh culture media. PC-3 cells were incubated with various weight ratio (20, 40, 60, 80, 100 and 120 w/w)of chitosan/siRNAcomplex (corresponded amounts to 2 μg of siRNA per well)for 48 h in a 5% CO_2 atmosphere with 95% relative humidity at 37℃. Cells were lysed with the addition of 500 μl cell lysis buffer (Cell Signaling Technology, Inc., Danvers, MA, USA)

and collected. Cell lysates were centrifuged at 12,000 rpm for 20 min and 100 μl supernatant was used for subsequent assay. Assay diluent(100 μl) and collected samples (100 μl) were mixed and stirred at 500 rpm for 2 h. Upon washing 4 times, SVN conjugate (200 μl) was added and stirred for 2 h at room temperature. After washing 4 times again, substrate solution (200 μl) was added and incubated for 30 min at dark place.The reaction was terminated with the addition of stop solution (50 μl) and the absorbance at 450 nm was read by SpectraMax M2 microplate reader (Molecular Devices, Sunnyvale, CA, USA).The amount (%) of SVN was calculated by substituting absorbance values into the regression line obtained from standard solution.

2.4. Preparation of hybrid nanocomplex

Hybrid nanocomplexes were prepared by the combination of SVNsiRNA,protamine, lecithin, chitosan, and TPP (as shown in Table 2).Briefly, each substance, such as 10 mg SVN siRNA, 0.5 mg protamine sulfate, 4 mg chitosanHCl (150~400 kDa, FMC CL214, FMC BioPolymer, Philadelphia, PA, USA), and 20 mg TPP,was solubilized in 1 ml of

diethylpyrocarbonate-treated distilled water (DW), respectively, and filtered.In the case of lecithin (Lipoid S-100), 30mg was dissolved in ethanol (1ml) and filtered. The pre-complex was prepared by mixing and stirring SVN siRNA and protamine. Lecithin was added into that complex solution and stirred for 30 min. The final formulation, GP-L-CT, was developed by adding chitosan and TPPinto the above mixture. Other complexes (G-C, G-CT, GP, GP-C, GP-CT, GP-L) were also prepared following theabove order.

2.5. Particle size and zeta potential measurements

The mean diameter and zeta potential values of developed nanocomplexes were measured by a light-scattering spectrophotometer (ELS-Z, Otsuka Electronics, Tokyo, Japan) according to the manufacturer's protocol. Corresponded amounts of nanocomplexes (to 20 µg of siRNA) were dispersed in DW (0.5 ml) for their analysis. The stability of nanocomplexes was assessed in cell culture medium (RPMI 1640) and 50% (v/v) FBS. Similarly with the above method, corresponded amounts of nanocomplexes (to 20 µg of siRNA) were diluted in 0.5 ml of cell culture medium or 50% FBS.After

incubating for 3 h, the mean diameter and zeta potential values were measured by ELS-Z system.

2.6. Cryo-transmission electron microscopy (Cryo-TEM)

The morphology of developed nanocomplexes was observed by Cryo-TEM (Tecnai G2 F20 Cryo-TEM, FEI Company, Hillsboro, Oregon, USA) [28]. The specimen was applied to holey carbon affixed to the grid (Quantifoil Micro Tools GmbH, Jena, Germany), and rapidly cooled to -170℃. It was fixed in the cryo-holder and inserted into the Cryo-TEM at -170℃. Images of specimen were recorded under low electron dose conditions.

2.7. In vitro cellular uptake

Cellular uptake efficiency of siRNA was assessed by flow cytometry analysis [29].

PC-3 cells were seeded onto 6-well plate at a density of 1×10^5 cells per well and incubated for 48 h in a 5% CO_2 atmosphere with 95% relative humidity at 37℃. All formulations containing 10 μg of BLOCK-iT fluorescent oligo were prepared according to the composition described in Table 2. Nanocomplexes with BLOCK-iT fluorescent oligo were added and incubated for 24 h in the same culture condition. After incubating, cells were washed with PBS three times, collected by the treatment with 0.25% trypsin-EDTA, and analyzed by flow cytometry (BD FACS Canto II; Becton-Dickinson, San Jose, CA, USA).

2.8. In vitro transfection study of developed nanocomplexes

Nanocomplexes were prepared, according to the compositions in Table 2, to evaluate their gene silencing efficiency in PC-3 cells by the described method in section 2.3. In case of L2K group, the mixture of SVN siRNA(100 μg) and L2K (300 μl) was prepared and incubated for 20 min before its use. Loading amount of siRNA was also 2 μg/ml per well and SVN expression (%) in PC-3 cells was analyzed according to the

above method.

2.9. In vivo near-infrared fluorescence (NIRF) imaging

Biodistribution of developed siRNA-loaded hybrid nanocomplex was assessed in PC-3 tumor xenografted mouse model. To establish human prostate cancer xenografted mouse model, 2× 10^6PC-3 cells suspended in 50 µl cell culture media with 50 µl Matrigel were injected subcutaneously into the five-week-old male severe combined immunodeficient (SCID) mouse (Shizuoka Laboratory Animal Center, Hamamatsu, Japan). After attaining 100 mm^3 of tumor volume, naked cy5.5-siRNA or cy5.5-siRNA-loaded formulation was injected intravenously *via* tail vein at a dose of 80 µg siRNAper mouse. cy5.5-siRNA-loaded formulations were prepared using cy5.5-siRNA instead of SVN siRNA according to the described method in section 2.4 and 2.8.NIRF images of tumor region in mouse model were obtained by eXploreOptixsystem (Advanced Research Technologies-GE healthcare, St. Laurent, Quebec, Canada) 2h post-injection [30]. Laser power and count time settings were 25 µW and 0.3 s per point, respectively.

To excite the Cy5.5 molecules in the nanocomplex, the laser diode at 670 nm wavelength was used.

2.10. In vivo anti-tumor efficacy

Prostate cancer (PC-3 tumor) xenografted mouse model was used to assess siRNA delivery efficiency of developed nanocomplex formulations. As described, 2×10^6 PC-3 cells suspended in 50 µl cell culture media with 50 µl Matrigel (BD Biosciences, Bedford, MA, USA) were injected subcutaneously into the five-week-old male SCID mouse to prepare the mouse model. Luciferase siRNAwas used as a scrambled siRNA and the preparation method of luciferase-loaded GP-L-CT was identical to that of SVN siRNA. After reaching approximately 100 mm^3 tumor volume, corresponded amounts of formulations to 40 µgsiRNA were injected intravenously *via* the tail vein 6 times for 2 weeks. The tumor size was measured with Vernier calipers, and tumor volume was calculated according to following formula; $V = 0.5 \times$ longest diameter $\times$ shortest $diameter^2$.

2.11. Statistical analysis

All experiments in this investigation were conducted at least three times and data were represented as mean ± standard deviation (S.D.). Statistical analysis was based on analysis of variance (ANOVA).

3. Results and discussion

3.1. Selection of chitosan

Chitosan is a natural and cationic polymer, which exists in a variety of MW, salt type and deacetylation degree. In our preliminary study, various types of chitosan of differentMWs were tested for siRNA complex formation by gel retardation assay to select those with efficient complexation capabilities (data not shown).Based on these results, four chitosans which have 50~400 kDa MW and 83~95% deacetylation degree were selected (Table 1), and then thecomplex formation with siRNA(Fig.2) and the *in vitro*gene transfection efficiencies(Fig.3) were evaluated. Chitosan D (chitosan HCl with 150~400 kDa MW and 95% deacetylation degree) exhibited the highest complexationcapability and gene transfection efficiency among the four chitosanstested. Chitosan/siRNA complex was formed in the minimum weight ratio (chitosan to siRNA) of 10for Chitosan D (Fig. 2) which also showed lower SVN expression rate (%)compared to other chitosans(Fig.3).Therefore, chitosan D was finally selected for the preparation of the siRNA-loaded hybrid nanocomplexes.

3.2. Development and characterization of siRNA-loaded hybrid nanocomplexes

All of the nanocomplex formulations were prepared according to the composition presented in Table 2. In the G-CT formulation, TPP was addedto improve the binding capacity of chitosan to nucleic acid therapeutics in the physiological pH region, compared to G-C as the conventional formulation. For stabilized hybrid nanocomplexes using a pre-complex process, GP, GP-CT, GP-L, and GP-L-CT were prepared. GP was a pre-complex consisted of siRNA and protamine, based on their electrostatic interaction. GP-CT was produced by the addition of siRNA/protamine complex, instead of siRNA alone, into the G-CT formulation. GP-L and GP-L-CT were prepared by adding lecithin into GP and GP-CT for more stability improvement, respectively.

Considering the clinical dose of therapeutic siRNA, the lower weight ratio between chitosan and siRNAis preferred. In our preliminary study, optimum formulations of hybrid nanocomplexes (GP-L-CT) were prepared at different weight ratios of chitosan to siRNA (3.4, 6.8, 10.0, and 20.0). Since the proper gene silencing effect was observed

from the weight ratio of 6.8 (data not shown), it was estimated to be the minimum ratio to prepare stable hybrid nanocomplexes, which was also supported by the gel retardation assay of chitosan D (Fig. 2). The amount of protamine, for the pre-complex formation with siRNA, should be restricted to make complexation with positively charged chitosan. The weight ratio of protamine to siRNA was fixed as 0.6 because the aggregation and precipitation of nanocomplex were shown around 0.8, and zeta potential value of siRNA/protamine pre-complex was converted into a positive charge of over 1.

The mean diameter and zeta potential values of the developed nanocomplexes in DW were measured and stability of nanocomplexes, presented by the change of the mean diameter in cell culture media and serum, was also evaluated (Fig. 4). The mean diameters of G-C and G-CT in DW were 377 and 419 nm, respectively, but the particle size was increased in the cell culture media and 50% FBS. After incubating 3 h in cell culture media and 50% FBS conditions, the mean diameters of G-C were 1,773 and 1,128 nm, respectively, while those values of G-CT were 1,440 and 1,247 nm, respectively. Such an aggregation of nanocomplexes in biological fluids should be resolved for efficient *in vivo* gene transfection and the maintenance of stability after

intravenous injection. The mean diameters of GP, GP-CT, GP-L, and GP-L-CT in DW were 177, 604, 133, and 189 nm, respectively. Zeta potential values of GP and GP-L were negative due to the absence of the cationic substances, chitosan and TPP. In contrast, zeta potential values of GP-CT and GP-L-CT were positive which could guarantee the attachment of nanocomplexes to negatively charged cellular membrane for subsequent endocytosis. The mean diameters of GP, GP-CT, GP-L, and GP-L-CT nanocomplexes in cell culture media were 25, 1,512, 110, and 129 nm, respectively. These values in 50% serum condition were changed to 33, 1,051, 94, and 181 nm, respectively (Fig. 4b). The GP exhibited complex dissociation and the GP-CT showed increased the diameter caused by aggregation in cell culture media and serum conditions, compared to nanocomplexes in DW. On the other hand, lecithin-incorporated formulations (GP-L and GP-L-CT) suppliedthe maintained particle size without a significant change of the diameters.Especially, it is interesting to note that GP-L-CT had positive zeta potential and similar particle size both in DW and serum.

The morphology of GP, GP-L, and GP-L-CT was observed by Cryo-TEM because the nanocomplexes had < 200 nm diameters in DW, culture media, and 50% FBS without

aggregation or precipitation. As shown in Fig. 5, GP has reticulartexture with loosely disentangled particular shape. GP-L exhibited a partial reticular structure but showed a fused shape with spherical liposome. In the case of GP-L-CT, reticular texture was completely disappeared and opaque spot, a characteristic of nanoparticles, was presented (Fig. 5C).The Cryo-TEM images explained that although the complex could be stabilized by pre-complex processor addition of lecithin, the formation of nanoparticle should be completed by complexation with cationic substances, chitosan and TPP.

3.3. In vitro cellular uptake

Cellular uptake efficiency of developed nanocomplexes in PC-3 cells was evaluated by flow cytometer (Fig. 6). According to the result with nanocomplexes including fluorescent siRNA, the mean population percentages in P1 region of naked siRNA, L2K, G-C, and G-CT were 2.0, 40.0, 59.6, and 73.2%, respectively. The mean population percentages of GP, GP-CT, GP-L, and GP-L-CT were 3.3, 75.0, 2.8, and 83.9%, respectively. It was shown that the naked siRNA, GP, and GP-L could not be permeated into the cellular membrane, and G-C, G-CT, GP-CT and GP-L-CT have a higher cellular

uptake efficiency compared to the L2K-treated group, despite their large particle size in cell culture media and serum condition *in vitro*. Especially, G-CT, GP-CT, and GP-L-CT with both chitosan and TPP showed the highest level of cellular uptake efficiency.

3.4. In vitro gene silencing

In vitro gene silencing efficiency of developed nanocomplexes was assessed by measuring SVN expression in PC-3 cells. SVN expression (%) was measured after incubating SVN siRNA or its nanocomplex formulations for 48 h (Fig. 7). SVN expression (%) was reduced to 29.3 and 25.9% by the treatment of G-C and G-CT, respectively. Although L2K treatment produced lower SVN expression rate (6.8%), its systemic application *in vivo* has been restricted generally due to its toxicity and low efficacy *in vivo* compared to the *in vitro* effect. SVN expression rates of GP, GP-CT, GP-L, and GP-L-CT-treated groups were 99.6, 35.2, 100.0, and 21.8%, respectively. While naked siRNA, GP and GP-L formulations lacking chitosan did not have any *in vitro* gene silencing efficacy, G-C, G-CT, GP-CT and GP-L-CT groups containing chitosan alone orboth chitosan and TPP exerted higher gene silencing efficiency. So it was confirmed

that the stabilizing process including pre-complexationor lecithin incorporation did not reduced the gene silencing efficiency of chitosan nanocomplex.

Considering the particle size (< 200 nm) in serum conditionand gene silencing efficiency, GP-L-CT is considered to be the most appropriate nanocomplex for the systemic delivery of SVN siRNA for cancer therapy. The stability of siRNAnanocomplex in serum condition was insured only by both pre-complexation with protamine and lecithin incorporation process. And cellular uptake and gene silencing efficiency was highly induced by complexation process of chitosan and TPP. Therefore, GP-L-CT nanocomplex, as the final formulation, was used in further *in vivo* studies.

3.5. In vivo NIRF imaging

Tumor targetability of Cy5.5-siRNA-loaded GP-L-CTnanocomplex was investigated by *in vivo* NIRF imaging in PC-3 tumor xenografted mouse model. Fluorescence intensity in tumor region was scanned 2 h after intravenous injection. As shown in Fig. 8, fluorescence intensity in tumor region of Cy5.5-siRNA/GP-L-CT was

the highest in all of the experimental groups. Fluorescence intensities of the naked Cy5.5-siRNA and Cy5.5-siRNA/L2K were lower than of the GP-L-CT-treated group, and it is surmised that naked siRNA and L2K were inappropriate for systemic administration due to their low stability in the biological fluids.

Though normal vasculature has packed structure with < 10 nm pore size, neovasculature in tumor region has an abnormally aligned endothelium with wide fenestrations (100~700 nm pore size) and defective lymphatic drainage [31]. As a result, *in vivo* stabilized and circulating nano-sized drug delivery systems can be easily permeated and accumulated in the tumor region. This phenomenon has been known as the enhanced permeability and retention (EPR) effect which explains the *in vivo*stability and tumor targetability of GP-L-CT.

3.6. In vivo anti-tumor efficacy

In vivo anti-tumor efficacy of control, SVN siRNA-loaded GP-L-CT nanocomplex was tested in PC-3 tumor xenografted mouse model by monitoring tumor growth inhibition (Fig. 9). As a scrambled siRNA, luciferase siRNA was incorporated into GP-L-

CT and used as a control group. In our preliminary study, naked siRNA did not produce an anti-tumor efficacy in PC-3 tumor bearing mouse model (data not shown). Mean tumor volumes, at day 14, of control, scrambled siRNA/GP-L-CT, and SVN siRNA/GP-L-CT treated groups were 615, 550, and 226 mm^3, respectively. At day 18, mean tumor volumes of control, scrambled siRNA/GP-L-CT, and SVN siRNA/GP-L-CT treated groups were 754, 742, and 277 mm^3, respectively. It is particularly notable that the tumor volume of SVN siRNA/GP-L-CT group was smaller than the scrambled siRNA/GP-L-CT group ($P< 0.05$). It indicated that the *in vivo* anti-tumor efficacy was induced by SVN siRNA delivery.

In vivo tumor targetability and anti-tumor efficacy of SVN siRNA/GP-L-CTafter intravenous injection have been demonstrated in this study.Although further investigation is needed for fully elucidating the specific mechanism of the developed nanocomplex, the feasibility as a nano-sized vehicle for the systemic application of siRNA therapeutics has been shown. Though chitosan could be used as a cationic polymer for *in vitro* gene transfection, it is difficult to verify its*in vivo* performance due to the weakened binding affinity with nucleic acids and the aggregation resulted by the interaction with

endogenous components in the biological system. The significance of this study is in successfully identifying thethe systemic application of the GP-L-CT formulation in cancer therapy and diagnosis.

4. Conclusions

The low cytotoxicity, high biocompatibility, high mucoadhesiveness, and high cell permeability of chitosan has made it widely used for the delivery of nucleic acid therapeutics. However,the reduction of its*in vivo* gene delivery efficiency should be overcome,even whenits*in vitro* gene transfection efficiency was properly maintained.A pre-complex based on siRNA and protamine was formed and lecithin, chitosan, and TPP were added to develop a more stable and efficient hybrid nanocomplex (GP-L-CT) in this study. GP-L-CT provided suitable physicochemical properties (< 200 nm mean diameter in serum and positive zeta potential) for intravenous injection of siRNAas well as superior *in vitro* cellular uptake and gene silencing efficiencies. Furthermore, *in vivo* tumor targetability and anti-tumor efficacy in tumor xenografted mouse model have been proven. The newly developed theranostic hybrid nanocomplex can therefore be used efficiently for the systemic siRNA delivery in cancer therapy.

References

[1] S.H. Chen, G. Zhaori, Potential clinical applications of siRNA technique: benefits and limitations, Eur J Clin Invest 41 (2011) 221–232.

[2] J. Wang, Z. Lu, M. G. Wientjes, J. L.-S. Au, Delivery of siRNA Therapeutics: Barriers and Carriers, AAPS J 12 (2010) 492–503.

[3] M.A. Behlke, Progress towards in vivo use of siRNAs, MolTher 13 (2006) 644–670.

[4] K.A. Whitehead, R. Langer, D.G. Anderson, Knocking down barriers: advances in siRNA delivery, Nat Rev Drug Discov 8 (2009) 129–138.

[5] S. Zhang, Y. Zhao, D. Zhi, S. Zhang, Non-viral vectors for the mediation of RNAi, Bioorg Chem 40 (2012) 10–18.

[6] I.A. Khalil, K. Kogure, H. Akita, H. Harashima, Uptake pathways and subsequent intracellular trafficking in nonviral gene delivery, Pharmacol Rev 58 (2006) 32–45.

[7] Y. Ping, C. Liu, Z. Zhang, K.L. Liu, J. Chen, J. Li, Chitosan-graft-(PEI-β-cyclodextrin) copolymers and their supramolecularPEGylation for DNA and siRNA

delivery, Biomaterials 32 (2011) 8328–8341.

[8] K. Singha, R. Namgung, W.J. Kim, Polymers in Small-Interfering RNA Delivery, Nucleic Acid Ther 21 (2011) 133–147.

[9] S. Mao, W. Sun, T. Kissel, Chitosan-based formulations for delivery of DNA and siRNA, Adv Drug Deliv Rev 62 (2010) 12–27.

[10] J. Malmo, S. Hanne, K. M. Vårum, S. P. Strand, siRNA delivery with chitosan nanoparticles: Molecular properties favoring efficient gene silencing, J Control Release 158 (2012) 261–268.

[11] S. Techaarpornkul, S. Wongkupasert, P. Opanasopit, A. Apirakaramwong, J. Nunthanid, U. Ruktanonchai, Chitosan-mediated siRNA delivery in vitro: effect of polymer molecular weight, concentration and salt forms, AAPS PharmSciTech 11 (2010) 64–72.

[12] S. Park, E. J. Jeong, J. Lee, T. Rhim, S. K. Lee, K. Y. Lee, Preparation and characterization of nonaarginine-modified chitosan nanoparticles for siRNA delivery, Carbohydr Polym 92 (2013) 57–62.

[13] J.C. Fernandes, X, Qiu, F. M. Winnik, M. Benderdour, X. Zhang, K. Dai, Q. Shi,

Low molecular weight chitosan conjugated with folate for siRNA delivery in vitro: optimization studies, Int J Nanomedicine 7 (2012) 5833–5845.

[14] M. Malhotra, C. Tomaro-Duchesneau, S. Prakash, Synthesis of TAT peptide-tagged PEGylated chitosan nanoparticles for siRNA delivery targeting neurodegenerative diseases, Biomaterials 34 (2013) 1270–1280.

[15] H.D. Han, L.S. Mangala, J.W. Lee, M.M. Shahzad, H.S. Kim, D. Shen, E.J. Nam, E.M. Mora, R.L. Stone, C. Lu, S.J. Lee, J.W. Roh, A.M. Nick, G. Lopez-Berestein, A.K. Sood, Targeted gene silencing using RGD-labeled chitosan nanoparticles, Clin Cancer Res. 16 (2010) 3910–3922.

[16] M. Malhotra, C. Lane, C. Tomaro-Duchesneau, S. Saha, S. Prakash, A novel method for synthesizing PEGylated chitosan nanoparticles: strategy, preparation, and in vitro analysis, Int J Nanomedicine 6 (2011) 485–494.

[17] P. P. Karmali, D. Simberg, Interactions of nanoparticles with plasma proteins: implication on clearance and toxicity of drug delivery systems, Expert Opin Drug Deliv 8 (2011) 343–357.

[18] A. Radomski, P. Jurasz, D. Alonso-Escolano, M. Drews, M. Morandi, T. Malinski,

M. W. Radomski, Nanoparticle-induced platelet aggregation and vascular thrombosis, Br J Pharmacol 146 (2005) 882–893.

[19] M. A. Dobrovolskaia, P. Aggarwal, J. B. Hall, S. E. McNeil, Preclinical Studies To Understand Nanoparticle Interaction with the Immune System and Its Potential Effects on Nanoparticle Biodistribution, Mol Pharm 5 (2008) 487–495.

[20] M. Matsuura, Y. Yamazaki, M. Sugiyama, M. Kondo, H. Ori, M. Nango, N. Oku, Polycation liposome-mediated gene transfer in vivo, Biochim Biophys Acta 1612 (2003) 136– 143.

[21] S. Xu, M. Dong, X. Liu, K.A. Howard, J. Kjems, F. Besenbacher, Direct force measurements between siRNA and chitosan molecules using force spectroscopy, Biophys J 93 (2007) 952–959.

[22] T. Rojanarata, P. Opanasopit, S. Techaarpornkul, T. Ngawhirunpat, U. Ruktanonchai, Chitosan-Thiamine Pyrophosphate as a Novel Carrier for siRNA Delivery, Pharm Res 25 (2008) 2807–2814.

[23] H. Doolittle, A. Morel, D. Talbot, Survivin-directed anticancer therapies – A review of pre-clinical data and early-phase clinical trials, European Oncology 6 (2010) 10–

14.

[24] A.K. Kundu, P.K. Chandra, S. Hazari, Y.V. Pramar, S. Dash, T.K. Mandal, Development and optimization of nanosomal formulations for siRNA delivery to the liver, Eur J Pharm Biopharm 80 (2012) 257–267.

[25] D. Delgado, A. Pozo-Rodríguez, M.A. Solinís, A. Rodríguez-Gascón, Understanding the mechanism of protamine in solid lipid nanoparticle-based lipofection: The importance of the entry pathway, Eur J Pharm Biopharm 79 (2011) 495–502.

[26] R.K. DeLong, U. Akhtar, M. Sallee, B. Parker, S. Barber, J. Zhang, M. Craig, R. Garrad, A.J. Hickey, E. Engstromd, Characterization and performance of nucleic acid nanoparticles combined with protamine and gold, Biomaterials 30 (2009) 6451–6459.

[27] M.S. Suh, G. Shim, H.Y. Lee, S.E. Han, Y.H. Yu, Y. Choi, K. Kim, I.C. Kwon, K.Y. Weon, Y.B. Kim, Y.K. Oh, Anionic amino acid-derived cationic lipid for siRNA delivery, J Control Release 140 (2009) 268–276.

[28] R. Crawford, B. Dogdas, E. Keough, R.M. Haas, W. Wepukhulu, S. Krotzer, P.A.

Burke, L.S. Lorenzino, A. Bagchi, B.J. Howell, Analysis of lipid nanoparticles by Cryo-EM for characterizing siRNAdelivry vehicles, Int J Pharm 403 (2011) 237–244.

[29] J. Malmo, H. Sorgard, K.M. Varum, S.P. Strand, siRNA delivery with chitosan nanoparticles: Molecular properties favoring efficient gene silencing, J Control Release 158 (2012) 261–268.

[30] N. Yagi, I. Manabe, T. Tottori, A. Ishihara, F. Ogata, J.H. Kim, S. Nishimura, K. Fujiu, Y. Oishi, K. Itaka, Y. Kato, M. Yamauchi, R. Nagai, A Nanoparticle System Specifically Designed to Deliver Short Interfering RNA Inhibits Tumor Growth In vivo, Cancer Res 69 (2009) 6531–6538.

[31]R. Juliano, J. Bauman, H. Kang, X Ming, Biological barriers to therapy with antisense and siRNA oligonucleotides, Mol Pharm 6 (2009) 685-695.

Table 1.Specifications of the chitosans used in this study.

	Chitosan	Molecular weight (MW:kDa)	Deacetylation degrees (%)
A	Chitosan acetate	100	84
B	Chitosan acetate	300	84
C	Chitosan HCl	50 ~ 150	83
D	Chitosan HCl	150 ~ 400	95

Table 2.Compositions of SVN siRNA-loaded chitosan-based nanocomplexes.

components	G-C	G-CT	GP	GP-CT	GP-L	GP-L-CT
SVN siRNA	1	1	1	1	1	1
Protamine	-	-	0.6	0.6	0.6	0.6
Lecithin	-	-	-	-	8	8
Chitosan	6.8	6.8	-	6.8	-	6.8
TPP	-	1.2	-	1.2	-	1.2

All values were presented as weight ratios.

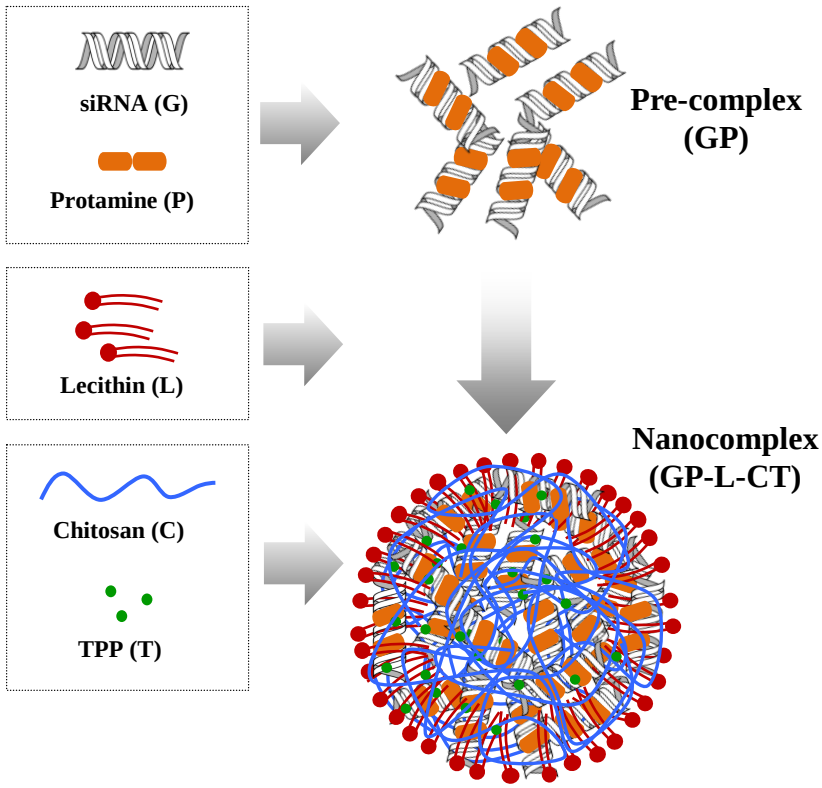

Fig.1. Schematic illustration of GP-L-CT hybrid nanocomplex preparation

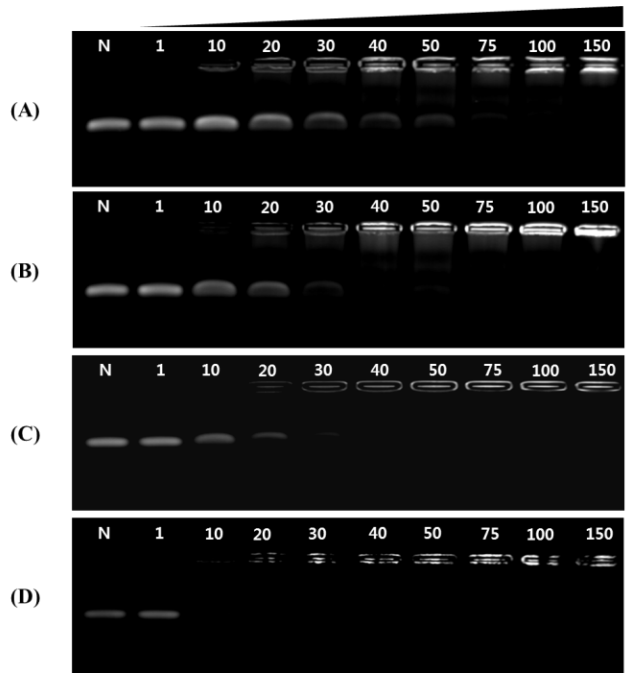

Fig.2. Gel retardation assays of siRNA with different chitosans; (A) chitosan acetate (MW: 100 kDa), (B) chitosan acetate (MW: 300 kDa), (C) chitosan HCl (MW: 50~150 kDa), and (D) chitosan HCl (MW: 150~400 kDa). Complex formation according to the weight ratios between chitosan and siRNA was investigated by gel electrophoresis in 2.5% agarose gel.

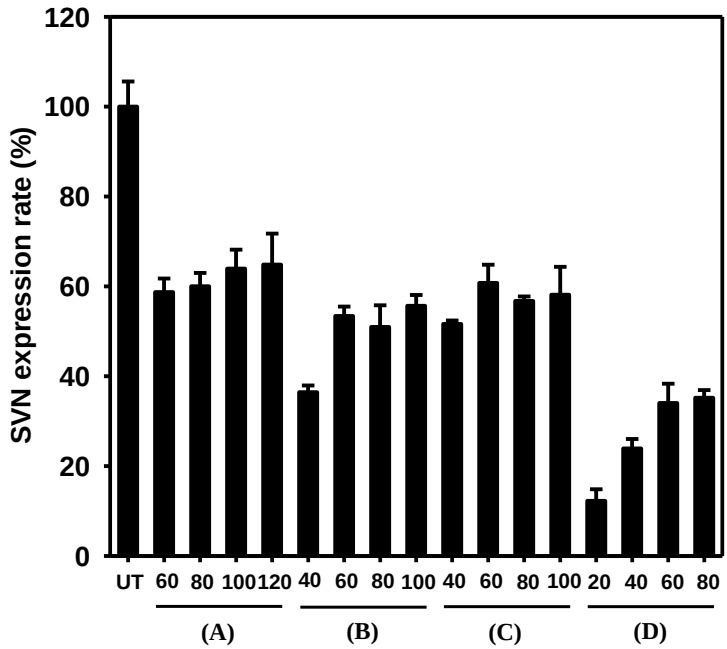

Fig.3.*In vitro* gene transfection efficiency of different chitosans; (A) chitosan acetate (MW: 100 kDa), (B) chitosan acetate (MW: 300 kDa), (C) chitosan HCl (MW: 50~150 kDa), and (D) chitosan HCl (MW: 150~400 kDa). SVN expression rate (%) was shown after incubating for 48 h with various weight ratios between chitosan and SVN siRNA in PC-3 cells. Each value was presented as the mean ± S.D. (n = 3).

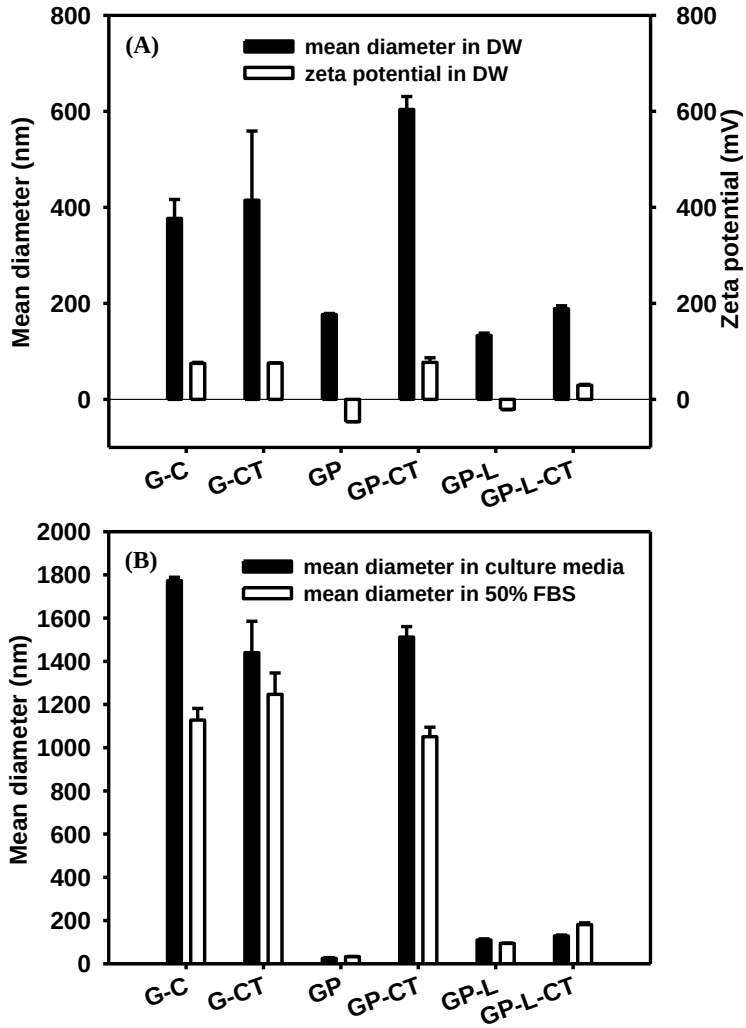

Fig.4. Characterization of SVN siRNA-loaded hybrid nanocomplex. (A) Particle size and zeta potential values of nanocomplex formulations in DW. (B) Mean diameters of nanocomplexes in cell culture media and FBS. Each value represents the mean ± S.D. (n = 3).

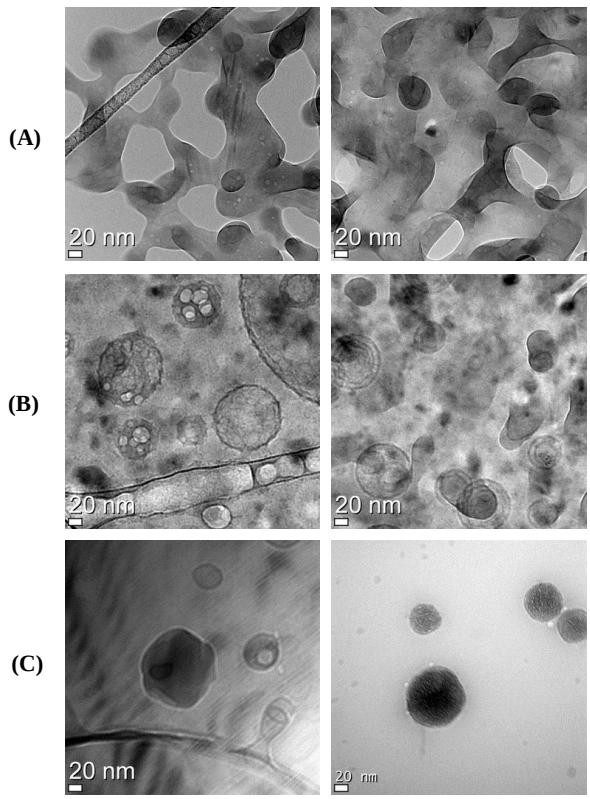

Fig.5. Morphology of nanocomplex formulations observed by cryo-transmission electron microscopy (cryo-TEM).Images of (A) siRNA/protamine (GP), (B) siRNA/protamine/lecithin complex (GP-L), (C) siRNA/protamine/lecithin/chitosan/TPP complex (GP-L-CT). The length of scale bar is 20 nm.

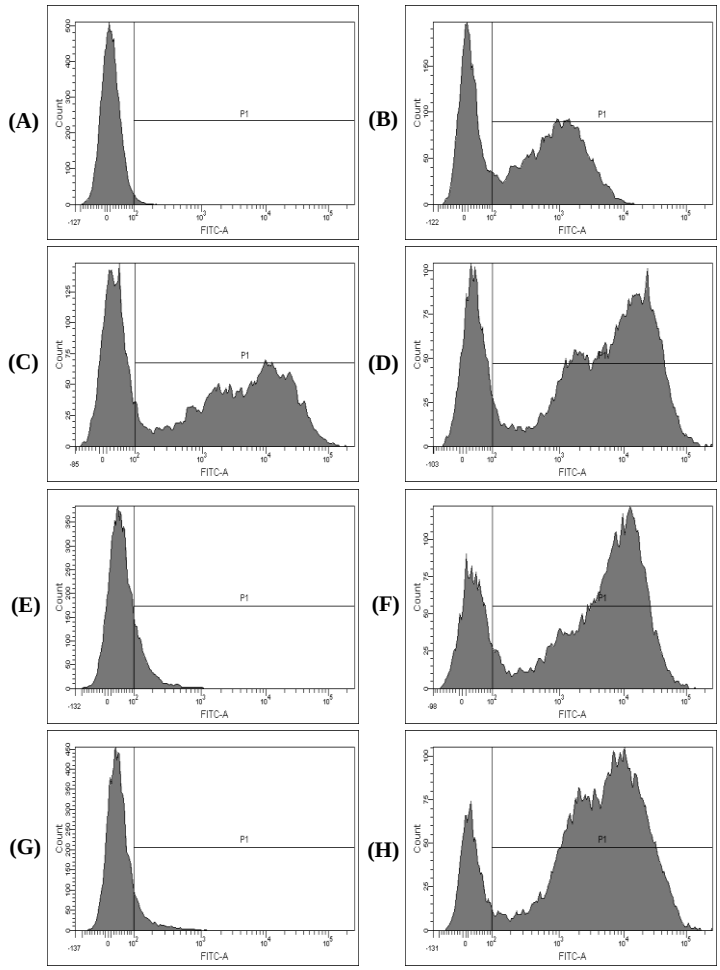

Fig.6. *In vitro* cellular uptake efficiency of the nanocomplexes in PC-3 cells. Fluorescent siRNA was loaded into various nanocomplex formulations and fluorescence intensity was measured by flow cytometry after incubating for 24 h. Plots, between cell count and fluorescence intensity, of (A) naked siRNA, (B) siRNA/Lipofectamine 2000 (L2K), (C) siRNA/chitosan (G-C), (D) siRNA/chitosan/TPP (G-CT), (E) siRNA/protamine (GP), (F) siRNA/protamine/chitosan/TPP (GP-CT), (G) siRNA/protamine/lecithin (GP-L), and (H) siRNA/protamine/lecithin/chitosan/TPP (GP-L-CT) are presented.

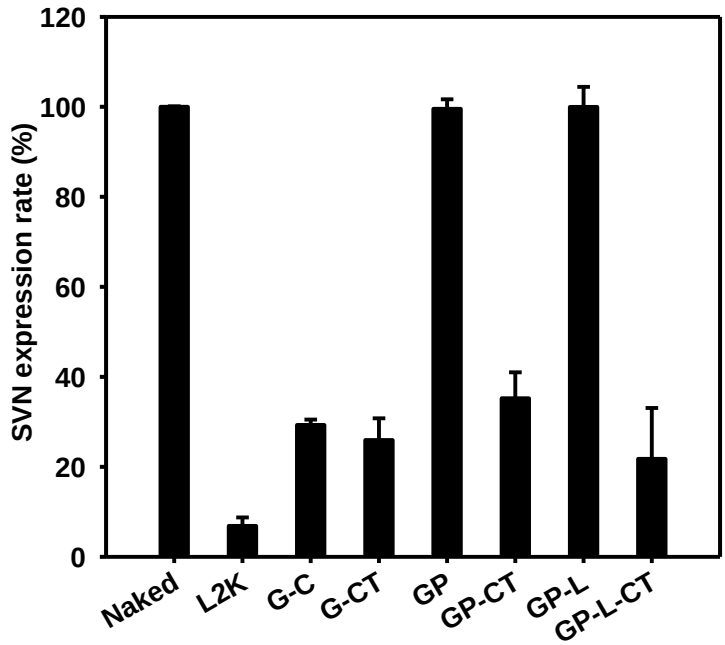

Fig.7. *In vitro* transfection efficiency of SVN siRNA-loaded nanocomplex formulations in PC-3 cells. SVN expression levels (%) of naked siRNA (naked), siRNA/Lipofectamine 2000 (L2K), siRNA/chitosan (G-C), siRNA/chitosan/TPP (G-CT), siRNA/protamine (GP), siRNA/protamine/chitosan/TPP (GP-CT), siRNA/protamine/lecithin (GP-L), and siRNA/protamine/lecithin/chitosan/TPP (GP-L-CT)-incubated groups (for 48 h) are presented. Each value represents the mean ± S.D. (n = 3).

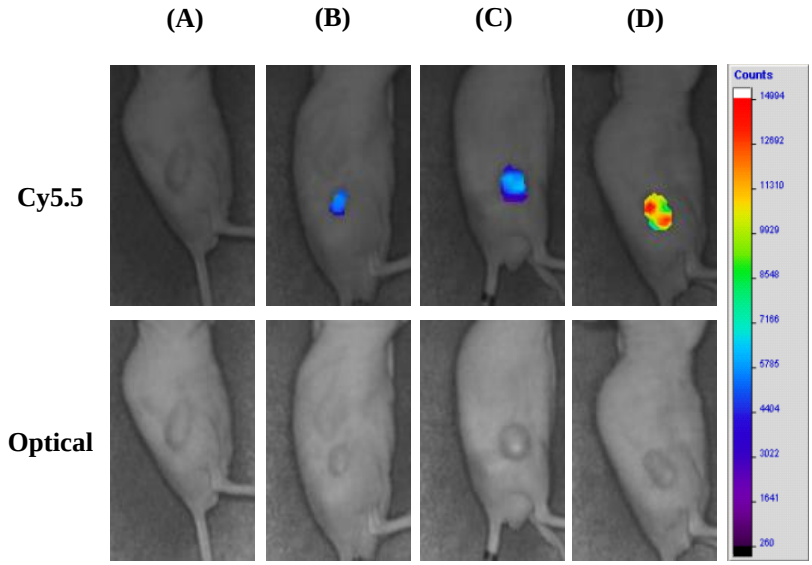

Fig.8. *In vivo* NIRF images of siRNA-loaded nanocomplex formulations in PC-3 tumor-xenografted mouse model. Cy5.5-filtered and optical images of tumor in (A) control, (B) naked cy5.5-siRNA, (C) cy5.5-siRNA/Lipofectamine 2000 (Cy5.5-siRNA/L2K), (D) cy5.5-siRNA/protamine/lecithin/chitosan/TPP complex (Cy5.5-siRNA/GP-L-CT) groups 2 h post-injection via intravenous route.

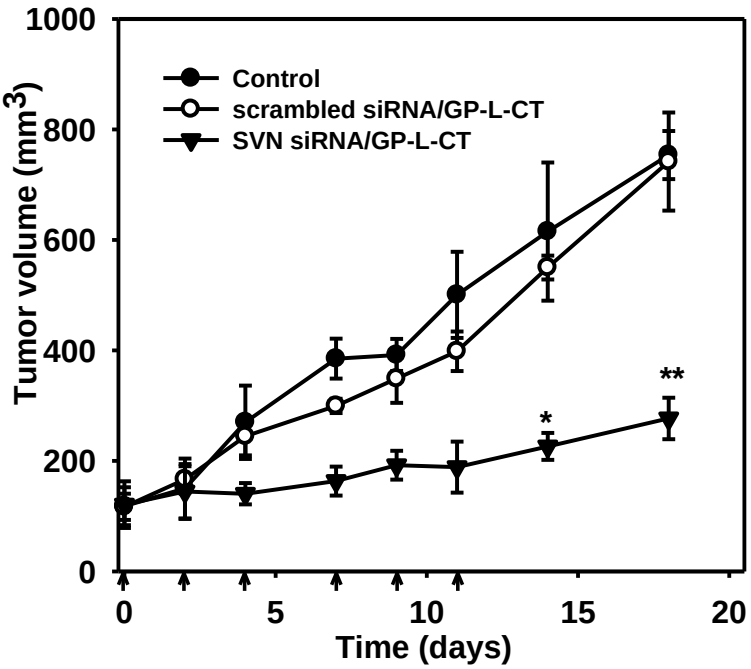

Fig.9. *In vivo* anti-tumor efficacy test of siRNA-loaded nanocomplex in PC-3 tumor-xenografted mouse model.Tumor volume profiles of control, luciferase-siRNA/protamine/lecithin/chitosan/TPP (scrambled siRNA/GP-L-CT), survivin-siRNA/protamine/lecithin/chitosan/TPP complex (SVN siRNA/GP-L-CT).Nanocomplexes were injected 6 times for 2 weeks via intravenous route. **P*< 0.05 and ***P*< 0.01 are established between scrambled siRNA/GP-L-CT and SVN siRNA/GP-L-CT. Data represents the mean ± S.D. (n ≥ 3).

요약 (국문 초록)

제목 :Chitosan을 이용한 siRNA 전달용 융합 나노복합체와 항암치료로의 활용

학교 : 서울대학교 약학대학원

학과 및 전공 : 제약학과 약제과학 전공

성명 : 기 민 효

천연의 생체적합성 양이온성폴리머인 chitosan 은 siRNA 전달을 위한 매력적인 전달체이지만 in vivo 환경에서 유전자 전달력이 감소되는 단점을 가지고 있다. 본 연구에서는 이러한 기존의 chitosan 나노입자의 문제점을 극복하기 위하여 혈액 내 안정성이 개선된 새로운 chitosan 융합 나노복합체를 개발하여 in vitro 및 in vivo 전달효력을 향상시키고자 하였다. Chitosan 융합 나노복합체는 survivin (SVN) siRNA 의 전달을 위하여 chitosan

및 protamine, lecithin, thiamine pyrophosphate (TPP)를 구성성분으로 하여 제조되었다. 먼저 정제수 및 세포배양액, 50% fetal bovine serum (FBS) 내에서 나노입자의 안정성을 포함한 물리화학적 특성을 평가하였고 전립선암세포주 (prostate cancer cells, PC-3)를 이용하여 세포 내로의 유전자 전달효과를 측정하였다. 그 결과, SVN siRNA 를 로딩한 융합 나노복합체 (GP-L-CT)는 혈청 내에서도 200 nm 이하의 평균 입자도와양이온성 표면전하를 유지하였고 PC-3 세포에서 SVN 발현율을 21.8%로 감소시켰다. 그리고 PC-3 암종을이종이식한 마우스 모델에서 근적외선 형광 (near-infrared fluorescence, NIRF)을 이용하여 나노복합체의 암으로의 이행성과 항암 효력을 평가하였을 때, GP-L-CT 는 정맥주사를 통해 암조직의 형광강도 증가와 암성장 억제 효력을 나타내어 전신투여를 통한 치료 및 진단 가능성을 보여주었다. 결론적으로 chitosan 을 이용한 융합 나노복합체는 SVN siRNA 의 전신투여 전달에 활용이 가능하고 또한 혈청 내에서 안정성이 낮은 기존의 양이온성폴리머나노입자의 문제점에 대한 대안이 될 수 있음이 확인되었다.

주요어 :chitosan, lecithin, nanocomplex, protamine, survivinsiRNA, thiamine pyrophosphate

학번 : 2005-31162

APPENDIX

Curriculum Vitae

Personal

Name: Min-Hyo Ki

Affiliation: Department of Pharmaceutics

College of Pharmacy, Seoul National University

1 Gwanak-ro, Gwanak-gu, Seoul 151-742, Korea

Contact: Tel. 82-2-884-3170

Fax. 82-2-885-8317

E-mail: mh_ki@naver.com

Citizenship

Republic of Korea

Education

Ph. D. in Pharmacy (Department of Pharmaceutics)

Seoul National University, Seoul, Korea

Advisor: Dae-Duk Kim, Ph. D., professor

Thesis Title: Chitosan-based hybrid nanocomplex for siRNA delivery and its application for cancer therapy

September 2005 – August 2014

M.S. in Pharmacy (Department of Pharmacy)

Busan National University, Pusan, Korea

Advisor: Nam Deuk Kim, Ph. D., professor

Thesis Title: All trans-retinoic acid induced differentiation of rat mammary epithelial cells cultured in serum free media

March 1993 – February 1995

B.S. in Pharmacy (Department of Pharmacy)

Busan National University, Pusan, Korea

March 1989 – February 1993

Experience

Chief of DDS Research Lab.

Chong Kun Dang Research Institute, Chong Kun Dang Pharmaceutical Corp., Yongin-si, Gyeonggi-do, Korea

January 2003 – present

Visiting Scholar in College of Pharmacy

University of Utah, Salt Lake City, UT, USA

April 2001 – April 2002

Researcher of Pharmaceutical Technology Lab.

Chong Kun Dang Research Institute, Chong Kun Dang Pharmaceutical Corp., Cheonan-si, ChungNam, Korea

December 1994 – December 2002

Honors

New Excellent Technology Award by Ministry of Science and Technology, “New Polymeric Salt Technology for Anti-coagulant Drug as Drug-carrier” (August 2007)

International Publication (SCI, SCIE)

1. Ki MH, Kim JE, Lee YN, Noh SM, An SW, Cho HJ, Kim DD, Chitosan-Based Hybrid Nanocomplex for siRNA Delivery and Its Application for Cancer Therapy, Pharm Res. 2014 May 24. [Epub ahead of print]
2. Ki MH, Lim JL, Ko JY, Park SH, Kim JE, Cho HJ, Park ES, Kim DD, A new injectable liquid crystal system for one month delivery of leuprolide, J Control Release. 2014 Jul 10;185:62-70
3. Kim JE, Ki MH, Yoon IS, Cho HJ, Kim RS, Tae Kim G, Kim DD, Pharmacokinetic properties and bioequivalence of 2 formulations of valsartan 160-mg tablets: A randomized, single-dose, 2-period crossover study in healthy Korean male volunteers, Clin Ther. 2014 Feb 1;36(2):273-9
4. Park MR, Chun C, Ahn SW, Ki MH, Cho CS, Song SC, Sustained delivery of human growth hormone using a polyelectrolyte complex-loaded thermosensitive polyphosphazene hydrogel, J Control Release. 2010 Nov 1;147(3):359-67
5. Park MR, Chun C, Ahn SW, Ki MH, Cho CS, Song SC, Cationic and thermosensitive protamine conjugated gels for enhancing sustained human growth hormone delivery, Biomaterials. 2010 Feb;31(6):1349-59
6. Ki MH, Choi MH, Ahn KB, Kim BS, Im DS, Ahn SK, Shin HJ, The efficacy and safety of clopidogrel resinate as a novel polymeric salt form of clopidogrel, Arch Pharm Res. 2008 Feb;31(2):250-8
7. Kim JH, Lee SK, Ki MH, Choi WK, Ahn SK, Shin HJ, Hong CI, Development of parenteral formulation for a novel angiogenesis inhibitor, CKD-732 through complexation with hydroxypropyl-beta-cyclodextrin, Int J Pharm. 2004 Mar 19;272(1-2):79-89
8. Min Hyo Ki, Kee-Joo Paik, Ji Hyeon Lee, Hae Young Chung, Kyung Hee Lee, Kyu-Won Kim, Nam Deuk Kim, All-trans retinoic acid induced differentiation of rat mammary epithelial cells cultured in serum-free medium, Arch Pharm Res. 1998 Jun;21(3):298-304

References

Dae-Duk Kim, Ph. D.

Department of Pharmaceutics, College of Pharmacy, Seoul National University,

1 Gwanak-ro, Gwanak-gu, Seoul 151-742, Korea

Tel. +82-2-880-7870, Fax. +82-2-873-9177

E-mail: ddkim@snu.ac.kr

Chang-Koo Shim, Ph. D.

Department of Pharmaceutics, College of Pharmacy, Seoul National University,

1 Gwanak-ro, Gwanak-gu, Seoul 151-742, Korea

Tel. +82-2-880-7873, Fax. +82-2-888-5969

E-mail: shimck@sun.ac.kr

Suk-Jae Chung, Ph. D.

Department of Pharmaceutics, College of Pharmacy, Seoul National University,

1 Gwanak-ro, Gwanak-gu, Seoul 151-742, Korea

Tel. +82-2-880-7865, Fax. +82-2-885-8317

E-mail: sukjae@snu.ac.kr

Publications

Pharm Res
DOI 10.1007/s11095-014-1422-3

RESEARCH PAPER

Chitosan-Based Hybrid Nanocomplex for siRNA Delivery and Its Application for Cancer Therapy

Min-Hyo Ki • Ji-Eon Kim • Young-Nam Lee • Sang Myoung Noh • Sung-Won An • Hyun-Jong Cho • Dae-Duk Kim

Received: 28 February 2014 / Accepted: 12 May 2014

ABSTRACT

Purpose Chitosan, a natural and biocompatible cationic polymer, is an attractive carrier for small interfering RNA (siRNA) delivery. The purpose of this study was to develop a chitosan-based hybrid nanocomplex that exhibits enhanced physical stability in the bloodstream compared with conventional chitosan complexes. Hybrid nanocomplexes composed of chitosan, protamine, lecithin, and thiamine pyrophosphate were prepared for systemic delivery of survivin (SVN) siRNA.

Methods Physicochemical properties of the nanoparticles including mean diameters and zeta potentials were characterized, and target gene silencing and cellular uptake efficiencies of the siRNA nanocomplexes in prostate cancer cells (PC-3 cells) were measured. *In vivo* tumor targetability and anti-tumor efficacy by systemic administration were assessed in a PC-3 tumor xenograft mouse model by near-infrared fluorescence (NIRF) imaging and tumor growth monitoring, respectively.

Results Mean diameters of the SVN siRNA-loaded hybrid nanocomplex (GP-L-CT) were less than 200 nm with a positive zeta potential value in water and were maintained without aggregation in culture media and 50% fetal bovine serum. SVN expression in PC-3 cells was reduced to 21.9% after treating with GP-L-CT. The tumor targetability and growth inhibitory efficacies of GP-L-CT supported the use of this novel hybrid nanocomplex as a cancer therapeutic and as a theranostic system for systemic administration.

Conclusions A chitosan-based hybrid nanocomplex was successfully developed for the systemic delivery of SVN siRNA, which could serve as an alternative to cationic polymeric nanoparticles that are unstable in serum.

KEY WORDS chitosan · lecithin · nanocomplex · protamine · survivin siRNA · thiamine pyrophosphate

ABBREVIATIONS

Cryo-TEM	Cryo-transmission electron microscopy
EPR	Enhanced permeability and retention
NIRF	Near-infrared fluorescence
RNAi	RNA interference
SCID	Severe combined immunodeficiency
siRNA	Small interfering ribonucleic acid
TPP	Thiamine pyrophosphate

INTRODUCTION

Various preclinical and clinical studies have been tried for the development of small interfering RNA (siRNA) therapeutics based on RNA interference (RNAi) technology (1). These studies have indicated that overcoming low cellular permeability of nucleic acids, as well as low stability against serum proteins and degradative enzymes, are prerequisites for therapeutic applications (2, 3). One of ways to solve these difficulties is the development of highly efficient nucleic acid delivery systems, which protect siRNA from nucleases presented in the body fluids, improve low cellular membrane permeability, and ameliorate endosomolysis (4).

Many strategies have been developed using non-viral vehicles for the delivery of RNAi (5). The primary approach has

Electronic supplementary material The online version of this article (doi:10.1007/s11095-014-1422-3) contains supplementary material, which is available to authorized users.

M.-H. Ki • Y.-N. Lee • S. M. Noh • S.-W. An
Chong Kun Dang Research Institute, Chong Kun Dang Pharm.
Yongin 446-916, Republic of Korea

H.-J. Cho
College of Pharmacy, Kangwon National University
Chuncheon 200-701, Republic of Korea

M.-H. Ki • J.-E. Kim • D.-D. Kim (✉)
College of Pharmacy and Research Institute of Pharmaceutical Sciences
Seoul National University, Seoul 151-742, Republic of Korea
e-mail: ddkim@snu.ac.kr

Published online: 24 May 2014

been the addition of cationic and lipophilic properties that overcome the limited cellular permeability of anionic and hydrophilic nucleic acids. Among these approaches, nucleic acid delivery systems based on cationic polymers and lipids has gained attention (6). Typical cationic polymers could be classified into synthetic polymers (i.e., polyethyleneimine, poly-L-lysine, poly-L-arginine) and natural polymers (i.e., chitosan) (7, 8). Chitosan has been widely used in the development of nucleic acid delivery systems due to its low cytotoxicity, high biocompatibility, and high cellular permeability (9). Its nucleic acid binding and delivery capacity can be influenced by its molecular weight and the degree of deacetylation (10, 11). Moreover, chitosan conjugated with a cationic polymer, peptide, and hydrophobic residue exhibits improved gene transfection efficiency (12–15), while the introduction of polyethylene glycol can increase chitosan hydrophilicity and stability in biological fluids (16).

However, clinical application and commercialization of synthetic chitosan conjugates could be hampered by toxicity of the delivery vehicle. Thus, a non-modified (i.e., natural) chitosan-based gene delivery system would be preferable if gene transfection efficiency could be maintained. Nevertheless, there are also some obstacles in using natural chitosan for siRNA delivery. Conventional siRNA delivery of cationic nanoparticles using chitosan can induce protein binding and aggregation in the bloodstream, resulting in peripheral vascular thrombosis and hemolysis as the surface charge increases (17–19). These phenomena in nanoparticle formulations can also influence the delivery accuracy and efficiency of therapeutics (20). Because of these reasons, few studies have described the intravenous administration of siRNA/chitosan nanoparticles until now (10, 21). In addition, even though chitosan may exhibit high binding affinity with siRNA due to its cationic charge density in acidic pH, the siRNA/chitosan complex tends to be physically unstable in neutral and basic pH conditions (22). These problems need to be solved through the optimal design of a stable chitosan-based nanocomplex in physiological conditions for successful siRNA delivery using natural chitosan.

Survivin (SVN) is an inhibitor of apoptosis and is thought to be a promising target for cancer therapy. It is minimally expressed in normal tissues and up-regulated in many cancers, including prostate cancer (23). Thus, SVN could be a good target protein for siRNA nanocomplex studies. In addition, several studies have shown that protamine, which binds to nucleic acids to form a stable nanocomplex via ionic and hydrophobic interactions, could be used for pre-complex preparation in the development of a nucleic acid nanocomplex (24–26). Herein, we thus prepared pre-complex with siRNA and protamine, which has a negative net charge for subsequent binding with cationic chitosan, by combining a limited amount of protamine. Phospholipid was then introduced into the siRNA/protamine pre-complex for the enhancement of nanocomplex stability in the bloodstream because protamine is known to have a binding affinity for the lipophilic moiety in a phospholipid (27, 28). In order to enhance the transfection efficiency of siRNA through the addition of a positive surface charge on this complex, chitosan was added together with thiamine pyrophosphate (TPP). TPP, combined with chitosan, is known to maintain the delivery efficiency of the siRNA/chitosan complex in neutral physiological pH, because the positively charged amine group of thiazolium in TPP stabilizes the complex regardless of the pH conditions (29). Following preparation of the nanoparticle complex, the physicochemical properties and siRNA delivery efficiency were assessed *in vitro* and *in vivo*.

MATERIALS AND METHODS

Materials

siRNA for SVN, luciferase, and Cy5.5-SVN (Cy5.5-siRNA) were provided by Bioneer Co. (Daejeon, Korea). Their sequences were as follows: SVN siRNA [sense: 5'-AAGGAG AUCAACAUUUUCA (dTdT)-3', anti-sense: 5'-UGAAAA UGUUGAUCUCCUU (dTdT)-3'], luciferase siRNA [sense: 5'-UUGUUUUGGAGCACGGAAA (dTdT)-3', anti-sense: 5'-UUUCCGUGCUCCAAAACAA (dTdT)-3']. Chitosan acetate and chitosan hydrochloride (HCl) were purchased from Heppe Medical Chitosan (Halle, Germany) and FMC BioPolymer (Philadelphia, PA, USA), respectively. BLOCK-iT fluorescent oligo and Lipofectamine 2000 (L2K) were obtained from Invitrogen (Carlsbad, CA, USA), and GelRed was acquired from Biotium, Inc. (Hayward, CA, USA). Lecithin, protamine, and TPP were purchased from Alps Pharmaceutical (Hida, Japan), Lipoid (Ludwigshafen, Germany), and Sigma-Aldrich (St. Louis, MO, USA), respectively. A human SVN Quantikine ELISA kit was obtained from R&D Systems (Minneapolis, MN, USA), and Matrigel was acquired from BD Biosciences (Bedford, MA, USA). Fetal bovine serum (FBS), penicillin, streptomycin, RPMI 1640 (developed at Roswell Park Memorial Institute), phosphate-buffered saline (PBS), Tris-borate-EDTA, and trypsin-EDTA were obtained from Gibco Life Technologies, Inc. (Grand Island, NY, USA). All other chemicals were of analytical grade.

Preparation of Hybrid Nanocomplex

Hybrid nanocomplexes were prepared by the combination of SVN siRNA, protamine, lecithin, chitosan, and TPP. Briefly, 10 mg of siRNA, 0.5 mg of protamine sulfate, 4 mg of chitosan HCl (150–400 kDa, FMC CL214, FMC BioPolymer, Philadelphia, PA, USA), and 20 mg of TPP were each solubilized

in 1 mL of diethylpyrocarbonate-treated distilled water (DW) and individually filtered. For lecithin (Lipoid S-100), 30 mg were dissolved in 1 mL of ethanol and filtered. The pre-complex was prepared by mixing and stirring SVN siRNA and protamine solutions. A lecithin solution was added into the pre-complex solution and stirred for 30 min. The final formulation, GP-L-CT, was prepared by adding chitosan and TPP solutions into the mixture. All components in the formulation were added and mixed according to weight ratios of the compositions. Other complexes were also prepared according to the manufacturing order of GP-L-CT. For siRNA/L2K complex as the control, a mixture of SVN siRNA (100 μg) and L2K (300 μL) was prepared and incubated for 20 min before use.

Particle Size and Zeta Potential Measurements

The mean diameter and zeta potential values of the developed complexes were measured by a light-scattering spectrophotometer (ELS-Z, Otsuka Electronics, Tokyo, Japan), according to the manufacturer's protocol. Complexes corresponding to 20 μg of siRNA were dispersed in DW (0.5 mL) for analysis. The stability of complexes was assessed in cell culture medium (RPMI 1640) and 50% (v/v) FBS. FBS was used after removing the flocculence (centrifugation at 400*g* and 0.2 μm filtration) according to the user's guide. Similarly, complexes corresponding to 20 μg of siRNA were diluted in 0.5 mL of cell culture medium and 50% FBS. After incubation for 3 h, the mean diameter and zeta potential values were measured by the ELS-Z system.

Cryo-Transmission Electron Microscopy (Cryo-TEM)

The morphology of the developed complexes was observed by cryo-TEM (Tecnai G2 F20 Cryo-TEM, FEI Company, Hillsboro, Oregon, USA) (30). The specimen was applied to holey carbon affixed to the grid (Quantifoil Micro Tools GmbH, Jena, Germany) and rapidly cooled to−170°C. It was fixed in the cryo-holder and inserted into the cryo-TEM at−170°C. Images were recorded under low electron dose conditions.

Gel Retardation Assays

Each sample was separated in a 2.5% agarose gel that included 0.001% GelRed in a Tris-borate-EDTA buffer at 50 V for 15 min. After electrophoresis, complex formation was evaluated by scanning with MiniBIS Pro (DNR Bio-imaging Systems, USA).

Quantification of Non-loaded Free siRNA

Non-loaded free SVN siRNA was assayed by high performance liquid chromatography (HPLC) after ultracentrifugation, to estimate loading amount of siRNA. Free SVN siRNA was separated from nanocomplexes by ultracentrifugation at 100,000*g* for 60 min at 15°C using Optimal-100XP ultracentrifuge (Beckman Coulter, Brea, CA, USA) (31). The free siRNA in the obtained supernatant was assayed using Waters Alliance 2695 HPLC system (Waters, Milford, MA, USA) and the Xterra® C18 column (5 μm, 4.6×150 mm, Waters, Milford, MA, USA). The mobile phase consisted of 100 mM triethylammonium acetate with pH 7.0 in water (MP-A) and acetonitrile (MP-B), and the flow rate was 0.5 mL/min. The gradient elution programs of the mobile phases were as follows: 93–90% MP-A; 7–10% MP-B, 0.0–30.0 min; 90–50% MP-A; 10–50% MP-B, 30.0–35.0 min; 50–20% MP-A; 50–80% MP-B, 35.0–40.0 min; 20–93% MP-A; 80–7%, 40.0–40.1 min; and 93% MP-A; 7% MP-B, 40.1–60 min. The samples were prepared by diluting 0.1 mL of the supernatant with 0.9 mL of MP-A. The standard were prepared by dissolving SVN siRNA to 30 μg/mL with MP-A. The sample or standard (10 μL each) was injected and detected by UV at a wavelength of 260 nm. The good linearity in a calibration curve of HPLC analysis was obtained at the concentration ranges of 1.0–100.0 μg/mL for anti-sense siRNA strands as demonstrated by the high correlation coefficient (R2) value of above 0.99 (Fig. S1).

In Vitro Transfection Study

For the *in vitro* transfection study, gene-silencing efficiency was evaluated in a human prostate cancer cell, PC-3, purchased from the Korea Cell Line Bank (KCLB; Seoul, Korea). Cells were cultured with RPMI 1640 containing 10% FBS, 100 U/mL penicillin, and 100 μg/mL streptomycin in a 5% CO_2 atmosphere with 95% relative humidity at 37°C. To evaluate gene-silencing efficiency, SVN expression (%) was measured by a human SVN Quantikine ELISA kit. In brief, PC-3 cells were seeded into a 6-well plate at a density of 1×10^5 cells/well and cultured for 48 h. Before loading the samples with SVN siRNA or luciferase siRNA as control, cells were stabilized for 2 h with fresh culture media. PC-3 cells were incubated with complexes corresponding to 2 μg of siRNA/well for 48 h in a 5% CO_2 atmosphere with 95% relative humidity at 37°C. Cells were lysed with the addition of 500 μL of cell lysis buffer (Cell Signaling Technology, Inc., Danvers, MA, USA) and collected. Cell lysates were centrifuged at 12,000 rpm for 20 min and 100 μL of the supernatant was used for the subsequent assay. Assay diluent (100 μL) and collected supernatant (100 μL) were mixed and stirred at 500 rpm for 2 h. Upon washing four times, the SVN conjugate (200 μL) was added and stirred for 2 h at room temperature. After washing additional four times, the substrate solution (200 μL) was added and incubated for 30 min in the dark. The reaction was terminated with the addition of stop solution (50 μL), and the absorbance at 450 nm was read by a SpectraMax M2

microplate reader (Molecular Devices, Sunnyvale, CA, USA). The amount (%) of SVN was calculated by substituting absorbance values into the regression line obtained from a standard solution. SVN expression rate was measured, regarding that of the untreated group as 100%. Gene-silencing efficiency was calculated according to following formula: efficiency = (1 − SVN expression rate in test group/SVN expression rate in control group) × 100.

In Vitro Cellular Uptake

Cellular uptake efficiency of siRNA was assessed by flow cytometry analysis (12). PC-3 cells were seeded onto 6-well plates at a density of 1×10^5 cells/well and incubated for 48 h in a 5% CO_2 atmosphere with 95% relative humidity at 37°C. All formulations were prepared using BLOCK-iT fluorescent oligo instead of SVN siRNA, as described above. PC-3 cells were incubated with naked siRNA (Naked) or complexes corresponding to 2 μg of BLOCK-iT fluorescent oligo/well for 24 h in a 5% CO_2 atmosphere with 95% relative humidity at 37°C. After incubating, cells were washed with PBS three times, and the fluorescence and optical photographs of cells were taken with the inverted microscope (Inverted Research Microscope ECLIPSE Ti, Nikon, Tokyo, Japan). Cells were collected by treatment with 0.25% trypsin-EDTA, and analyzed by flow cytometry (BD FACS Canto II; Becton-Dickinson, San Jose, CA, USA).

In Vivo Near-Infrared Fluorescence (NIRF) Imaging

The biodistribution of the complexes by systemic administration was assessed in a PC-3 tumor xenograft mouse model. Briefly, 2×10^6 PC-3 cells suspended in 50 μL of cell culture media with 50 μL of Matrigel were injected subcutaneously into 5-week-old male severe combined immunodeficiency (SCID) mice (Shizuoka Laboratory Animal Center, Hamamatsu, Japan). After attaining a tumor volume of 100 mm^3, complexes were injected intravenously via the tail vein at a dose of 80 μg siRNA (about 266 μL) per mouse. For NIRF imaging, Cy5.5-siRNA-loaded formulations were prepared using Cy5.5-siRNA instead of SVN siRNA, according to the method described above. NIRF images of the tumor region were obtained by the eXplore Optix system (Advanced Research Technologies-GE healthcare, St. Laurent, Quebec, Canada) at 2 and 5 h post-injection (32). Laser power and count time settings were 25 μW and 0.3 s per point, respectively. To excite the Cy5.5 molecules in the complexes, a laser diode at 670 nm was used.

In Vivo Anti-Tumor Efficacy

The PC-3 tumor xenograft mouse model was used to assess siRNA delivery efficiency of complexes of test or control groups. As described previously, 2×10^6 PC-3 cells suspended in 50 μL of cell culture media with 50 μL of Matrigel (BD Biosciences, Bedford, MA, USA) were injected subcutaneously into the 5-week-old male SCID mice. Luciferase siRNA was used as a irrelevant siRNA, and the preparation method of luciferase siRNA-loaded GP-L-CT was identical to that of SVN siRNA. After reaching a tumor volume of 100 mm^3, complexes corresponding to 40 μg siRNA (about 133 μL) per mouse were injected intravenously *via* the tail vein six times for 2 weeks. Tumor size was measured with Vernier calipers, and tumor volume and tumor inhibition rate (%) were calculated according to the following formula: $V = 0.5 \times \text{longest diameter} \times \text{shortest diameter}^2$; growth inhibition rate (%) = $[1 - (V_f - V_0 \text{ in test group})/(V_f - V_0 \text{ in control group})] \times 100$, where V_0 and V_f are the tumor volume at the initial day and final day tested, respectively.

Statistical Analysis

All experiments were conducted at least three times, and data are represented as means ± standard deviation (SD). Statistical analysis was based on analysis of variance (ANOVA).

RESULTS AND DISCUSSION

Determination of Nanocomplex Composition

To produce stable nanocomplexes without aggregation under physiological conditions *in vitro* and *in vivo*, optimal composition of the siRNA hybrid nanocomplexes was determined at each step in the preparation. All complex formulations were prepared according to the compositions presented in Table I. Protamine was introduced to form SVN siRNA/protamine pre-complexes and then chitosan + TPP was added to produce the SVN siRNA/chitosan/TPP complexes.

For the siRNA pre-complex formation, several weight ratios of siRNA and protamine were tested, ranging from 1:0.4 to 1:1 (w/w) (Table I). The pre-complexes with 1:0.4, 1:0.6, and 1:1 ratios had mean diameters of 261.9, 192.3, and 225.8 nm in DW, respectively, while the complex with a 1:0.8 ratio resulted in severe aggregation without measurable diameter and zeta potential values (Fig. 1a). Although it is not clear why aggregation was observed, a similar case was reported previously (33). The complexes with 1:0.4 and 1:0.6 ratios had negative surface charges according to zeta potential values and the complex with 1:1 converted to a positive surface charge. Thus, the amount of protamine in the pre-complex should be restricted to maintain the negative surface charge for the next step, which requires the addition of chitosan as a cationic polymer. The pre-complex with a 1:0.6 weight ratio

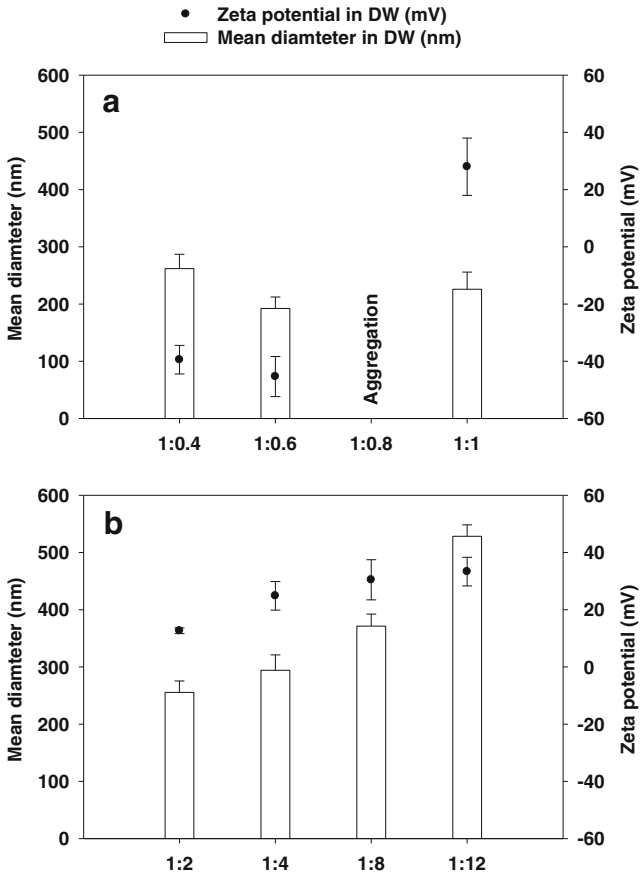

Fig. 1 Mean diameter and zeta potential values of siRNA/protamine pre-complexes and siRNA/chitosan/TPP complexes. (**a**) SVN siRNA/protamine pre-complexes with various siRNA:protamine ratios. (**b**) SVN siRNA/chitosan/TPP complexes with various siRNA:chitosan + TPP ratios. Chitosan + TPP was prepared at a ratio of 85/15 (w/w, %). Each value represents the mean ± SD ($n = 3$).

was selected for siRNA pre-complex formation because it showed the smallest diameter and a negative surface charge.

The mixture of chitosan and TPP (85:15, w/w) was used for complex formation with siRNA to complement the weak binding affinity of chitosan with siRNA in neutral physiological pH conditions (29). Several weight ratios of siRNA and chitosan + TPP were tested, ranging from 1:2 to 1:12 (w/w) corresponding to 3.5 to 21.1 of N/P (chitosan/siRNA) ratio (Table I). All siRNA/chitosan/TPP complexes had positive surface charges, reaching a plateau at a 1:8 ratio and showed larger mean diameters with increased amounts of chitosan + TPP (Fig. 1b). The complex of siRNA and chitosan + TPP with a 1:8 ratio was considered to be the optimal combination for efficient siRNA delivery because they had a high zeta potential value and relatively small mean diameter.

Based on these results, the siRNA pre-complex with siRNA and protamine (1:0.8, w/w) was subsequently complexed with chitosan + TPP at the 1:8 ratio of siRNA and chitosan + TPP. However, this resulted in a bulky complex with a mean diameter >600 nm. To ameliorate this phenomenon, lecithin was incorporated between the protamine pre-complex and chitosan complex steps, since protamine has a nanocomplex-stabilizing effect when it binds to the lipophilic moiety in a phospholipid (27, 28). The optimal lecithin amount was determined by comparing the mean diameters of the final nanocomplexes in DW, as well as in cell culture media and in 50% FBS. Lecithin was incorporated in ratios ranging from 1:5 to 1:15 (w/w) of siRNA and lecithin (Table II). The 1:10 ratio of siRNA and lecithin showed the smallest mean diameter nanocomplex compared with the 1:5 and 1:15 ratios in various media including serum conditions (Fig. 2). The mean diameter of the 1:10 ratio was 189, 129, and 181 nm in DW, culture media, and 50% FBS, respectively. However, that of the 1:15 ratio was 312, 340, and 404 nm, respectively, while that of the 1:5 ratio was >500 nm in DW and even larger in culture media and 50% FBS due to the aggregation. Therefore, we concluded that lecithin should be incorporated at no less than 10-fold the weight of the siRNA to stabilize the nanocomplex in culture media and 50% FBS. However, lecithin at a ratio >1:15 induced reversible bulky or loosened complexes that resulted in a slightly increased mean diameter. Therefore, the nanocomplex with the 1:10 ratio of siRNA and lecithin (GP-L-CT) was used as the final formulation and compared with comparative example formulations (Table III and Fig. 3) in further studies.

Before determination of the component compositions of the nanocomplex, the proper chitosan for siRNA delivery had been selected. Chitosan is a natural cationic polymer, which exists in a variety of molecular weights (MWs), salt types and deacetylation degrees. In our preliminary study, four chitosans with MWs of 50–400 kDa and 83–95% deacetylation degrees were tested (Table SI). The influences of chitosan MW and deacetylation on complex formation with SVN siRNA were investigated by gel retardation assay, as reported in the literature (34). Based on this result, chitosan D (chitosan HCl with a MW of 150–400 kDa and 95% deacetylation) exhibited higher siRNA-binding capability (Fig. S2) and resulted in lower SVN expression indicative of siRNA transfection efficiency, compared to other chitosans (Fig. S3). Therefore, chitosan D was selected and used for preparation of the chitosan-based complexes in the experiments.

Characterization of siRNA-Loaded Hybrid Nanocomplexes

The GP-L-CT nanocomplex (GP-L-CT) was prepared as described in Fig. 3 and the composition presented in Table III. The GP pre-complex (GP) was produced by mixing siRNA and protamine and the GP-L complex (GP-L) was produced by incorporating lecithin into GP. The final GP-L-CT was prepared by coating chitosan and TPP onto GP-L based on their electrostatic interaction. The morphology of GP, GP-L, and GP-L-CT was observed by cryo-TEM at each

Table I Composition of SVN siRNA/Protamine Pre-complexes and SVN siRNA/Chitosan/TPP Complexes

Components	siRNA:protamine (w/w)				siRNA:(chitosan + TPP) (w/w)			
	1:0.4	1:0.6	1:0.8	1:1	1:2	1:4	1:8	1:12
SVN siRNA	1	1	1	1	1	1	1	1
Protamine	0.4	0.6	0.8	1	-	-	-	-
Chitosan + TPP[a]	-	-	-	-	2	4	8	12

[a] Chitosan + TPP was prepared at a ratio of 85/15 (w/w, %).

All values are presented as weight ratios.

preparation step for the chitosan-based hybrid nanocomplex. As shown in Fig. 3a, GP had a reticular texture with a loosely disentangled particular shape. GP-L exhibited a partial reticular structure but showed a fused shape with a spherical liposome (Fig. 3b). In the case of GP-L-CT, the reticular texture completely disappeared and an opaque spot, characteristic of polymeric nanocomplexes, was presented (Fig. 3c). The cryo-TEM images demonstrated that the formation of tightly compacted nanocomplexes should be completed by complexing with cationic substances, chitosan and TPP, although the complexes could be stabilized by pre-complexing with protamine or lecithin incorporation processes. Other complex formulations were prepared for comparison with GP, GP-L, and GP-L-CT (Table III). As comparative examples, a G-C complex (G-C) was prepared by mixing siRNA and chitosan and a G-CT complex (G-CT) was made by mixing siRNA, chitosan and TPP. GP-CT complex (GP-CT) was produced using the same preparation method as GP-L-CT without lecithin incorporation.

The mean diameter and zeta potential values of the developed nanocomplexes in DW were measured and stability of the nanocomplexes was evaluated as the change in mean diameter in cell culture media and 50% FBS (Fig. 4). The mean diameters of GP, GP-L, and GP-L-CT in DW were 177, 133, and 189 nm, while those of G-C, G-CT, GP-CT as comparative examples were 377, 371, and 604 nm, respectively (Fig. 4a). Although FBS contained background signal of around 25 nm mean diameter (data not shown), the size measurement of nanocomplexes does not seem to be influenced by those smaller nanoparticles. Zeta potential values of GP and GP-L were negative due to the absence of the cationic substances, chitosan and TPP. In contrast, zeta potential values of GP-L-CT, G-C, G-CT, and GP-CT were positive due to the inclusion of chitosan, which is necessary for interaction with the negatively charged cellular membrane. Lecithin incorporation reduced the positive charge, seen when comparing the zeta potential value of GP-L-CT with that of GP-CT, due to lecithin itself having a slight negative charge. When the complexes were exposed to cell culture media and 50% FBS for 3 h, the complexes showed extremely different

Table II Composition of Chitosan-Based Hybrid Complexes with Lecithin Incorporation

Components	siRNA:lecithin (w/w)		
	1:5	1:10	1:15
SVN siRNA	1	1	1
Protamine	0.6	0.6	0.6
Lecithin	5	10	15
Chitosan	6.8	6.8	6.8
TPP	1.2	1.2	1.2

All values are presented as weight ratios.

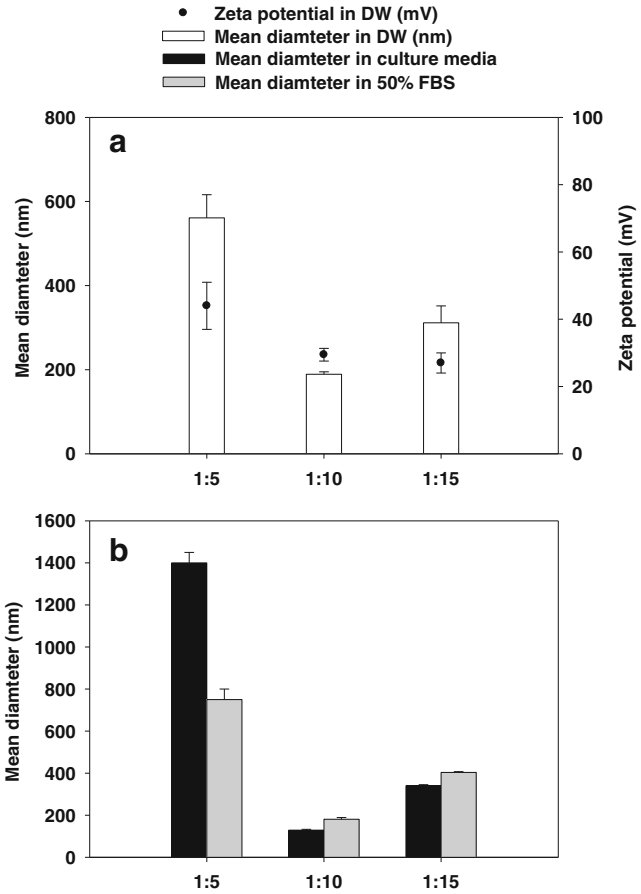

Fig. 2 Mean diameter and zeta potential values of chitosan-based complexes with various siRNA:lecithin ratios. (**a**) Mean diameters and zeta potentials of chitosan-based complexes with lecithin incorporation in DW. (**b**) Mean diameters of chitosan-based complexes with lecithin incorporation in culture media and 50% FBS. Each value represents the mean ± SD ($n = 3$).

Table III Compositions of SVN siRNA-Loaded Nanocomplexes and Comparative Examples

Components	GP	GP-L	GP-L-CT	G-C [a]	G-CT [a]	GP-CT [a]
SVN siRNA	1	1	1	1	1	1
Protamine	0.6	0.6	0.6	-	-	0.6
Lecithin	-	8	8	-	-	-
Chitosan	-	-	6.8	6.8	6.8	6.8
TPP	-	-	1.2	-	1.2	1.2

[a] G-C, G-CT, and GP-CT were prepared as comparative examples of GP-L-CT.

All values are presented as weight ratios.

changes in mean diameters. The mean diameters of GP, GP-L, and GP-L-CT were 25, 110, and 129 nm in culture media, and 33, 94, and 181 nm in 50% FBS, respectively (Fig. 4b). The mean diameters of G-C, G-CT, and GP-CT increased to >1,400 nm in culture media, and >1,000 nm in 50% FBS. The mean diameter of GP in culture media and 50% FBS was 20% smaller than that in DW and finally overlapped with the background signal of FBS (<30 nm), possibly due to dissociation of the complex. GP-L and GP-L-CT had a stable mean diameter, although it decreased slightly in culture media. In contrast, the mean diameters of G-C, G-CT, and GP-CT, which are conventional chitosan complexes that did not include protamine or lecithin, increased significantly with the precipitation of large particles in culture media and 50% FBS. GP-L-CT was more stable in the serum because of the formation of the liposomal complex (35, 36) as well as the reduction of the zeta potential (29.5 mV), compared to those of G-C, G-CT, and GP-CT (74.9–77.1 mV). Because the serum content in 50% FBS is similar to that in whole blood, G-C, G-CT, and GP-CT can form the aggregation *in vivo* that can result in the decrease of siRNA delivery efficiency and peripheral vascular thrombosis via intravenous injection.

When the influences of compositions on complex formation with SVN siRNA were investigated by gel retardation assay, GP-L-CT, G-C, G-CT, and GP-CT exhibited higher binding capabilities compared to GP and GP-L (Fig. 4c). It was supported by assay of non-loaded free siRNA using HPLC, in which GP and GP-L showed 31.7 ± 5.1 and 20.9 ± 2.9% of free siRNA, respectively, while other complexes had no detectable amount of free siRNA. To prepare a chitosan-based hybrid nanocomplex that can be systemically administered, GP-L-CT were evaluated with GP and GP-L as intermediate steps of GP-L-CT in further studies, excluding comparative examples such as G-C, G-CT, and GP-CT, which are physically unstable under physiological conditions.

In Vitro Gene Silencing and Cellular Uptake

In vitro gene silencing efficiency of the developed complexes was assessed by measuring SVN expression in PC-3 cells after incubating with SVN siRNA or luciferase siRNA as control for 48 h (Fig. 5). SVN expression rates were reduced to 7.0 and 21.9% by treatment with L2K and GP-L-CT containing SVN siRNA, while those were 68.5 and 105.5% with L2K and GP-L-CT containing luciferase siRNA, respectively. Thus, the gene silencing efficiencies of L2K and GP-L-CT were calculated as 89.8 and 79.2%, respectively. The high efficiencies were also supported by the siRNA-binding capacity of L2K and GP-L-CT exhibited in gel retardation assay (Fig. S4). Although L2K treatment resulted in higher gene silencing efficiency, its systemic application *in vivo* has been

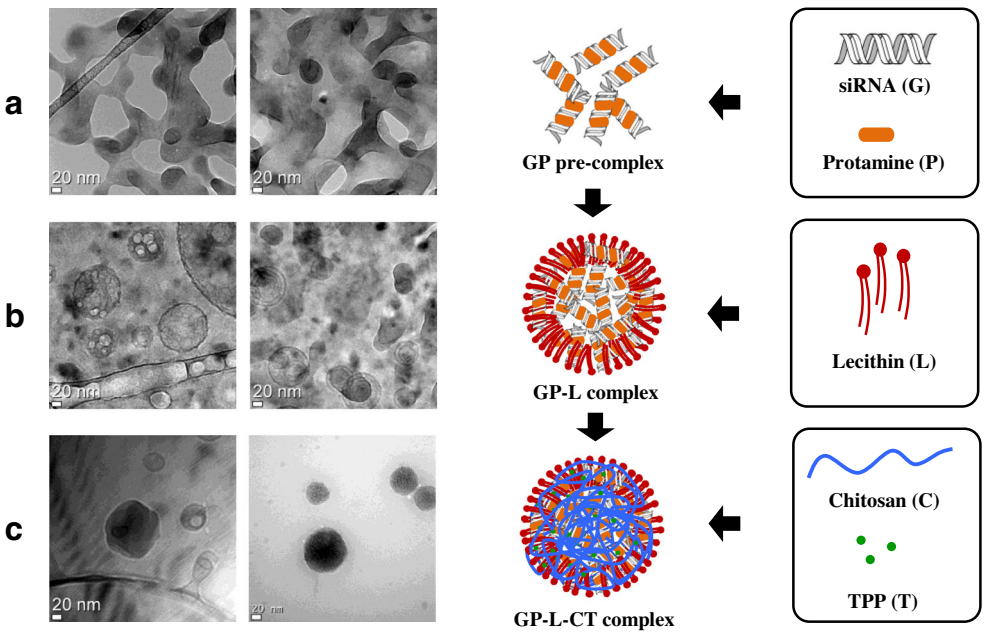

Fig. 3 Morphology of nanocomplex formulations observed by cryo-transmission electron microscopy (cryo-TEM) and schematic illustration of GP-L-CT hybrid nanocomplex preparation. Images of (**a**) siRNA/protamine pre-complex (GP), (**b**) siRNA/protamine/lecithin complex (GP-L), (**c**) siRNA/protamine/lecithin/chitosan/TPP complex (GP-L-CT) are presented. Scale bar = 20 nm.

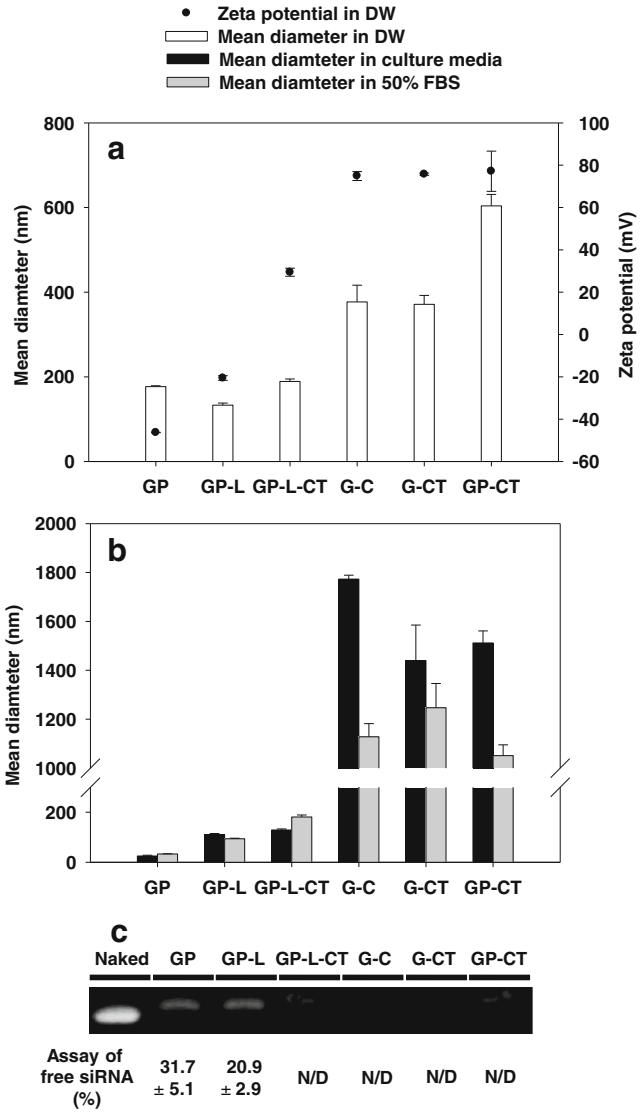

Fig. 4 Characterization of nanocomplex formulations by measurement of diameter and zeta potential values of complexes using a light-scattering spectrophotometer, gel retardation assay, and quantification of non-loaded free siRNA. The siRNA/protamine/lecithin/chitosan/TPP hybrid complex (GP-L-CT) was prepared through an intermediate step that included the siRNA/protamine pre-complex (GP) and siRNA/protamine/lecithin complex (GP-L). The siRNA/chitosan complex (G-C), siRNA/chitosan/TPP complex (G-CT), and siRNA/protamine/chitosan/TPP complex (GP-CT) were prepared as comparative examples of GP-L-CT. (**a**) Mean diameters and zeta potentials of chitosan-based nanocomplexes in DW are presented. (**b**) Mean diameters of chitosan-based nanocomplexes in culture media and 50% FBS are presented. (**c**) The gel retardation results by electrophoresis in 2.5% agarose gel and the quantified ratios of non-loaded free siRNA from complexes are presented. Each value represents the mean ± SD ($n = 3$).

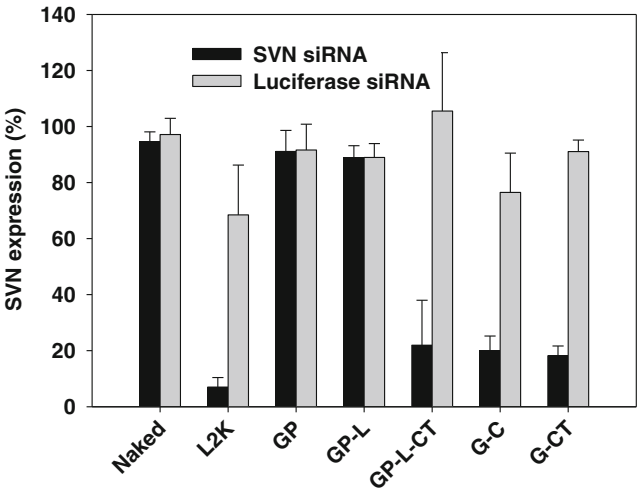

Fig. 5 *In vitro* transfection efficiency of SVN siRNA and luciferase siRNA-loaded complexes in PC-3 cells. SVN expression levels (%) following a 48-h transfection with naked siRNA (Naked), siRNA/Lipofectamine 2000 complex (L2K), siRNA/protamine pre-complex (GP), siRNA/protamine/lecithin complex (GP-L), siRNA/protamine/lecithin/chitosan/TPP complex (GP-L-CT), siRNA/chitosan complex (G-C) and siRNA/chitosan/TPP complex (G-CT)-incubated groups are presented. Each value represents the mean ± SD ($n = 3$).

restricted generally due to toxicity, which was implied by the decreased SVN expression rate in the control group (68.5%), as well as its low efficacy *in vivo* compared to *in vitro*. In the transfection study of conventional chitosan nanocomplexes, the gene silencing efficiencies of G-C and G-CT were 73.9% and 80.0%, respectively (Fig. 5), which means the efficiency of GP-L-CT was not reduced in spite of the composition of nanocomplex-stabilizing components, lecithin and protamine. In Naked, GP, and GP-L complexes that do not have cationic charges, SVN expression rates were not silenced at all, which indicates that complexes lacking a cationic moiety (i.e., chitosan and TPP) could not efficiently induce gene silencing. The control groups for Naked, GP, GP-L, and GP-L-CT complexes showed negligible cytotoxicity, which was supported by >90% SVN expression. Consequently, GP-L-CT was the most effective nanocomplex which induced *in vitro* gene silencing efficiency with SVN siRNA and did not decrease SVN expression rate with control siRNA indicating its low cytotoxicity.

Cellular uptake efficiency of developed complexes in PC-3 cells was evaluated by flow cytometry using complexes that included fluorescent siRNA (Fig. 6). The mean population percentages in P1 regions of L2K and GP-L-CT were 40.0 and 83.9%, respectively. A greater population shift into the P1 region is observed when more fluorescent siRNA is delivered into the cells through nanocomplexes. The mean population percentages in P1 regions of Naked, GP, and GP-L were 2.0, 3.3, and 2.8%, respectively, which indicates that the cells do not take up complexes without a cationic charge. Mean florescence intensity in Fig. 6 highly increased with GP-L-CT among the test groups, indicative of increased cellular uptake efficiency, which was also observed in dot plots by flow cytometry (Fig. S5). When the fluorescence and optical microscope images of cells on the well plate were taken after cellular uptake study, L2K and GP-L-CT showed fluorescent cell images by cellular uptake, while the Naked did not have fluorescence intensity (Fig. S6).

Based on a mean diameter <200 nm in serum and efficient gene silencing and cellular uptake, GP-L-CT was considered to

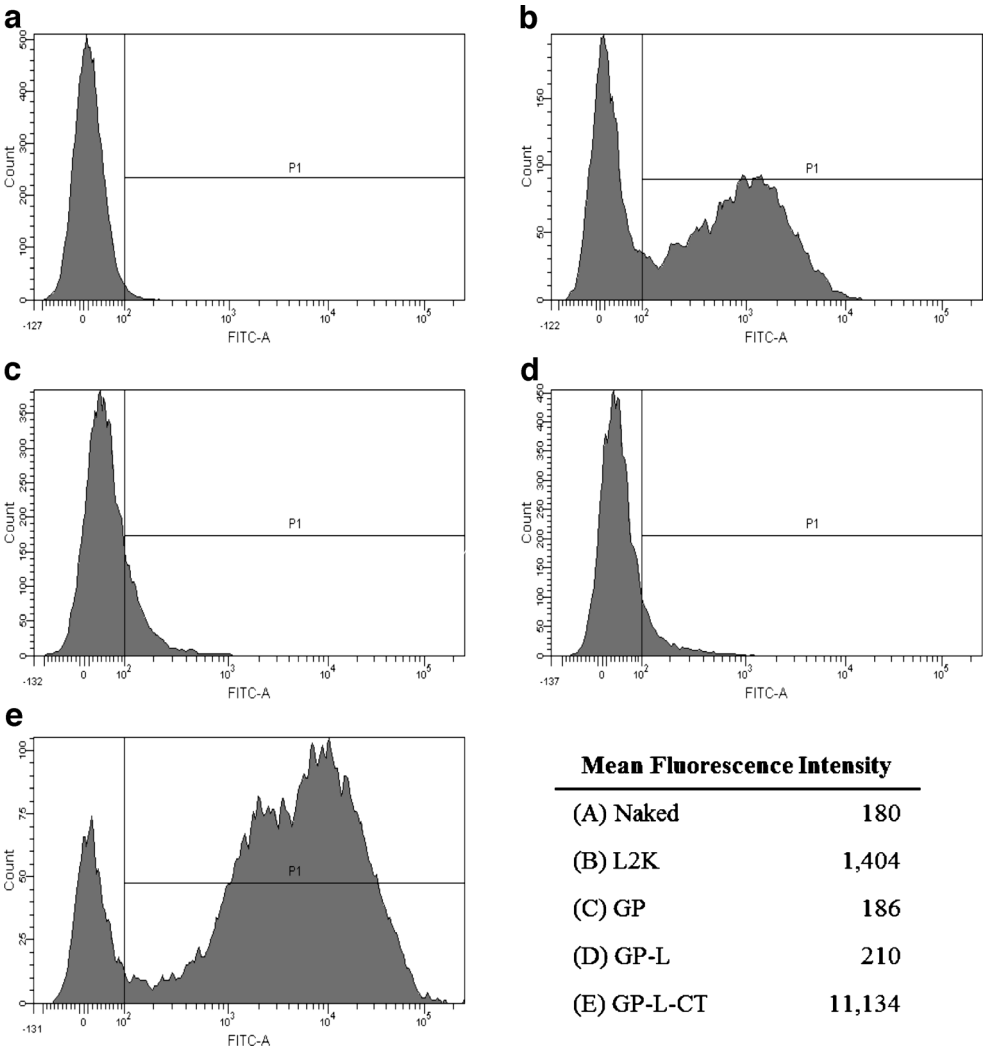

Mean Fluorescence Intensity	
(A) Naked	180
(B) L2K	1,404
(C) GP	186
(D) GP-L	210
(E) GP-L-CT	11,134

Fig. 6 *In vitro* cellular uptake efficiency of the nanocomplexes in PC-3 cells. Fluorescent siRNA was loaded into various nanocomplex formulations and fluorescence intensity measured by flow cytometry after incubating for 24 h. Plots are presented of cell count and fluorescence intensity from (**a**) naked siRNA (Naked), (**b**) siRNA/Lipofectamine 2000 (L2K), (**c**) siRNA/protamine (GP), (**d**) siRNA/protamine/lecithin (GP-L), and (**e**) siRNA/protamine/lecithin/chitosan/TPP (GP-L-CT).

be the most appropriate nanocomplex for the systemic delivery of SVN siRNA for cancer therapy. Stability of the siRNA nanocomplex in serum was ensured only in the hybrid nanocomplex, GP-L-CT, by pre-complexing with protamine (24–26) and incorporation of lecithin. Moreover, gene silencing and cellular uptake efficiencies were highly induced by complexing with chitosan and TPP (29), without interference of stabilizing components, protamine and lecithin, used in intermediate steps of the hybid nanocomplex preparation. Therefore, GP-L-CT was selected and evaluated as the final formulation in *in vivo* studies.

In Vivo NIRF Imaging and Anti-Tumor Efficacy

Tumor targetability of Cy5.5-siRNA-loaded GP-L-CT was investigated by *in vivo* NIRF imaging in a PC-3 tumor xenograft mouse model. Fluorescence intensity in the tumor region was scanned 2 and 5 h after intravenous injection, according to the previous study (32). As shown in Fig. 7, fluorescence intensity in the tumor region of Cy5.5-siRNA-loaded GP-L-CT was the highest of the experimental groups. Fluorescence intensities of the naked Cy5.5-siRNA and Cy5.5-siRNA loaded L2K were lower than that of GP-L-CT, suggesting that naked siRNA and L2K were inappropriate for systemic administration due to their low stability and delivery effect in biological fluids. Normal vasculature has a packed structure with a pore size <10 nm, however, neovasculature in the tumor region has an abnormally aligned endothelium with wide fenestrations with a pore size of 100–700 nm and defective lymphatic drainage (37). As a result, *in vivo* stabilized and circulating nano-sized drug delivery systems can easily permeate and accumulate in the tumor region. This phenomenon is known as the enhanced permeability and retention (EPR) effect, which explains the *in vivo* stability and tumor targetability of GP-L-CT. The EPR effect observed in Cy5.5-siRNA loaded GP-L-CT demonstrated that GP-L-CT was circulated in the

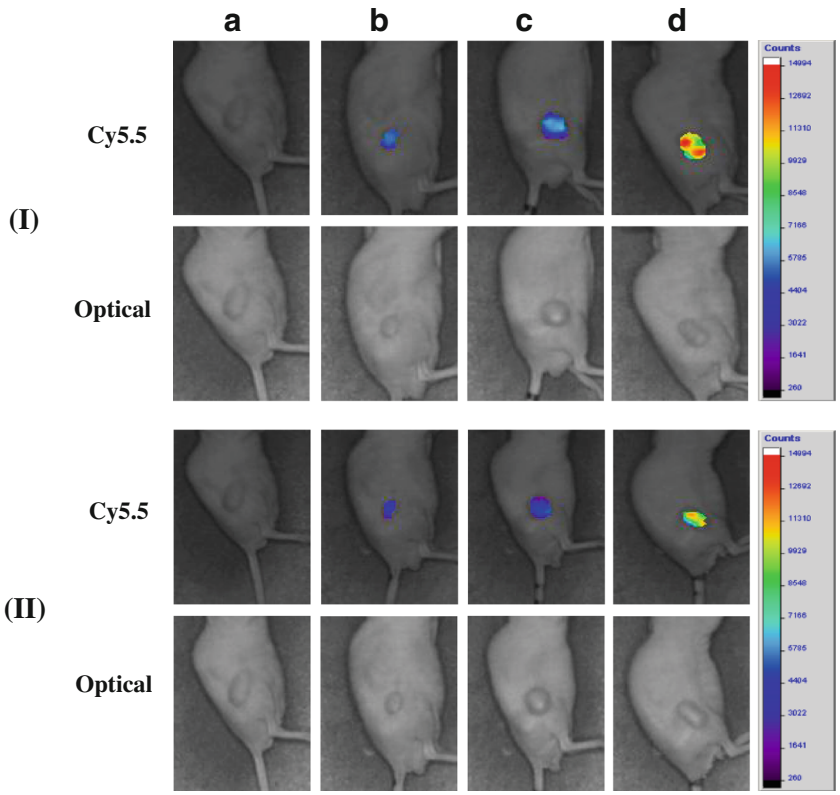

Fig. 7 *In vivo* NIRF images of siRNA-loaded nanocomplex formulations in a PC-3 tumor-xenograft mouse model. Cy5.5-filtered and optical images of tumor in (**a**) control, (**b**) naked Cy5.5-siRNA, (**c**) Cy5.5-siRNA/Lipofectamine 2000 (Cy5.5-siRNA loaded L2K), (**d**) Cy5.5-siRNA/protamine/lecithin/chitosan/TPP complex (Cy5.5-siRNA loaded GP-L-CT) groups 2 h (I) and 5 h (II) post-intravenous injection.

bloodstream and permeated into the tumor tissue as a nano-sized drug delivery system after intravenous injections.

In vivo anti-tumor efficacy of GP-L-CT nanocomplexes was tested in a PC-3 tumor xenograft mouse model by monitoring tumor growth inhibition (Fig. 8). Luciferase siRNA was incorporated into GP-L-CT for the irrelevant siRNA group. In our preliminary study, naked siRNA did not have any anti-tumor efficacy in a PC-3 tumor-bearing mouse model (data not shown). The mean tumor volumes of the PBS (control), Luciferase siRNA GP-L-CT, and SVN siRNA GP-L-CT treated groups were 615, 550, and 226 mm^3 at day 14, and 754, 742, and 277 mm^3 at day 18, respectively. The growth inhibition rate of GP-L-CT was calculated to be 75.5% at day 18 compared to the control group. It is particularly notable that the tumor volume of the SVN siRNA GP-L-CT group was significantly smaller than those of the control and Luciferase siRNA GP-L-CT groups ($P<0.05$). This indicated that anti-tumor efficacy was induced by *in vivo* systemic siRNA delivery of the chitosan-based hybrid nanocomplex.

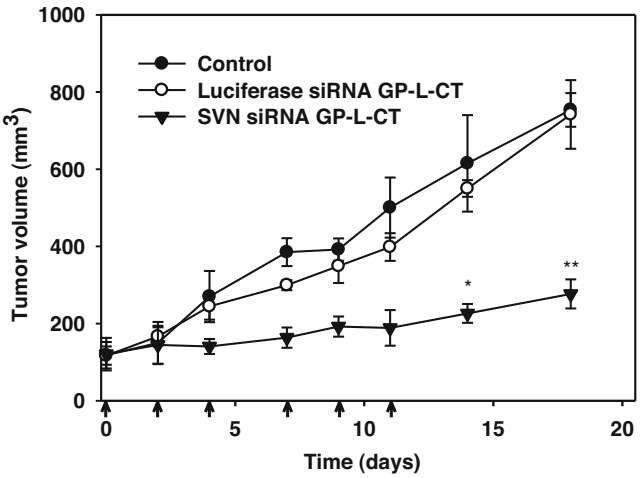

Fig. 8 *In vivo* anti-tumor efficacy of siRNA-loaded nanocomplex in a PC-3 tumor-xenograft mouse model. Tumor volume profiles of PBS (Control), luciferase siRNA/protamine/lecithin/chitosan/TPP (Luciferase siRNA GP-L-CT), SVN siRNA/protamine/lecithin/chitosan/TPP complex (SVN siRNA GP-L-CT). Nanocomplexes were injected intravenously six times for 2 weeks. $*P<0.05$ and $**P<0.01$ are established between Luciferase siRNA GP-L-CT and SVN siRNA GP-L-CT. Data represent means ± SD ($n\geq3$).

Based on its tumor targetability and anti-tumor efficacies, GP-L-CT can circulate in the bloodstream and exhibit an EPR effect with systemic administration, resulting in reduced tumor growth in a tumor xenograft mouse model. Although chitosan could be used as a cationic polymer for *in vitro* gene transfection, it is difficult to verify its *in vivo* performance due to its weakened binding affinity with nucleic acids and the aggregation that was resulted from interaction with endogenous components (17–19, 22). The significance of this study is that it identified a method for systemic application of the GP-L-CT formulation in cancer therapy and diagnosis, overcoming difficulties with instability of conventional cationic nanoparticles under physiological conditions using the hybrid nanocomplex system. Although further investigation is needed

to fully elucidate the specific mechanism and detailed *in vivo* efficacy of the developed nanocomplex, its feasibility as a nano-sized vehicle for systemic application of siRNA therapeutics was verified.

CONCLUSIONS

The low cytotoxicity, high biocompatibility, high mucoadhesiveness, and high cell permeability of chitosan have made it widely used for the delivery of nucleic acid therapeutics. However, a reduction in its *in vivo* gene delivery efficiency must be overcome. In this study, a pre-complex based on siRNA and protamine was formed and lecithin, chitosan, and TPP were added to develop a more stable and efficient hybrid nanocomplex (GP-L-CT). GP-L-CT provided suitable physicochemical properties with a positive zeta potential in DW and mean diameter <200 nm in 50% FBS for intravenous injection of siRNA, as well as superior *in vitro* cellular uptake and gene silencing efficiencies. Furthermore, systemic administration of GP-L-CT improved *in vivo* tumor targetability and anti-tumor efficacy in a tumor xenograft mouse model compared to other formulations. This novel chitosan-based hybrid nanocomplex was successfully developed for the systemic delivery of SVN siRNA, which could serve as an alternative to cationic polymeric nanoparticles that are unstable in serum.

ACKNOWLEDGMENTS AND DISCLOSURES

This work was supported by the Ministry of Knowledge Economy of Korea (10030044, SM. Noh).

REFERENCES

1. Davaa E, Ahn IH, Kang BS, Lee SE, Myung CS, Park JS. Preliminary study to determine the optimal conditions for the simultaneous complexation of siRNA and plasmid DNA. J Pharm Invest. 2013;43:499–505.
2. Wang J, Lu Z, Wientjes MG, Au JL-S. Delivery of siRNA therapeutics: barriers and carriers. AAPS J. 2010;12:492–503.
3. Behlke MA. Progress towards *in vivo* use of siRNAs. Mol Ther. 2006;13:644–70.
4. Whitehead KA, Langer R, Anderson DG. Knocking down barriers: advances in siRNA delivery. Nat Rev Drug Discov. 2009;8:129–38.
5. Zhang S, Zhao Y, Zhi D, Zhang S. Non-viral vectors for the mediation of RNAi. Bioorg Chem. 2012;40:10–8.
6. Khalil IA, Kogure K, Akita H, Harashima H. Uptake pathways and subsequent intracellular trafficking in nonviral gene delivery. Pharmacol Rev. 2006;58:32–45.
7. Ping Y, Liu C, Zhang Z, Liu KL, Chen J, Li J. Chitosan-graft-(PEI-β-cyclodextrin) copolymers and their supramolecular PEGylation for DNA and siRNA delivery. Biomaterials. 2011;32:8328–41.
8. Singha K, Namgung R, Kim WJ. Polymers in small-interfering RNA delivery. Nucleic Acid Ther. 2011;21:133–47.
9. Mao S, Sun W, Kissel T. Chitosan-based formulations for delivery of DNA and siRNA. Adv Drug Deliv Rev. 2010;62:12–27.
10. Malmo J, Hanne S, Vårum KM, Strand SP. SiRNA delivery with chitosan nanoparticles: molecular properties favoring efficient gene silencing. J Control Release. 2012;158:261–8.
11. Techaarpornkul S, Wongkupasert S, Opanasopit P, Apirakaramwong A, Nunthanid J, Ruktanonchai U. Chitosan-mediated siRNA delivery *in vitro*: effect of polymer molecular weight, concentration and salt forms. AAPS PharmSciTech. 2010;11:64–72.
12. Park S, Jeong EJ, Lee J, Rhim T, Lee SK, Lee KY. Preparation and characterization of nonaarginine-modified chitosan nanoparticles for siRNA delivery. Carbohydr Polym. 2013;92:57–62.
13. Fernandes JC, Qiu X, Winnik FM, Benderdour M, Zhang X, Dai K, *et al.* Low molecular weight chitosan conjugated with folate for siRNA delivery *in vitro*: optimization studies. Int J Nanomedicine. 2012;7:5833–45.
14. Malhotra M, Tomaro-Duchesneau C, Prakash S. Synthesis of TAT peptide-tagged PEGylated chitosan nanoparticles for siRNA delivery targeting neurodegenerative diseases. Biomaterials. 2013;34:1270–80.
15. Han HD, Mangala LS, Lee JW, Shahzad MM, Kim HS, Shen D, *et al.* Targeted gene silencing using RGD-labeled chitosan nanoparticles. Clin Cancer Res. 2010;16:3910–22.
16. Malhotra M, Lane C, Tomaro-Duchesneau C, Saha S, Prakash S. A novel method for synthesizing PEGylated chitosan nanoparticles: strategy, preparation, and *in vitro* analysis. Int J Nanomedicine. 2011;6:485–94.
17. Karmali PP, Simberg D. Interactions of nanoparticles with plasma proteins: implication on clearance and toxicity of drug delivery systems. Expert Opin Drug Deliv. 2011;8:343–57.
18. Radomski A, Jurasz P, Alonso-Escolano D, Drews M, Morandi M, Malinski T, *et al.* Nanoparticle-induced platelet aggregation and vascular thrombosis. Br J Pharmacol. 2005;146:882–93.
19. Dobrovolskaia MA, Aggarwal P, Hall JB, McNeil SE. Preclinical studies to understand nanoparticle interaction with the immune system and its potential effects on nanoparticle biodistribution. Mol Pharm. 2008;5:487–95.
20. Matsuura M, Yamazake Y, Sugiyama M, Kondo M, Ori H, Nango M, *et al.* Polycation liposome-mediated gene transfer *in vivo*. Biochim Biophys Acta. 2003;1612:136–43.
21. Ragelle H, Vandermeulen G, Préat V. Chitosan-based siRNA delivery systems. J Control Release. 2013;172:207–18.
22. Xu S, Dong M, Liu X, Howard KA, Kjems J, Besenbacher F. Direct force measurements between siRNA and chitosan molecules using force spectroscopy. Biophys J. 2007;93:952–9.
23. Doolittle H, Morel A, Talbot D. Survivin-directed anticancer therapies – A review of pre-clinical data and early-phase clinical trials. Eur Oncol. 2010;6:10–4.
24. Kundu AK, Chandra PK, Hazari S, Pramar YV, Dash S, Mandal TK. Development and optimization of nanosomal formulations for siRNA delivery to the liver. Eur J Pharm Biopharm. 2012;80:257–67.
25. Delgado D, Pozo- Rodríguez A, Solinís MA, Rodríguez-Gascón A. Understanding the mechanism of protamine in solid lipid nanoparticle-based lipofection: The importance of the entry pathway. Eur J Pharm Biopharm. 2011;79:495–502.
26. DeLong RK, Akhtar U, Sallee M, Parker B, Barber S, Zhang J, *et al.* Characterization and performance of nucleic acid nanoparticles combined with protamine and gold. Biomaterials. 2009;30:6451–9.
27. Li S, Huang L. *In vivo* gene transfer via intravenous administration of cationic lipid–protamine–DNA (LPD) complexes. Gene Ther. 1997;4:891–900.

28. Yuan H, Zhang W, Du Y, Hu F. Ternary nanoparticles of anionic lipid nanoparticles/protamine/DNA for gene delivery. Int J Pharm. 2010;392:224–31.
29. Rojanarata T, Opanasopit P, Techaarpornkul S, Ngawhirunpat T, Ruktanonchai U. Chitosan-thiamine pyrophosphate as a novel carrier for siRNA delivery. Pharm Res. 2008;25:2807–14.
30. Crawford R, Dogdas B, Keough E, Haas RM, Wepukhulu W, Krotzer S, *et al.* Analysis of lipid nanoparticles by Cryo-EM for characterizing siRNA delivery vehicles. Int J Pharm. 2011;403: 237–44.
31. Mayen V, Wutikhun T, Ketchart O, Kopermsub P. Adsorption of siRNA into mesoporous silica nanoparticles. J Microsc Soc Thai. 2012;5:10–3.
32. Cho HJ, Yoon HY, Koo H, Ko SH, Shim JS, Lee JH, *et al.* Self-assembled nanoparticles based on hyaluronic acid-ceramide (HA-CE) and Pluronic® for tumor-targeted delivery of docetaxel. Biomaterials. 2011;31:7181–90.
33. Kalsin AM, Kowalczyk B, Smoukov SK, Klajn R, Grzybowski BA. Ionic-like behavior of oppositely charged nanoparticles. J Am Chem Soc. 2006;128:15046–7.
34. Suh MS, Shim G, Lee YH, Han SE, Yu YH, Choi Y, *et al.* Anionic amino acid-derived cationic lipid for siRNA delivery. J Control Release. 2009;140:268–76.
35. Sternberg B, Hong K, Zheng W, Papahadjopoulos D. Ultrastructural characterization of cationic liposome-DNA complexes showing enhanced stability in serum and high transfection activity *in vivo*. Biochim Biophys Acta. 1998;1375:23–35.
36. Han SE, Kang H, Shim GY, Suh MS, Kim SJ, Kim JS, *et al.* Novel cationic cholesterol derivative-based liposomes for serum-enhanced delivery of siRNA. Int J Pharm. 2008;353:260–9.
37. Juliano R, Bauman J, Kang H, Ming X. Biological barriers to therapy with antisense and siRNA oligonucleotides. Mol Pharm. 2009;6:685–95.

Journal of Controlled Release 185 (2014) 62–70

Contents lists available at ScienceDirect

Journal of Controlled Release

journal homepage: www.elsevier.com/locate/jconrel

A new injectable liquid crystal system for one month delivery of leuprolide

Min-Hyo Ki [a,b], Jong-Lae Lim [a,c], Jin-Young Ko [a], So-Hyun Park [a], Ji-Eon Kim [b], Hyun-Jong Cho [d], Eun-Seok Park [c], Dae-Duk Kim [b,*]

[a] Chong Kun Dang Research Institute, CKD Pharmaceuticals Inc., 464-3 Jung-dong, Giheung-gu, Yongin-si, Gyeonggi-do 446-916, Republic of Korea
[b] College of Pharmacy and Research Institute of Pharmaceutical Sciences, Seoul National University, Seoul 151-742, Republic of Korea
[c] School of Pharmacy, Sungkyunkwan University, 300 Cheoncheon-dong, Jangan-gu, Suwon 440-746, Republic of Korea
[d] College of Pharmacy, Kangwon National University, Chuncheon 200-701, Republic of Korea

ARTICLE INFO

Article history:
Received 8 January 2014
Accepted 19 April 2014
Available online 29 April 2014

Keywords:
Liquid crystal
Hexagonal phase
Leuprolide
Sustained release injection
Pharmacokinetics

ABSTRACT

An injectable liquid crystal-forming system (LCFS) was prepared by using sorbitan monooleate (SMO) as a new liquid crystal-forming material for injections, and its potential use of clinically available sustained-release formulation was evaluated. LCFS was prepared using SMO mixed with phosphatidyl choline and tocopherol acetate, and contained 3.75 mg of leuprolide acetate as a monthly dose in 90 μl in liquid form. The semi-solid mesophase was formed from the liquid LCFS when it contacted water. The mesophase showed typical characteristics of the liquid crystalline phase, which was classified as the hexagonal phase. The safety of the LCFS was studied by an *in vitro* extraction colony assay and by examining the injection site in rats and white rabbits after an autopsy. Both *in vitro* release test and *in vivo* pharmacokinetic and pharmacodynamic studies showed a sustained release of leuprolide. When compared with a commercial depot formulation of leuprolide, the LCFS showed a similar AUC_{last} value and significantly reduced initial burst with sufficient suppression of testosterone after subcutaneous injections in rats and dogs. The LCFS can serve as a new type of sustained-release injection formulation for its safety, ease of preparation, and sustained release properties.

1. Introduction

Sustained-release (SR) injections are designed to release a drug substance at a predetermined rate to maintain its effective plasma concentration for a specific period of time for months. Leuprolide (pGlu-His-Trp-Ser-Tyr-D-Leu-Leu-Arg-Pro-NHEt) is one of the most successful drugs in SR depot injection formulation of poly(lactic-co-glycolic acid) (PLGA) microspheres [1–4]. It is a potent luteinizing hormone-releasing hormone (LHRH) analog that stimulates the release of luteinizing hormones. Leuprolide has been used in treating prostate cancer by saturating and down-regulating pituitary receptors, thereby suppressing testosterone production. Though PLGA microspheres are available for clinical application, they are difficult to prepare and are known to decrease the stability of protein drugs [5–7]. Unfortunately, alternative polymers with proven safety for injectable excipients have not been reported yet in spite of many research efforts [8].

Recently, liquid crystal technology has emerged as a new, injectable SR formulation for its sustained drug release properties. Although no commercial product based on this technology has been developed, it has gained increasing interest for drug delivery [9,10]. Lyotropic liquid crystal systems composed of amphiphiles can be classified into lamellar (La), hexagonal and cubic phases based on their assembly shape. Among them, the reversed hexagonal phase (H_2) and the reversed cubic phase (Q_2) have been extensively investigated for their ability to control the release rate of numerous drug substances, from low-molecular-weight chemicals to macromolecular drugs (proteins, peptides and nucleic acids) [11]. Their structures consist of a linear arrangement of alternating lipid bilayers and of aqueous channels arranged in periodic minimal surface geometries. The reversed hexagonal phase consists of an infinite rod-type water channel arranged in a two-dimensional lattice and separated by lipid bilayers, and the reversed cubic phase comprises a curved water channel and a bicontinuous lipid bilayer that extends in three dimensions. The reversed hexagonal and cubic mesophases are spontaneously formed from the liquid crystal-forming system (LCFS) in an aqueous fluid. The formed tortuous networks of aqueous nano-channels in the mesophases or mesophase particles play important roles as passageways for the sustained release of drugs from liquid crystals [9–12].

Various amphiphilic liquid crystal-forming materials (LCFMs), such as glycerol monooleate (GMO), glycerol dioleate (GDO), glycerol oleyl ether, oleyl glycerate, phytanyl glycerate and phytantriol, have been reported [13–16]. The drug release patterns of different types of LCFMs have been evaluated for the development of lyotropic liquid crystals as

* Corresponding author. Tel.: +82 2 880 7870; fax: +82 2 873 9177.
E-mail address: ddkim@snu.ac.kr (D.-D. Kim).

http://dx.doi.org/10.1016/j.jconrel.2014.04.034
0168-3659/

controlled release dosage forms. The results show that the drug release rate was reduced as the diameter of the aqueous channel, located inside the liquid crystal, was decreased and the drug in the similar molecular structure was more hydrophobic [17,18]. Aside from LCFMs, additives that change the physical properties of liquid crystal have also been investigated, such as fat materials including phospholipid, tocopherol, tocopherol acetate and tri-acyl glycerol. A mixture of phospholipid and GDO (45/55 to 55/45%, w/w) that formed the liquid crystalline phase has been used for subcutaneous drug delivery [19]. Fat materials, such as tocopherol, tocopherol acetate and tricaprylin, that are added to LCFMs (up to 10 or 15% weight ratio), could help the fabrication of cubic or hexagonal phase by increasing the curvature of the bicontinuous layer inside the liquid crystal [20,21].

Although there were many results regarding *in vitro* drug release tests of LCFSs, their *in vivo* pharmacokinetic study over one month was not thoroughly investigated. Moreover, while many studies on SR injections using LCFMs, such as GMO, GDO, oleyl glycerate or phytantriol, have been conducted, no drug delivery systems based on LCFM have been approved by the FDA. In this study, sorbitan monooleate (SMO) (also known as Span 80) was used as a new LCFM because it has been used as a pharmaceutical excipient with acceptable daily intakes up to 25 mg/kg/day [22]. Unlike other LCFMs reported, SMO is regarded as safe for injection formulations. To the best of our knowledge, this study is the first case of applying SMO in SR (monthly) injections based on liquid crystal technology which could replace the PLGA depot systems. The non-polar tail structure of SMO is made up of oleic acid, the same as the previously used LCFMs. But its polar head group has a distinguished sorbitan structure, compared to the polyol structures in other LCFMs, such as glycerol or glycerate (Fig. 1) [13–16]. SMO has advantages in terms of safety and quality control when it is applied in SR injections, because it is an injectable emulsifier that has been used in various pharmaceutical formulations.

In this study, the LCFS composed of leuprolide acetate and SMO was assessed for its use as a SR injection formulation. The inner structure and the drug release profiles of liquid crystal phases from the LCFS were investigated. Also, the pharmacokinetic and pharmacodynamic properties of leuprolide acetate from the developed LCFS were compared to the commercial PLGA depot formulation.

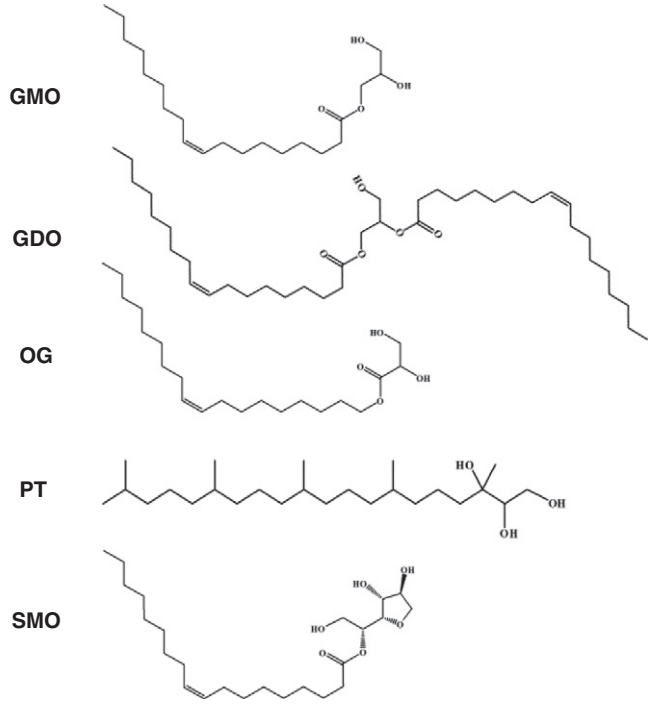

Fig. 1. Chemical structures of liquid crystal-forming materials, GMO: glyceryl monooleate; GDO: glyceryl dioleate; OG: oleyl glycerate; PT: phytantriol and SMO: sorbitan monooleate.

2. Materials and methods

2.1. Materials

Leuprolide acetate and leuprolide-d_5 acetate were obtained from Teva (Petah-Tiqva, Israel) and Toronto Research Chemicals (Ontario, Toronto, Canada), respectively. Testosterone and testosterone-d_3 were obtained from TLC PharmaChem (Ontario, Toronto, Canada) and BDG Synthesis (Wellington, New Zealand), respectively. SMO, phosphatidyl choline, tocopherol acetate, and Tween 80 were purchased from Seppic (Puteaux, France), Lipoid GmBH (Ludwigshafen, Germany), DSM Nutritional Products Limited (Sisseln, Switzerland), and Croda (Edison, NJ, USA), respectively. Leuprolide acetate conforms to 97–103% of the assay specification. SMO and phosphatidyl choline correspond to 65–88% as oleic acid and >94% of the assay specification, respectively. Na-heparin was obtained from JW Pharma(Seoul, Korea) and aprotinin solution (30 TIU/5 mL) was purchased from Phoenix Pharmaceuticals (Hanau, Germany). The mouse fibroblast (NIH 3T3) was obtained from ATCC (Manassas, VA, USA). Giemsa stain solution 5% and fetal bovine serum (FBS) were purchased from Santa Cruz Biotechnology (Santa Cruz, CA, USA) and NOVA Biologics (Oceanside, CA, USA), respectively. Penicillin, streptomycin, Eagle's minimum essential medium (EMEM) and trypsin-ethylenediaminetetraacetic acid (EDTA) were purchased from Gibco (Grand Island, NY, USA). All the other chemicals were of analytical grade.

2.2. Preparation of LCFS and its formation test

The LCFS was prepared by adding and mixing a leuprolide solution into the LCFS vehicle solution. The leuprolide solution was prepared by dissolving 3.75 mg of leuprolide acetate in 5 μl of DMSO. The LCFS vehicle solution was prepared by mixing SMO, phosphatidyl choline, tocopherol acetate, Tween 80, and ethanol (33:45:10:2:10, w/w%). SMO, phosphatidyl choline, and tocopherol acetate were used as core components for the LCFS, and Tween 80 and ethanol were used to prevent the separation of components which could make a homogenized vehicle solution. The final LCFS was designed to contain 3.75 mg of leuprolide acetate for one month dose in 90 μl. The viscosity of the liquid form, being approximately 650 cPs, was suitable for injection. The commercialized Leuplin DPS Injection® 3.75 mg (Takeda Pharmaceutical Company Limited, Osaka, Japan) was used as a reference product.

To confirm the transition from the oil phase to the gel-like mesophase after the LCFS came in contact with water, 100 μl of the LCFS in the oil phase was added to 3 ml of phosphate buffered saline (PBS, pH 7.4) at room temperature. The apparent appearance and the half-dissected section of the mesophases were observed after water on the surface of the formed liquid crystalline mesophases was cautiously wiped off at 0.5, 6, 72, 168, 240 and 336 h after the loading. The water content of the mesophases was measured by Karl Fischer titration (758 KFD Titrino, Metrohm, Herisau, Switzerland).

2.3. Cryo-transmission electron microscopy (Cryo-TEM) and polarized optical microscopy

Cryo-TEM (Tecnai G2 F20 Cryo-TEM, FEI Company, Hillsboro, OR, USA) was used to observe the inner structure of the liquid crystal that was formed with exposure to water [23–25]. For convenient observation of the liquid crystalline phase, 15 μl of the LCFS in the oil phase was added to 3 ml of triple distilled water and dispersed using a probe sonicator (CL-334, Qsonica, LLC, Newtown, CT, USA) to form mesophase particles. The dispersed liquid crystalline phase was placed on the holey carbon-coated grid (Quantifoil Micro Tools GmbH, Jena, Germany) like a water film and quickly frozen at −170 °C. The frozen grid was fixed in

the cryo-holder and moved to the Cryo-TEM at −170 °C. The sample was observed at the 80–200 kV dose.

Polarized optical microscopy (BA 300 Pol, Motic, British Columbia, Canada) was also used to investigate the structure of the liquid crystal phase [26–29]. LCFS (15 μl) was dropped and thinly spread on the glass slide. The glass slide was placed in a petri dish that contained 10 ml of triple distilled water for 15 min to form the liquid crystalline phase on the glass. The cover glass was placed slowly on the glass slide so as not to form air bubbles, and then the cover glass was sealed with silicone grease to prevent water evaporation at 25 °C. All the photographs were taken under the condition of the cross-polarizer.

2.4. In vitro release test

The drug release test was evaluated in triplicate with the modified method, based on the USP rotating-basket method [30]. The LCFS containing 3.75 mg of leuprolide acetate was loaded in 3 ml of purified water to form a liquid crystalline mesophase. The Hanson SR8 Plus dissolution tester (Hanson Research Corp., Chatsworth, CA, USA) was used as a basket dissolution apparatus (USP apparatus 1) for the release test. When the basket was fully submerged in the release medium, the liquid crystalline phase was placed in the basket. The vessel was filled with 500 ml of the release medium, and the basket was rotated at 100 rpm at 37 °C. Aliquots of the medium (5 ml) were taken at 0, 1, 3, 6, 12, 18, 24, 48, 72, 120 and 168 h and an equivalent volume of the medium was refilled. The medium that was taken at each time point was filtered using a 0.22 μm syringe filter and analyzed quantitatively by high performance liquid chromatography (HPLC). As for the release medium, 20.95 ml triethylamine was dissolved in 1000 ml of water, and then 85% phosphoric acid was added to it to adjust the pH to 7.0. Finally, sodium azide (0.02%) and Tween 80 (0, 0.02, 0.2 and 2.0%, w/v) were added to it.

The Waters Alliance 2695 HPLC system (Waters, Milford, MA, USA) and the Spherisorb® C18 column (3 μm, 4.6 × 100 mm, Waters, Milford, MA, USA) were used for the analysis of the drug. The mobile phase was prepared as a mixture of a pH 3.0 buffer, acetonitrile, and n-propyl alcohol (80: 12: 8, volume ratio) and flowed through the column at the rate of 1.0 ml/min and room temperature. For the pH 3.0 buffer, 20.95 ml triethylamine was dissolved in 1000 ml of water, and then 85% phosphoric acid was added to adjust its pH to 3.0. The samples (20 μl each) were injected and detected by UV at a wavelength of 220 nm.

2.5. Animals

Male Sprague–Dawley (SD) rats (8 weeks old, about 300 g body weight) were obtained from Orient Bio, Inc. (Seongnam, Korea). Female New Zealand white rabbits (approximately 2.5–3.5 kg) were acquired from Roberto C. Hartelust (Tilburg, the Netherlands). Rats and rabbits were acclimated for approximately 7 days before dosing. They had free access to food and water. Male beagle dogs (5–6 months old, about 10 kg body weight) were purchased from Beijing Marshall Biotechnology (Beijing, China). Beagle dogs were acclimated for approximately 14 days before dosing. They were fed approximately 300 g dog diet once daily and municipal water was supplied *ad libitum*. All animals were cared for in accordance with OECD guideline for the testing of chemicals (the standards of toxicity study for medicinal products No. 2013–121).

2.6. Safety test

As the LCFS forms a gel-like mesophase in contact with water, an extraction colony assay (colony-forming assay) was used to evaluate the toxicity of the liquid crystalline phase *in vitro*. The extraction colony assay can be used to test the toxicity of solid materials inserted into the human body, such as polymers, dental materials and implant devices [31,32]. Leuplin DPS Injection® 3.75 mg (reference) and LCFS containing 3.75 mg of leuprolide acetate were added to each 2 ml of EMEM with 10% FBS, respectively, and incubated at 37 °C for 24 h. After centrifugation, the supernatant was taken for a medium extract which was diluted serially using EMEM with 10% FBS to achieve the final concentrations of 25, 50, 75 and 100%. NIH 3T3 (mouse fibroblast) cells were seeded in 6 wells at a density of 1×10^2 per well, and 2 ml of 10% EMEM with 10% FBS was added to the well and incubated at 37 °C in a 5% CO_2 incubator. After 24 h incubation, the medium was exchanged with 2 ml of the serially diluted medium extract or the medium without the medium extract for control, and the cells were cultured for 7 days at 37 °C in the 5% CO_2 incubator. The cells were fixed with a 10% formalin solution for 5 min, and the cell colonies attached to the well plate were stained with a 5% Giemsa stain solution. The number of stained colonies in each well was counted, and the relative colony-forming capacity was calculated as the ratio of the number of colonies in the sample to that in the control. The cytotoxicity of the reference and LCFS were evaluated using the half-maximal inhibitory concentration (IC_{50}) of the relative colony-forming capacity compared to that of the reference. The IC_{50} (%) values were calculated from dose–response curves.

The *in vivo* safety of LCFS was investigated in rats and rabbits. An oil free syringe was filled with LCFS without air bubbles. After the hair on the back of the rats and rabbits was shaven, the injection site was sterilized with 70% (v/v) ethanol, and then LCFS containing 3.75 mg of leuprolide acetate was injected. The rats and rabbits were sacrificed 7, 14 and 28 days from the injection date, and the injection sites were dissected to observe the appearance of the formed liquid crystalline phase and the surrounding tissues.

2.7. Pharmacokinetic and pharmacodynamic studies

Leuplin DPS Injection® 3.75 mg (reference) and LCFS containing 3.75 mg of leuprolide acetate were subcutaneously injected into the back of the rats and beagle dogs (five animals per group). For pharmacokinetic study, blood samples of the rats were collected from the tail vein at 0, 0.5, 1, 3 and 6 h, and 1, 3, 5, 7, 10, 14, 21 and 28 days, while blood samples of the beagle dogs were collected from the cephalic vein at 0, 1, 3, 6 and 12 h and 1, 2, 3, 5, 7, 10, 14, 21 and 28 days after the injection. For pharmacodynamic study, reference and LCFS were injected into beagle dogs additionally in the same manner 28 days after the first injection after which blood samples were collected at 35, 42, 49, and 56 days. Each blood sample of the rats (0.75 ml) or beagle dogs (2 ml) were mixed with Na-heparin, resulting in about 15 IU/ml of Na-heparin in blood and centrifuged at 4 °C and 4000 rpm for 20 min. The centrifuged 100 μl of plasma sample was mixed with a 10 μl of aprotinin solution (30 TIU/5 ml) and stored at −80 °C before analysis. The concentration of leuprolide was analyzed for pharmacokinetic evaluation using plasma samples of the rats and beagle dogs, and the concentration of testosterone was analyzed for pharmacodynamic evaluation using plasma samples of the beagle dogs.

For the analysis of leuprolide, a stock solution of leuprolide acetate (20.0 μg/ml in 50% methanol) was prepared. A working standard solution was prepared by diluting a stock solution to 10.0, 8.0, 2.5, 1.0, 0.25, 0.1, 0.05, 0.025 and 0.005 μg/ml with 50% methanol. An internal standard solution was prepared by dissolving leuprolide-d_5 acetate to 20.0 μg/ml with 50% methanol and diluting it to 0.025 μg/ml with 50% methanol. Sequentially, a series of calibration standards was prepared by diluting 10 μl of a working standard solution with 0.99 ml of plasma. The final concentrations of the calibration standards were 100, 80.0, 25.0, 10.0, 2.5, 1.0, 0.5, 0.25 and 0.05 ng/ml. Each calibration standard (100 μl) was mixed with aprotinin solution (10 μl). Then, the plasma samples (50 μl) and the calibration standards were mixed with the internal standard solution (10 μl) and centrifuged for 1 min at 13,000 rpm after vortexing for 1 min. After the organic layer was separated, acetonitrile (150 μl) was put in each sample and standard, and centrifuged for 3 min after vortexing for 1 min. Each supernatant

separated (150 μl) was put in a 96-well round plate, and 350 μl of 0.05% (v/v) acetic acid was added onto the plate. The 96-well round plate was centrifuged for 1 min at 4000 rpm at room temperature after mixing for 3 min. The prepared samples (20 μl) were injected into an ultra performance liquid chromatography–tandem-mass spectrometry (UPLC–MS/MS) system. The UPLC–MS/MS system consisted of the Waters ACQUITY UPLC System (Waters, Milford, MA, USA) and the Waters XEVO TQ-S (Waters, Milford, MA, USA). Chromatographic separation was achieved on an ACQUITY UPLC® BEH C18 column (100 × 2.1 mm, 1.7 μm, Waters, Milford, MA, USA) with a column temperature of 35 °C. The mobile phase consisted of 0.05% acetic acid in water (MP-A) and 0.05% acetic acid in acetonitrile (MP-B), and the flow rate was 0.4 ml/min. The gradient elution programs of the mobile phases were as follows: 75% MP-A; 25% MP-B, 0–0.4 min; 75–60% MP-A; 25–40% MP-B, 0.4–2.0 min; 60–10% MP-A; 40–90% MP-B, 2.0–2.01 min; 10% MP-A; 90% MP-B, 2.01–2.5 min; 10–75% MP-A; 90–25% MP-B, 2.5–2.51 min; and 75% MP-A; 25% MP-B, 2.51–3.0 min. The UPLC–MS/MS system was interfaced with an electrospray ionization (ESI) probe. The ion source and desolvation temperatures were set at 150 °C and 500 °C, respectively. The flow rates of the cone gas and the desolvation gas were kept at 150 l/h and 800 l/h, respectively. The voltages were set at 30 V for the entrance potential, and at 16 V for the collision energy. The ions for selective monitoring were chosen *via* positive scanning from 100 to 800 m/z; and for the quantification, the product ions were monitored. The protonated molecule ions of leuprolide were monitored at 605.53 m/z $[M + H]^+$ for the precursor ions and at 299.34 m/z $[M + H]^+$ for the product ions. The protonated molecule ions of leuprolide-d_5 were monitored at 608.02 m/z $[M + H]^+$ for the precursor ions and at 304.34 m/z $[M + H]^+$ for the product ions. Using the above UPLC–MS/MS analysis method, good linearity in a calibration curve was obtained at the concentration range of 0.05–100 ng/ml for leuprolide in the rat and dog plasmas, as demonstrated by the high correlation coefficient (R^2) value of above 0.99 (Fig. S1). The developed assay exhibited acceptable precision and accuracy, and 0.05 ng/ml of lower limit of quantification (LLOQ) in both rat and dog plasma.

For the analysis of testosterone, a stock solution of testosterone (50.0 μg/ml in 50% methanol) was prepared. A calibration standard was prepared by diluting a stock solution to 10.00, 5.00, 2.00, 0.50, 0.20, 0.10, 0.05 and 0.02 ng/ml with plasma. An internal standard solution was prepared by dissolving testosterone-d_3 to 0.02 μg/ml with 50% methanol. Then, each calibration standard (200 μl) was mixed with the internal standard solution (10 μl) and centrifuged for 1 min at 13,000 rpm after vortexing for 1 min. The mixed solvent (1.0 ml) of n-hexane and ethyl acetate (60:40, v/v) was put in each sample and standard, and centrifuged for 3 min at 13,000 rpm at room temperature after vortexing for 10 min. After separating into aqueous and organic phases, the aqueous layer (lower layer) was frozen at −60– -80 °C for 30 min. The organic layer (upper layer) was put in 1.5 ml polypropylene tube and then evaporated completely in a centrifugal vacuum concentrator for 30 min. Each residue in the tube was dissolved with 0.2 ml of 85% (v/v) methanol and centrifuged for 1 min at 13,000 rpm at room temperature after vortexing for 10 min. After 0.3 ml of 0.05% (v/v) acetic acid was put in the tube and vortexed for 1 min, the centrifugation was carried out for 1 min at 13,000 rpm at room temperature. All supernatants were put in a 96-well round plate. The prepared samples (50 μl) were injected into the UPLC–MS/MS system. Chromatographic separation was achieved on an ACQUITY UPLC® BEH C18 column (50 × 2.1 mm, 1.7 μm, Waters, Milford, MA, USA). The mobile phase consisted of 0.05% acetic acid in water (MP-A) and 0.05% acetic acid in acetonitrile (MP-B), and the flow rate was 0.4 ml/min. The gradient elution programs of the mobile phases were as follows: 65% MP-A; 35% MP-B, 0–0.2 min; 65–10% MP-A; 35–90% MP-B, 0.2–1.5 min; 10% MP-A; 90% MP-B, 1.5–2.0 min; 10%–65% MP-A; 90%–35% MP-B, 2.0–2.1 min and 65% MP-A; 35% MP-B, 2.1–2.5 min. The UPLC–MS/MS system was interfaced with an ESI probe. The ion source and desolvation temperatures were set at 150 °C and 600 °C, respectively. The flow rates of the cone gas and the desolvation gas were kept at 150 l/h and 1000 l/h, respectively. The voltages were set at 34–36 V for the entrance potential, and at 20–21 V for the collision energy. The protonated molecule ions of testosterone were monitored at 289.39 m/z $[M + H]^+$ for the precursor ions and at 97.13 m/z $[M + H]^+$ for the product ions. The protonated molecule ions of testosterone-16,16,17-d_3 were monitored at 292.42 m/z $[M + H]^+$ for the precursor ions and at 97.15 m/z $[M + H]^+$ for the product ions. Using the above UPLC-MS/MS analysis method, good linearity in a calibration curve was obtained at the concentration range of 0.02–10.00 ng/ml in dog plasmas, as demonstrated by the high correlation coefficient (R^2) value of above 0.99 (Fig. S1). The developed assay exhibited acceptable precision and accuracy, and 0.02 ng/ml of LLOQ in dog plasma.

2.8. Pharmacokinetic and statistical analysis

The maximum plasma concentration (C_{max}) of leuprolide and the time to reach the maximum concentration (T_{max}) were determined as the mean value directly from the data. Non-compartmental pharmacokinetic analysis was performed on the plasma concentration *versus* time curves using commercially available pharmacokinetic software. The area under the plasma concentration time curve from time zero to the last measurable concentration (AUC_{last}), the area under the curve from time zero to infinity (AUC_{inf}), and terminal half-life of the drug ($T_{1/2}$) were calculated by WinNonlin 5.3 (Pharsight Corporation, Mountain View, CA, USA). Statistical analysis was carried out using paired *t*-tests between pharmacokinetic parameters of reference and LCFS.

3. Results and discussion

3.1. Liquid crystal formation test

A LCFS based on SMO, phosphatidyl choline, and tocopherol acetate was developed for the subcutaneous delivery of leuprolide acetate. The LCFS was transformed into a gel-like mesophase by forming a lyotropic liquid crystal in 5 min after the LCFS containing SMO came in contact with PBS. As soon as the LCFS was injected into the water, it lost the flow property of a liquid and changed into a spherical semi-solid form to minimize the contact surface with water, exhibiting a semi-transparent and light yellow appearance (Fig. 2).

The formed gel-like mesophase was kept in PBS and observed up to 336 h. The internal part of the mesophase was not fully developed into a semi-solid form at 0.5 h and was squashed when dissected. The semi-solid state was reached, including the surface and internal part, at 6 h and maintained until the end of the observation period of 14 days. Water content continuously increased up to 21.4% at 240 h, but remained constant after that. About 21% of water content in the liquid crystalline phase is probably the maximum content that could be involved in the formation of a water channel inside the liquid crystal (Fig. 3).

The similar phenomenon of gel formation can be observed in a microemulsion preparation. Microemulsion gel in a temporal phase (between w/o and o/w) has similar characteristics to the liquid crystal. Though the microemulsion gel formed temporarily loses its semi-solid property by transformation into the liquid form of o/w microemulsion in the presence of excessive water, liquid crystal keeps its semi-solid mesophase for at least 14 days in spite of its continuous exposure to excessive amounts of water. SMO has been used for microemulsion gel formation as a minor component with large amount of oil and surfactants [33,34]. However, the LCFS in this study was prepared with SMO and phosphatidyl choline as core components providing the curvature in liquid crystals without oil or additional surfactants. The liquid crystal mesophases have shown that the longer half-life is achievable compared to microemulsion gels [34] as sustained release is maintained for several days to even several months. Formation of a

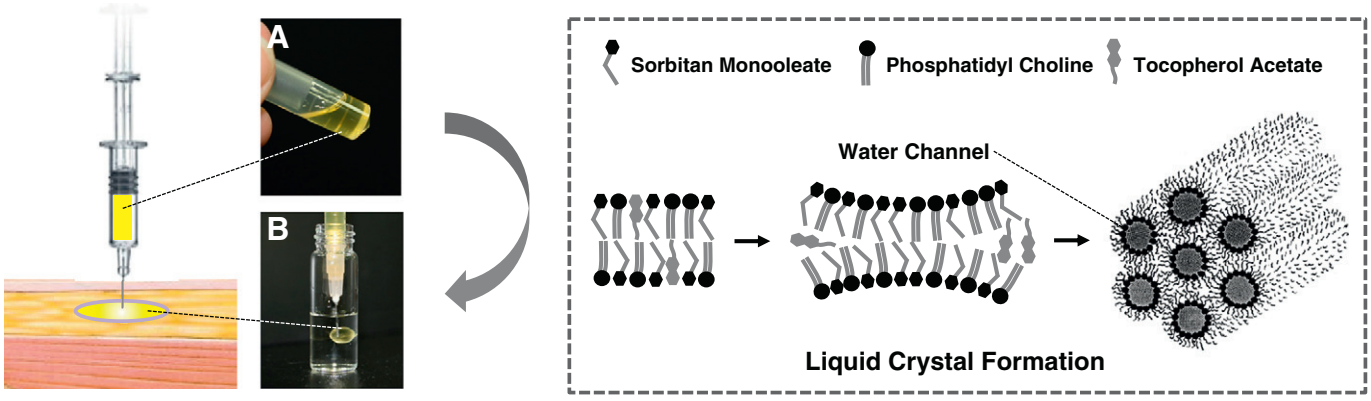

Fig. 2. Schematic illustration of liquid crystal formation in water after subcutaneous injection. Images of LCFS containing leuprolide acetate before injection (A) and liquid crystalline mesophase formed in PBS (pH 7.4) after injection (B) are shown.

liquid crystal using SMO was also confirmed in the following analysis of the inner structure, using Cryo-TEM and polarized optical microscopy.

3.2. Cryo-TEM and polarized optical microscopy

The crystallographic structures of the mesophases and the mesophase particles were determined *via* Cryo-TEM. The crystalline phase formed by SMO was observed to have mesophases with an internal curved longitudinal axis and mesophase particles with hexosome- or cubosome-like particles (Fig. 4). Fig. 4A and B show the striation texture in which the curved longitudinal axis has only one direction or many duplicated directions, while Fig. 4C and D show the mesophase particles with hexagonal or cubosomal symmetry. According to the shape and morphology of mesophase particles in previous literature, lamellar phases, including micelles, emulsions and liposomes, which have separated internal and external layers, exhibit a vesicle structure with a transparent or non-transparent inner single space in the particles [23,24]. However, the non-lamellar phases like liquid crystals, which have no separation between internal and external layers, show a lattice structure that is filled with many nano-sized units in the particles [23–25]. Results of this study confirmed that the structure of the mesophase particles from the LCFS was of the non-lamellar-phase type, which is known to be the major characteristic of liquid crystalline phase. The liquid crystalline phase can also be classified into the hexagonal phase and the cubic phase depending on the morphology. The hexagonal phase shows faceted particles, many of which exhibit curved striations, whereas others have textures with hexagonal symmetry. The cubic phase shows cubic symmetry accompanied by a vesicle or a vesicle-like structure on the contacting surface with water. The Cryo-TEM results confirmed that the liquid crystalline phase from the LCFS has characteristics that are similar to those of the hexagonal phase, since the phase mainly exhibited curved striations or hexagonal symmetries.

Since it is difficult to simply distinguish the hexagonal phase from the cubic phase based on the micrograph morphology, polarized optical microscopy was also performed. The result indicated that the liquid crystalline phase had an angular or anisotropic texture, based on the observation sites (Fig. 5). The optical texture in polarized optical microscopy can be used to distinguish the hexagonal phase from the cubic phase. In particular, an angular texture in Fig. 5A was the morphology mostly observed in the hexagonal liquid crystalline phase [26–28], as well as the anisotropic texture in Fig. 5B observed in the hexagonal phase [28,29]. All of the results from the Cryo-TEM and polarized optical microscopy revealed that the mesophase and mesophase particles from the LCFS with SMO exhibited typical characteristics of the liquid

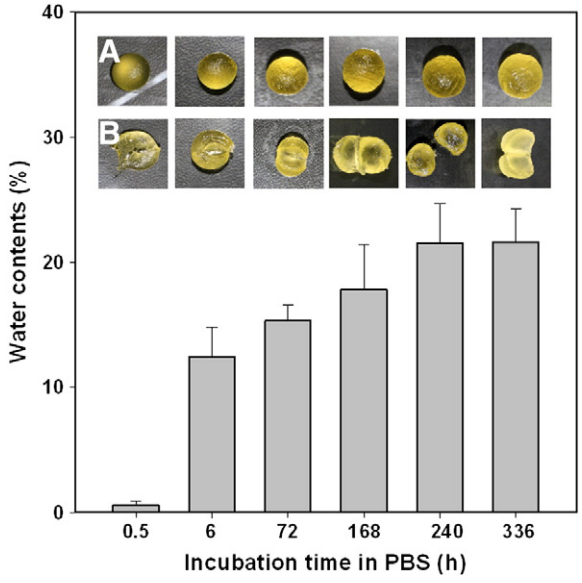

Fig. 3. Morphologies and water contents of liquid crystalline mesophases after incubation in PBS (pH 7.4). (A) Mesophases were formed after injections into PBS (pH 7.4). (B) Mesophases were cut in half after their formation. Water content was measured by Karl Fischer titration. Data are presented as mean ± SD (n = 3).

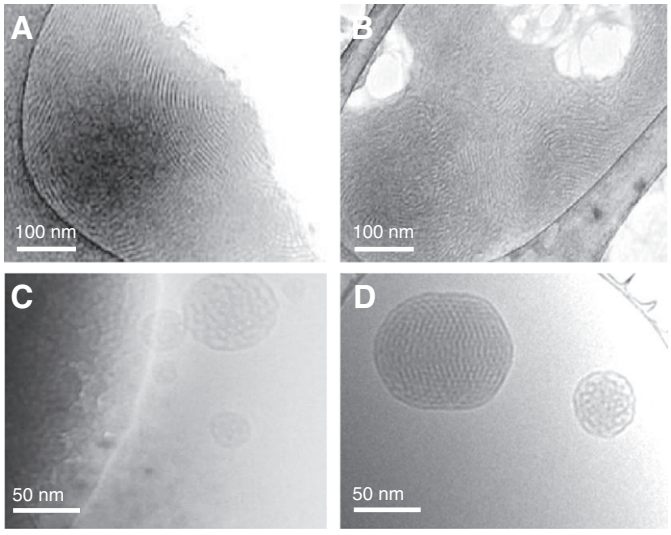

Fig. 4. Cryo-TEM micrographs of inner structure of mesophases and dispersed mesophase particles formed from LCFS. (A) and (B) Mesophases show striation texture in the mass. (C) and (D) Mesophase particles exhibit cubic or hexagonal symmetry inside the particles.

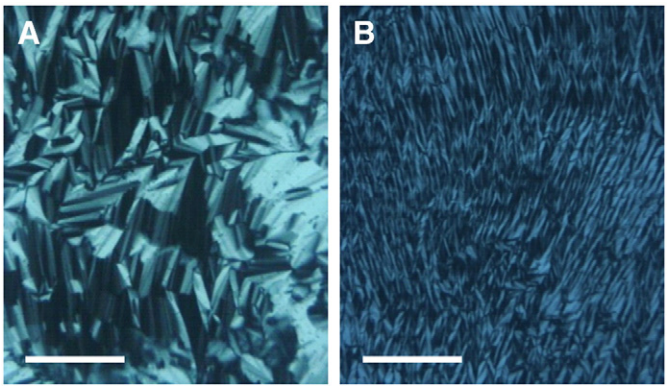

Fig. 5. Polarized optical microscope images of mesophases formed from LCFS. Optical images with (A) angular and (B) anisotropic textures. All images were taken at 100× magnification and the scale bar is 100 μm.

crystalline phase, which were classified into the hexagonal phase in terms of their structure.

3.3. In vitro release test

Drug release tests from the liquid crystal have been conducted by placing the formulation in a dialysis bag or a cuvette, wherein one or multiple planes of the liquid crystalline mesophases or particles were exposed to a release medium [17–19]. In this study, the liquid crystal mesophases containing 3.75 mg of leuprolide acetate were exposed to 500 ml of the release medium without using a cuvette or a dialysis bag surrounding the mesophase, for the simulation of subcutaneous conditions and easy observation of mesophases. As shown in Fig. 6, the release rate of leuprolide from the liquid crystalline phase was faster in the release medium with higher content of Tween 80. There seemed to be no initial burst in all drug release profiles. In the release medium without Tween 80, the released amount of drug was less than 5% at 168 h. The medium containing 0.02, 0.2 and 2.0% of Tween 80 showed 40.9, 71.2 and 94.3% of the released amounts at 168 h, respectively. In the test with the medium containing 2.0% of Tween 80, the steady state was already accomplished at 72 h with 87.5% of the released amount. A higher degree of erosion in the mass of the mesophase was observed in the medium with higher contents of Tween 80 during the test. Upon completion of the release test, over 80% of the mass remained in the medium with 0 and 0.02% of Tween 80, and about 40% and 10% of the mass remained in the medium with 0.2% and 2.0% of Tween 80, respectively. The release of leuprolide from the liquid crystalline phase was considered to be related to both the diffusion of the drug from the mass and the direct erosion of the mass (Fig. 6). In the condition of all drug release tests of this study, the solubility did not interfere with the release rate under the sink condition, because the solubility of leuprolide was known to be over 400 mg/ml in water at 25 °C [35].

Considering the results of the pharmacokinetic study presented below, the *in vitro* release condition, which mimics the *in vivo* condition of the SR injection for one month, was observed in the medium containing 0 and 0.02% of Tween 80. In this *in vitro* condition, it was assumed that the complete dissolution would be available in a month and similar velocity with the *in vivo* condition would be observed in the diffusion of the drug and the erosion of the mass. However, considering the drug stability of peptides and the practical test period for quality control, the medium containing between 0.2% and 2.0% of Tween 80 could be selected as a more appropriate medium for the test completion in a week. Although it may cause faster erosion of the mass compared to the *in vivo* condition, the medium with 0.2 to 2.0% of Tween 80 could be proper for the prompt evaluation of the reproducibility of controlled release.

3.4. Safety test

The extraction colony assay was conducted to evaluate the toxicity of the LCFS *in vitro*. The serially diluted medium extracts (25, 50, 75 and 100%) of reference were 96.3, 107.2, 78.3 and 48.0% of the relative colony-forming capacities, and IC_{50} of about 98.5% was obtained. For the LCFS, all of the medium extracts (25, 50, 75 and 100%) showed more than 100% of the relative colony-forming capacities resulting in IC_{50} of more than 100% (Fig. 7). The extraction colony assay can be used to evaluate the toxicity of solid materials in contact with the body or extracted materials from natural resources. The calculated IC_{50} from the assay was related to the cytotoxic effect on cell proliferation and differentiation [31,32]. IC_{50} of the LCFS is higher than that of the reference, and it means that the LCFS has less inhibitory effect on the proliferation and differentiation than the reference. Considering the

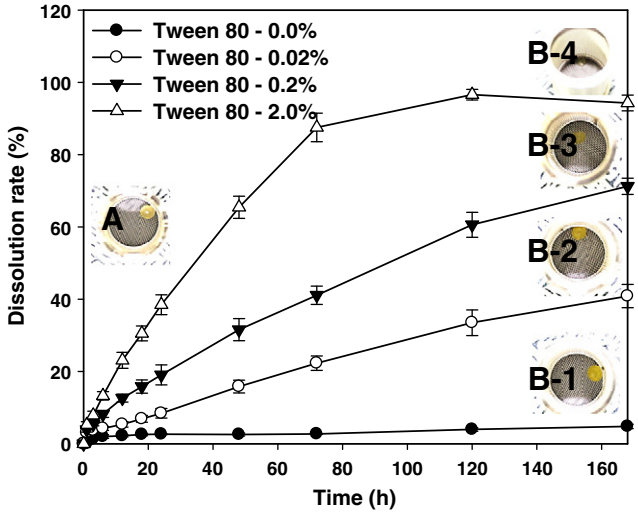

Fig. 6. *In vitro* release of leuprolide from LCFS in pH 7.0 buffer solutions containing 0, 0.02, 0.2, and 2.0% (w/v) of Tween 80 at 37 °C. Images of liquid crystal mesophases in the baskets showed their shapes due to erosion. The images of liquid crystal mesophases at the initial state (A) and after completion of release test in the buffer solutions containing 0% (B-1), 0.02% (B-2), 0.2% (B-3), and 2.0% (B-4) of Tween 80 are shown. Data are presented as mean ± SD (n = 3).

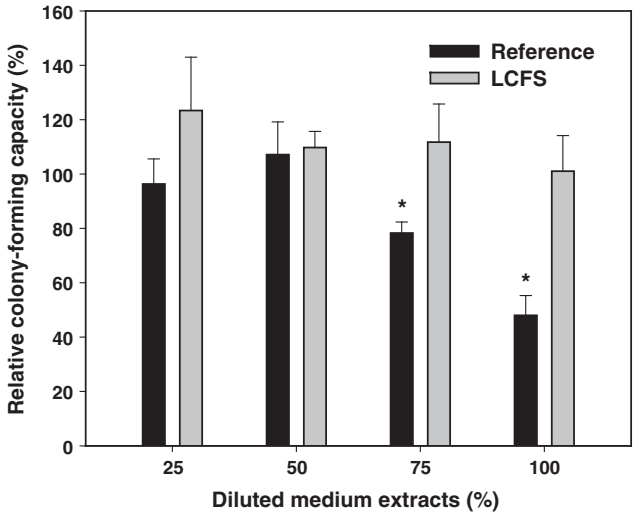

Fig. 7. Relative colony forming capacities of NIH 3T3 cells cultured with the medium extracts of reference and LCFS. For reference, Leuplin DPS Injection® 3.75 mg was extracted in EMEM with 10% FBS. For LCFS, it was extracted in EMEM with 10% FBS. *$P < 0.05$ is established between reference and LCFS. Data are presented as mean ± SD (n = 3).

low cytotoxicity of the commercially available PLGA depot injections, the LCFS can be regarded as a safe and proper SR injection in terms of cytotoxicity.

To assess *in vivo* safety of the LCFS against local tissue, a monthly dose of the LCFS was subcutaneously injected into the back of rats and rabbits. The appearance of the liquid crystal formed in the subcutaneous region and its injection site was observed after an autopsy. The liquid crystal phase in the subcutaneous region was a light yellow semi-transparent gel-like mesophase, similar to what was observed *in vitro*. A slightly flat mass, less than 1 cm in diameter, was observed in the *in vivo* state because it was located between the tissue and the skin (Fig. 8). Nothing unusual was found at the injection site and the surrounding tissue in all the animals at 7, 14 and 28 days after the injection when observed with the naked eye. There was also no significant pathological change, such as in the thickness of the tissue, an exudate, an inflammation of the tissue or an adhesion between the tissue and the liquid crystal mass during the test period.

The remaining amounts of the mesophases 28 days after injection were approximately 70% of the initial amounts observed by the naked eye. Considering that about 30% erosion of the mesophases took place in a month, it would take more than 3 months for the *in vivo* mesophases to be completely disintegrated, which would be similar to the 4 month erosion time of the commercially available PLGA depot injection [36].

3.5. Pharmacokinetic & pharmacodynamic studies

When the reference and the LCFS, containing 3.75 mg of leuprolide acetate as a monthly dose, were subcutaneously injected into the rat (at a dose of 12.5 mg/kg), similar plasma concentration profiles were observed except for the C_{max} values. T_{max} values of both groups were observed within 1 h and the difference of the plasma concentrations of the reference and LCFS was reduced after the T_{max} point. A similar pattern of plasma concentration profiles was observed from 6 h and a steady state of plasma concentration was achieved from 7 days in both groups. From 7 to 28 days, the reference and the LCFS maintained 1.7–5.7 and 2.7–3.6 ng/ml of plasma concentration, respectively (Fig. 9). The C_{max} values of the reference and LCFS were 155.7 ± 28.5 and 80.7 ± 13.6 ng/ml, respectively. The C_{max} value of the LCFS was about half that of the reference. The AUC_{last} values of the reference and LCFS for 28 days were 3358 ± 649 and 3233 ± 297 h.ng/ml, while the $T_{1/2}$ values of the reference and LCFS were 153.2 ± 20.7 and 168.2 ± 27.4 h, respectively. A paired *t*-test indicated that only the C_{max} value among pharmacokinetic parameters of the LCFS was significantly different from that of the reference (Table 1).

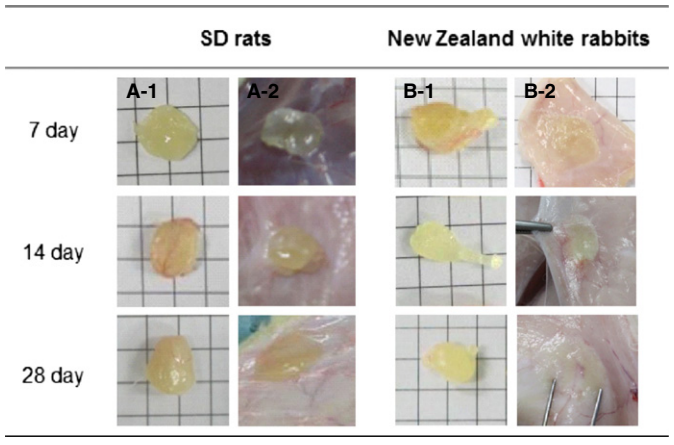

Fig. 8. Morphologies of liquid crystal mesophases and subcutaneous tissues around the mesophases after 7, 14, and 28 days of subcutaneous injections of LCFS into the back of rats and rabbits. (A-1) and (B-1) Mesophases separated from subcutaneous tissues in rats and rabbits. (A-2) and (B-2) Subcutaneous tissues around the mesophases in rats and rabbits.

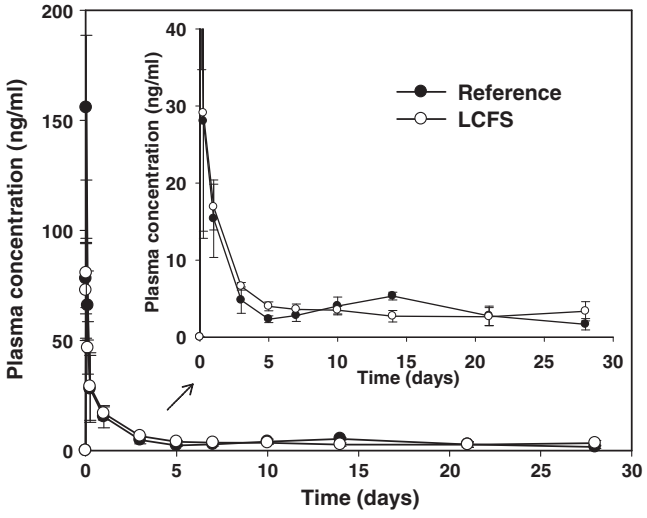

Fig. 9. Plasma concentrations of leuprolide after subcutaneous injections of reference and LCFS in rats. Data are presented as mean ± SD (n = 5).

When the reference and the LCFS, containing 3.75 mg of leuprolide acetate as a monthly dose, were subcutaneously injected into the beagle dog (at a dose of 0.375 mg/kg), similar plasma concentration profiles of leuprolide were observed except for the C_{max} value, as shown in the data of rats. T_{max} values of both groups were within 3 h and the difference in the plasma concentrations of the reference and LCFS was reduced after the T_{max} point. A similar pattern of plasma concentration profiles was observed from 1 day and a steady state of plasma concentration was achieved from 7 days in both groups. From 7 to 28 days, the reference and LCFS maintained 0.4–1.2 and 0.3–0.8 ng/ml of plasma concentration, respectively (Fig. 10A). C_{max} values of the reference and LCFS were 29.8 ± 21.5 and 12.7 ± 4.2 ng/ml, respectively. The C_{max} value of the LCFS was significantly lower than the reference. AUC_{last} values of the reference and LCFS for 28 days were 580.1 ± 370.1 and 538.5 ± 221.3 h.ng/ml, and $T_{1/2}$ values of the reference and LCFS were 185.8 ± 29.8 and 161.1 ± 31.6 h, respectively. A paired *t*-test showed that only the C_{max} value among pharmacokinetic parameters of the LCFS was significantly different from the reference (Table 2).

The LCFS showed significantly lower C_{max} values than the reference, as shown in the pharmacokinetic studies in rats and beagle dogs. The difference in C_{max} values was considered to be caused by the initial burst in drug release due to the characteristics of each formulation. Since a reference formulation is based on solid PLGA microparticles, the drug located on the surface or the external layer of the particles can be easily exposed to body fluids right after the injection, eventually causing an initial burst that induces higher C_{max} values. However, as the LCFS is a liquid formulation and can be transformed into the liquid crystalline mesophases bearing dissolved drug after injection, the drug is relatively unexposed to body fluids. Despite the significantly different C_{max} values, the plasma concentrations of the reference and LCFS went down quickly beyond T_{max}, which resulted in a similar steady state of plasma concentrations and AUC_{last} values. AUC_{inf} values extrapolated to time infinity were not significantly different either. The terminal half-life values of leuprolide in intravenous solutions were different according to the animals, showing 0.67 and 1.19 h in rats and dogs, respectively [39]. $T_{1/2}$ values of the reference and LCFS showed a prolonged terminal half-life up to 153.2–185.8 h regardless of experimental animals, because the half-life in the SR injection was mainly determined by the sustained release rate of a drug from the subcutaneous or intramuscular depot form instead of the drug metabolism rate of an experimental animal. The reference showed a slight increase in plasma concentration around 14 days in rats and dogs due to the characteristics of PLGA formulations [39,40], but the maintenance of the steady state was not influenced. The LCFS exhibited a plasma

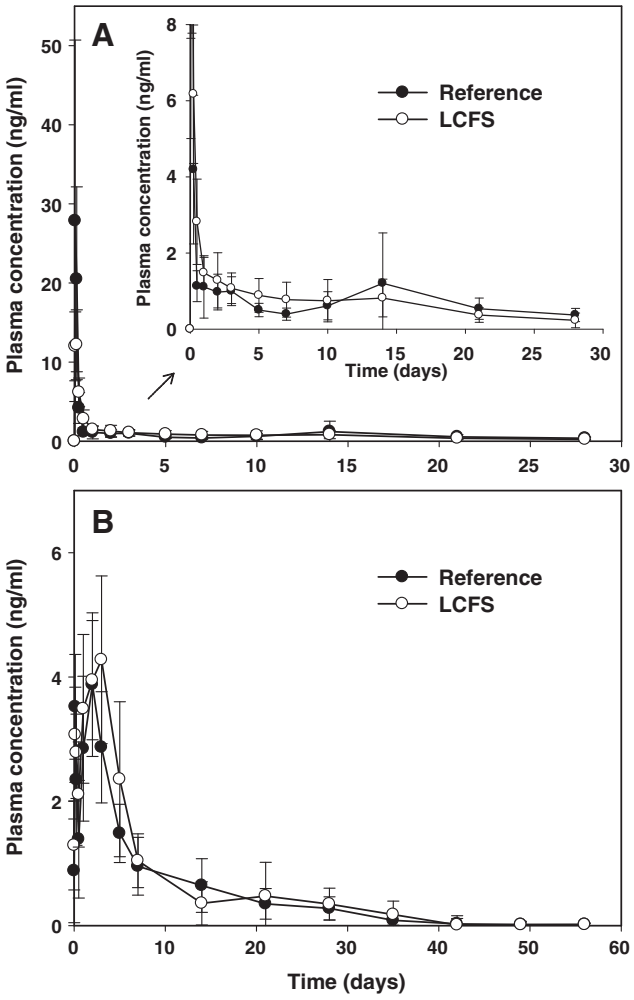

Fig. 10. Plasma concentrations of leuprolide (A) and testosterone (B) after subcutaneous injections of reference and LCFS in dogs. Data are presented as mean ± SD (n = 5).

concentration with a slowly decreasing pattern without a significant change from 7 to 28 days. Although their profiles after 7 days were slightly different due to the characteristics of each formulation, the steady state of plasma concentration in both groups was well maintained.

According to previous pharmacokinetic and pharmacodynamic studies, the serum level of leuprolide and testosterone was analyzed using radioimmunoassay (RIA) after injection of PLGA depot formulations. The serum level determined by RIA was not different from the plasma concentration in this study by UPLC-MS/MS. With the PLGA depot formulation, Okada et al. reported 27.8 ng/ml serum level of leuprolide was measured at 24 h in rats after injection of 14 mg/kg of leuprolide acetate in the once-a-month PLGA depot formulations [39].

Table 1
Pharmacokinetic parameters of leuprolide after subcutaneous injections of reference and LCFS in rats.

	Reference	LCFS
Dose (mg/kg)	12.5	12.5
C_{max} (ng/ml)	155.7 ± 28.5	80.7 ± 13.6[a]
T_{max} (h)	1.0 ± 0.0	1.0 ± 0.0
AUC_{last} (h·ng/ml)	3,358 ± 649	3,233 ± 297
AUC_{inf} (h·ng/ml)	3,736 ± 779	4,068 ± 580
$T_{1/2}$ (h)	153.2 ± 20.7	168.2 ± 27.4

Data are presented as mean ± SD (n = 5).
[a] $P < 0.01$ is established between reference and LCFS.

Table 2
Pharmacokinetic parameters of leuprolide after subcutaneous injections of reference and LCFS in dogs.

	Reference	LCFS
Dose (mg/kg)	0.375	0.375
C_{max} (ng/ml)	29.8 ± 21.5	12.7 ± 4.2[a]
T_{max} (h)	1.4 ± 0.9	2.2 ± 1.1
AUC_{last} (h·ng/ml)	580.1 ± 370.1	538.5 ± 221.3
AUC_{inf} (h·ng/ml)	673.8 ± 393.7	598.1 ± 237.8
$T_{1/2}$ (h)	185.8 ± 29.8	161.1 ± 31.6

Data are presented as mean ± SD (n = 5).
[a] $P < 0.05$ is established between reference and LCFS.

Also, they reported 0.5–1 ng/ml serum level of leuprolide at 2 weeks after the injection of leuprolide acetate (100 μg/kg/day; at a monthly dose of 3 mg/kg) into rats, and 0.5–1.5 ng/ml serum level of leuprolide and suppressed serum level of testosterone below 0.5 ng/ml at 2 weeks after the injection of the drug (25.6 μg/kg/day; at a monthly dose of 0.786 mg/kg) to dogs [37]. The plasma concentrations of leuprolide and testosterone in this study were similar to the serum levels in previous studies. Although the C_{max} value of the LCFS group was significantly different from that of the reference, the plasma concentration profile of testosterone in dogs as a pharmacodynamic marker was similar in both formulations. Compared to previous reports [37,38], a similar pharmacodynamic response, flare up and complete suppression of testosterone, was observed over the 56 day period (Fig. 10B).

The LCFS provided a significantly reduced initial burst due to its formulation characteristics and the lowered C_{max} values did not change the therapeutic effect. The C_{max} values of the one-month and three-month depot injections based on PLGA depot formulations of leuprolide were observed to be 10.7 and 20.8 ng/ml in clinical practice [40]. Although the C_{max} values of these two formulations were significantly different, they showed the same flare-up and complete down-regulation of testosterone to the castration range (≤0.5 ng/ml for testosterone) [40,41]. Moreover, Viadur®, a leuprolide implant, was shown to have the same therapeutic effect as the depot injection even if it reached a steady state of plasma concentration without C_{max} peaks generally observed in PLGA depot injections [42]. Accordingly, the lower C_{max} values in the SR injections of leuprolide probably did not affect or change the efficacy of the drug. Rather the maintenance of plasma concentration after the C_{max} point was considered to be an important factor in the therapeutic effect of leuprolide. This same therapeutic effect is remarkable considering the fact that only 90 μl of LCFS including solvent is used for one month SR injection and the injectable LCFS solution can be prepared by a simple mixing and dissolving process. Both *in vitro* and *in vivo* studies have shown that the LCFS with SMO could be developed into a novel SR injection system of leuprolide acetate in the liquid form.

4. Conclusions

Results of this work revealed that LCFS containing SMO could be used for SR injections of leuprolide acetate. The LCFS was formulated using SMO, phosphatidyl choline and tocopherol acetate as the core components while Tween 80 and ethanol were used as additives. The LCFS formed the hexagonal liquid crystalline phase, when a liquid crystal formation test, Cryo-TEM, and polarized optical microscopy were conducted. In the safety test, the LCFS was observed to have lower interference with the proliferation and differentiation of cells compared to the reference. The LCFS also did not cause a pathologic change in the injection site, including local inflammation. Finally, an *in vitro* release test and an *in vivo* pharmacokinetic study proved that the LCFS containing leuprolide acetate has the suitable controlled release property required for SR injection, despite the fact that the LCFS has less than 100 μl of total volume for one month SR injection and can be prepared by a simple mixing and dissolving process. In

particular, compared with a commercial depot formulation of leuprolide acetate, the LCFS showed a similar AUC_{last} value and significantly reduced initial burst after subcutaneous injections in rats and dogs. Consequently, the LCFS is believed to have a sufficient therapeutic effect when it is used for SR injection of leuprolide acetate. The LCFS composed of injectable excipients including SMO is expected to replace conventional depot injections in terms of safety, ease of preparation, and suitability of controlled release properties. It is also expected that the developed LCFS for SR injections in liquid form can be applied for the controlled release of a wide range of drugs from low molecular chemical entities to high molecular drugs, such as peptides and proteins.

Supplementary data to this article can be found online at http://dx.doi.org/10.1016/j.jconrel.2014.04.034.

References

[1] D. Teutonico, S. Montanari, G. Ponchel, Leuprolide acetate: pharmaceutical use and delivery potentials, Expert Opin Drug Deliv. 9 (2012) 343–354.
[2] R. Astaneh, N.N. Varcheh, M. Erfan, Zinc-leuprolide complex: preparation, physicochemical characterization and release behavior from in situ forming implant, J. Pept. Sci. 13 (2007) 649–654.
[3] A.C. Wilson, S.V. Meethal, R.L. Bowen, C.S. Atwood, Leuprolide acetate: a drug of diverse clinical applications, Expert Opin Drug Deliv. 16 (2007) 1–13.
[4] L.T. Sennello, R.A. Finley, S.Y. Chu, C. Jagst, D. Max, D.E. Rollins, K.G. Tolman, Single-dose pharmacokinetics of leuprolide in humans following intravenous and subcutaneous administration, J. Pharm. Sci. 75 (1986) 158–160.
[5] H. Okada, One- and three-month release injectable microspheres of the LH-RH super agonist leuprorelin acetate, Adv. Drug Deliv. Rev. 28 (1997) 43–70.
[6] J.A.M. Namur, C.S. Takata, A.M. Moro, M.J. Politi, P.S. Araujo, I.M. Cuccovia, M.H. Bueno da Costa, Lactic acid triggers, *in vitro*, thiomersal to degrade protein in the presence of PLGA microspheres, Int. J. Pharm. 273 (2004) 1–8.
[7] M. Weert, W.E. Hennink, W. Jiskoot, Protein instability in poly(lactic-co-glycolic acid) microparticles, Pharm. Res. 17 (2000) 1159–1167.
[8] C. He, S.W. Kim, D.S. Lee, In situ gelling stimuli-sensitive block copolymer hydrogels for drug delivery, J. Control. Release 127 (2008) 189–207.
[9] C. Guo, J. Wang, F. Cao, R.J. Lee, G. Zhai, Lyotropic liquid crystal systems in drug delivery, Drug Discov. Today 15 (2010) 23–24.
[10] J.C. Shah, Y. Sadhale, D.M. Chilukuri, Cubic phase gels as drug delivery systems, Adv. Drug Deliv. Rev. 47 (2001) 229–250.
[11] A. Angelova, B. Angelov, R. Mutafchieva, S. Lesieur, P. Couvreur, Self-assembled multicompartment liquid crystalline lipid carriers for protein, peptide, and nucleic acid drug delivery, Acc. Chem. Res. 44 (2011) 147–156.
[12] W. Fong, T.L. Hanley, B. Thierry, N. Kirby, B.J. Boyd, Plasmonic nanorods provide reversible control over nanostructure of self-assembled drug delivery materials, Langmuir 26 (2010) 6136–6139.
[13] B.J. Boyd, Y. Dong, T. Rades, Nonlamellar liquid crystalline nanostructured particles: advances in materials and structure determination, J. Liposome Res. 19 (2009) 12–28.
[14] H. Qiu, M. Caffrey, The phase diagram of the monoolein/water system: metastability and equilibrium aspects, Biomaterials 21 (2000) 223–224.
[15] J. Barauskas, C. Cervin, M. Jankunec, M. Spandyreva, K. Ribokaite, F. Tiberg, M. Johnsson, Interactions of lipid-based liquid crystalline nanoparticles with model and cell membranes, Int. J. Pharm. 391 (2010) 284–291.
[16] B.J. Boyd, D.V. Whittaker, S. Khoob, G. Davey, Lyotropic liquid crystalline phases formed from glycerate surfactants as sustained release drug delivery systems, Int. J. Pharm. 309 (2006) 218–226.
[17] J. Clogston, M. Caffrey, Controlling release from the lipidic cubic phase. Amino acids, peptides, proteins and nucleic acids, J. Control. Release 107 (2005) 97–111.
[18] J. Clogston, G. Craciun, D.J. Hart, M. Caffrey, Controlling release from the lipidic cubic phase by selective alkylation, J. Control. Release 102 (2005) 441–461.
[19] E. Rosenbaum, S. Tavelin, L.B.A. Johansson, A characterization study on the application of inverted lyotropic phases for subcutaneous drug release, Int. J. Pharm. 388 (2010) 52–57.
[20] I. Amar-Yuli, D. Libster, A. Aserin, N. Garti, Solubilization of food bioactives within lyotropic liquid crystalline mesophases, Curr. Opin. Colloid Interface Sci. 14 (2009) 21–32.
[21] I.A. Yuli, N. Garti, Transitions induced by solubilized fat into reverse hexagonal mesophases, Colloids Surf. B: Biointerfaces 43 (2005) 72–82.
[22] Evaluation of certain food additives and contaminants, World Health Organization Technical Report Series, 6831982.
[23] J. Kuntsche, J.C. Horst, H. Bunjes, Cryogenic transmission electron microscopy (cryo-TEM) for studying the morphology of colloidal drug delivery systems, Int. J. Pharm. 417 (2011) 1–18.
[24] J. Gustafsson, H. Ljusberg-Wahren, M. Almgren, K. Larsson, Submicron particles of reversed lipid phases in water stabilized by a nonionic amphiphilic polymer, Langmuir 13 (1997) 6964–6971.
[25] L. Sagalowicz, R. Mezzenga, M.E. Leser, Investigating reversed liquid crystalline mesophases, Curr. Opin. Colloid Interface Sci. 11 (2006) 224–229.
[26] I. Amar-Yuli, N. Garti, Transitions induced by solubilized fat into reverse hexagonal mesophases, Colloids Surf. B: Biointerfaces 43 (2005) 72–82.
[27] B.A. Pindzola, J. Jin, D.L. Gin, Cross-linked normal hexagonal and bicontinuous cubic assemblies *via* polymerizable gemini amphiphiles, J. Am. Chem. Soc. 125 (2003) 2940–2949.
[28] J. Gurfinkel, A. Aserin, N. Garti, Interactions of surfactants in nonionic/anionic reverse hexagonal mesophases and solubilization of chymotrypsinogen A, Colloids Surf. A Physicochem. Eng. Asp. 392 (2011) 322–328.
[29] E. Farkas, D. Kiss, R. Zelko, Study on the release of chlorhexidine base and salts from different liquid crystalline structures, Int. J. Pharm. 340 (2007) 71–75.
[30] M.G. Lara, M.V.L.B. Bentley, J.H. Collett, *In vitro* drug release mechanism and drug loading studies of cubic phase gels, Int. J. Pharm. 293 (2005) 241–250.
[31] K. Isama, A. Matsuoka, Y. Haishima, T. Tsuchiya, Proliferation and differentiation of normal human osteoblasts on dental Au-Ag-Pd casting alloy: comparison with cytotoxicity to fibroblast L929 and V79 cells, Mater. Trans. 43 (2002) 3155–3159.
[32] A. Sauerbrey, J.P. Mcpherson, S. Zhao, D. Banerjee, J.R. Bertino, Expression of a novel double-mutant dihydrofolate reductase-cytidine deaminase fusion gene confers resistance to both methotrexate and cytosine arabinoside, Hum. Gene Ther. 10 (1999) 2495–2504.
[33] X. Ren, D. Svirskis, R.G. Alany, S. Zargar-Shoshtari, Z. Wu, In-situ phase transition from microemulsion to liquid crystal with the potential of prolonged parenteral drug delivery, Int. J. Pharm. 431 (2012) 130–137.
[34] Z. Wu, R.G. Alany, N. Tawfeek, J. Falconer, W. Zhang, I.M. Hassan, M. Rutland, D. Svirskis, A study of microemulsions as prolonged-release injectables through in-situ phase transition, J. Control. Release 174 (2014) 188–194.
[35] E.J. McNally, J.E. Hastedt, Protein formulation and delivery, 2nd Ed. Informa Healthcare 28 (2008) 153–176.
[36] J.M. Anderson, M.S. Shive, Biodegradation and biocompatibility of PLA and PLGA microspheres, Adv. Drug Deliv. Rev. 28 (1997) 5–24.
[37] H. Okada, Y. Doken, Y. Ogawa, H. Toguchi, Sustained suppression of the pituitary-gonadal axis by leuprorelin three-month depot microspheres in rats and dogs, Pharm. Res. 11 (1994) 1199–1203.
[38] O. Sartor, Eligard: leuprolide acetate in a novel sustained-release delivery system, Urology 61 (2003) 25–31.
[39] H. Okada, Y. Inoue, T. Heya, H. Ueno, Y. ogawa, H. Toguchi, Pharmacokinetics of once-a-month injectable microspheres of leuprolide acetate, Pharm. Res. 8 (1991) 787–791.
[40] P. Periti, T. Mazzei, E. Mini, Clinical pharmacokinetics of depot leuprorelin, Clin. Pharmacokinet. 41 (2002) 485–504.
[41] R. Sharifi, R. Browneller, The Leuprolide Study Group, Serum testosterone suppression and potential for agonistic stimulation during chronic treatment with monthly and 3-month depot formulations of leuprolide acetate for advanced prostate cancer, J. Urol. 168 (2002) 1001–1004.
[42] J.E. Fowler, M. Flanagan, D.M. Gleason, I.W. Klimberg, J.E. Gottesman, R. Sharifi, Evaluation of an implant that delivers leuprolide for 1 year for the palliative treatment of prostate cancer, Urology 55 (2000) 639–642.

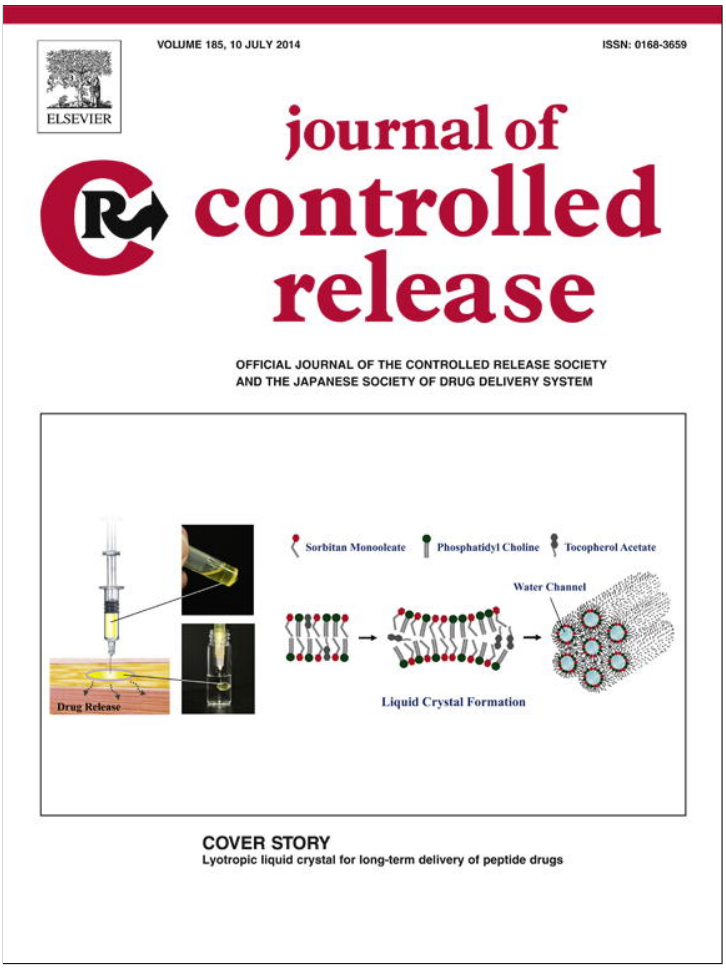

Journal of Controlled Release 185 (2014) 139

Contents lists available at ScienceDirect

Journal of Controlled Release

journal homepage: www.elsevier.com/locate/jconrel

Cover story

Lyotropic liquid crystal for long-term delivery of peptide drugs

Various injectable, sustained-release (SR) formulations have been developed for delivery of peptide drugs for extended periods of time, ranging from weeks to months. The current clinically used SR formulations are mostly based on poly(lactic-co-glycolic acid) (PLGA) microspheres. Since the first introduction of PLGA depot formulation of goserelin acetate in 1989, only less than 10 PLGA formulations have been clinically available for peptide delivery. Such a small number of PLGA depot formulations developed for peptide and protein deliveries over the last 25 years highlight various difficulties and significant challenges to overcome. Currently, PLGA is the only biodegradable polymer that has been used in products approved by the Food and Drug Administration of the United States (US FDA). It is time to explore other long-term peptide delivery systems beyond PLGA polymers.

Liquid crystal technology has gained increasing interest for developing *in situ* forming parenteral depot formulations [1,2]. Lyotropic liquid crystal systems, composed of amphiphiles, are usually classified into lamellar, hexagonal, and cubic phases based on their assembly shape. Among them, the reversed hexagonal phase (H_2) and the reversed cubic phase (Q_2) have been extensively investigated for their ability to control the release of diverse drugs, ranging from low-molecular-weight chemicals to macromolecular drugs (proteins, peptides and nucleic acids). Amphiphilic liquid crystal-forming materials (LCFMs) include glycerol monooleate, glycerol dioleate, glycerol oleyl ether, oleyl glycerate, phytanyl glycerate, and phytantriol [3]. A liquid crystal-forming system (LCFS) is formulated by mixing these with other hydrophobic materials, such as phospholipid, tocopherol, tocopherol acetate, and tricaprylin.

In this issue, the paper by Professor Dae-Duk Kim and his colleagues prepared a LCFS by mixing sorbitan monooleate (SMO, also known as Span 80), phosphatidyl choline, tocopherol acetate, Tween 80, and ethanol (33:45:10:2:10, w/w%) [4]. The SMO LCFS preparation contains 3.75 mg leuprolide acetate as a monthly dose in 90 μl of a liquid formulation. The semi-solid mesophase was formed upon contact with water. The mesophase showed typical characteristics of the liquid crystalline phase, which was classified as the hexagonal phase. The safety of the LCFS was studied by an *in vitro* extraction colony assay and by examining the injection site in rats and white rabbits after an autopsy. Both *in vitro* release test and *in vivo* pharmacokinetic and pharmacodynamic studies showed sustained release of leuprolide. When compared with the reference depot formulation of leuprolide acetate, the SMO LCFS showed a similar AUC_{last} value with a significantly reduced initial burst after subcutaneous injections in rats and dogs. Although the study by Professor Kim and his collaborators is focused on leuprolide in their current study, other peptide drugs can be certainly delivered.

It will take a while until a LCFS-based peptide depot formulation is approved by the FDA for clinical application. But a new opportunity for making an injectable depot formulation based on materials other than PLGA is encouraging. The new injectable SR formulations for clinical application need to improve a few shortcomings of the currently available formulations, mostly based on PLGA. First, the initial burst release has to be reduced dramatically. Most of the current formulations have significant initial burst release, reaching the drug concentration in the blood which is often two orders of magnitude higher than the steady state concentration. These formulations were still approved because such initial burst release was tolerable by patients. This, by no means, indicates that the huge initial burst release is acceptable. In addition, the drug loading needs to be increased. The higher drug loading usually results in a higher initial burst release. However, the high drug loading without initial burst release will allow longer release, *e.g.*, >6 months, without the side effects associated with large amounts of excipients. These are tall orders, but availability of injectable depot formulation materials different from PLGA will stimulate the development of various novel formulations. Clear understanding of the advantages and limitations of LCFMs as well as the problems associated with the current injectable depot formulations is essential in making the right step toward development of many clinically useful formulations.

References

[1] Z. Wu, R.G. Alany, N. Tawfeek, J. Falconer, W. Zhang, I.M. Hassan, M. Rutland, D. Svirskis, A study of microemulsions as prolonged-release injectables through *in-situ* phase transition, J. Control. Release 174 (2014) 188–194.
[2] C. Guo, J. Wang, F. Cao, R.J. Lee, G. Zhai, Lyotropic liquid crystal systems in drug delivery, Drug Discov. Today 15 (2010) 23–24.
[3] B.J. Boyd, D.V. Whittaker, S. Khoob, G. Davey, Lyotropic liquid crystalline phases formed from glycerate surfactants as sustained release drug delivery systems, Int. J. Pharm. 309 (2006) 218–226.
[4] M.-H. Ki, J.-L. Lim, J.-Y. Ko, S.-H. Park, J.-E. Kim, H.-J. Cho, E.-S. Park, D.-D. Kim, A new injectable liquid crystal system for one month delivery of leuprolide, J. Control. Release 185 (2014) 62–70.

Kinam Park
Purdue University
Departments of Biomedical Engineering and Pharmaceutics
West Lafayette, IN 47907, USA
E-mail address: kpark@purdue.edu

http://dx.doi.org/10.1016/j.jconrel.2014.05.047

논문요지 발표자료

Chitosan-based hybrid nanocomplex for siRNA delivery and its application for cancer therapy

2013년 11월 26일

기 민 효

제약학과 약제과학

Introduction

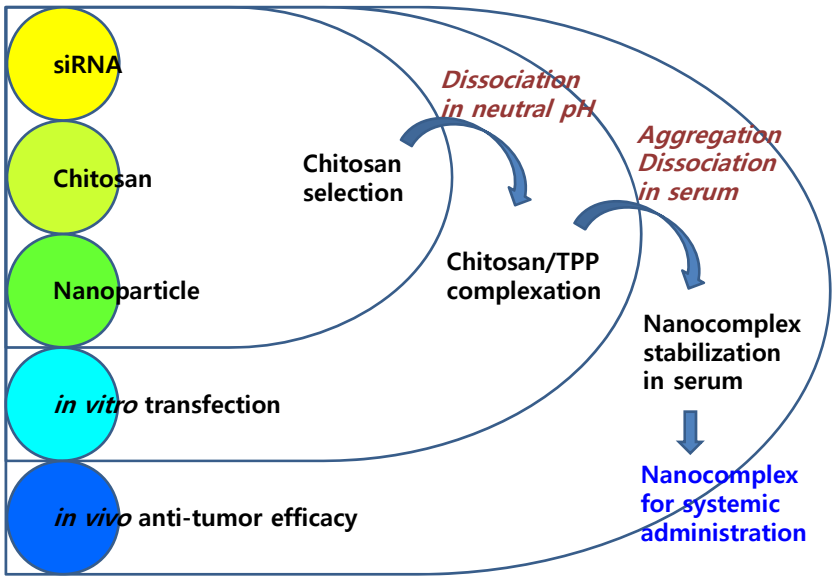

siRNA & miRNA

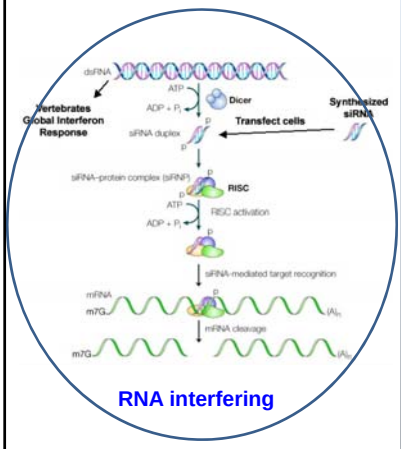

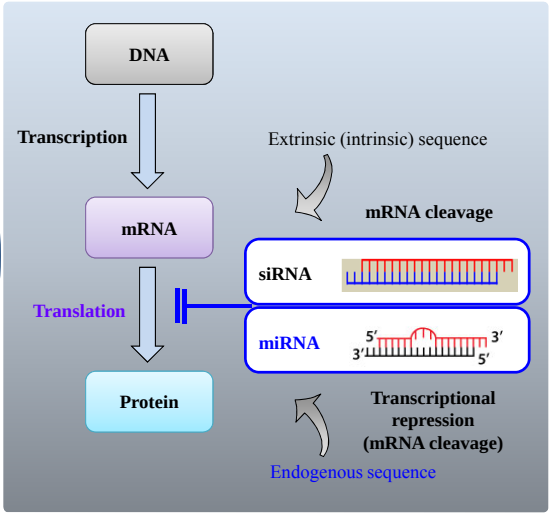

Delivery System of siRNA

기존 유전자 치료제의 한계성

- 신속한 배설
- 짧은 반감기
- 혈장 중 분해
- 표적 장기 전달이 어려움
- 세포로의 투과성이 매우 낮음

유전자 전달체의 종류

- Viral Vector
- Cationic Material or Lipid
- Cationic Polymer

유전자 치료제의 방향

➢ The system of Biodegradable polymeric nanocomplex

- 산업화 측면
  - ✓ 의약품 GMP 대량생산성 우수
  - ✓ 품질관리 규격화 용이
- 기술적 측면
  - ✓ 항원성이 낮고 안정성이 매우 우수
  - ✓ 표적지향화 유리 (Ligand Modification)
  - ✓ 유전자 지속적 체내방출

Eur J Clin Invest 41 (2011) 221–232
AAPS J. 12 (2010) 492–503
Mol Ther 13 (2006) 644–670
Nat Rev Drug Discov 8 (2009) 129–138.

Chitosan

Chitosan (Poly-(1-4)-2-Amino-2-deoxy-ß-D-Glucan)

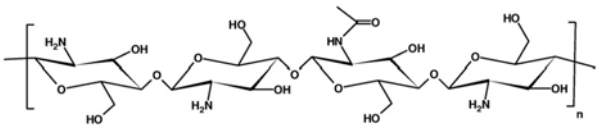

- pKa : A weak polybase with a pKa that is close to 6.6
- MW : ~ 2,000 kDa
- Deacetylation degree : 70% ~

Chitosan as a natural polymer has been widely used in the development of nucleic acid delivery systems as it is known to have low cytotoxicity, high biocompatibility and high cellular permeability

In addition, its nucleic acid binding and delivering capacity can be influenced by its molecular weight, the degree of deacetylation and its salt form

Adv Drug Deliv Rev 62 (2010) 12–27.
J Control Release 158 (2012) 261–268.
AAPS PharmSciTech 11 (2010) 64–72.

Complexation with Chitosan & TPP

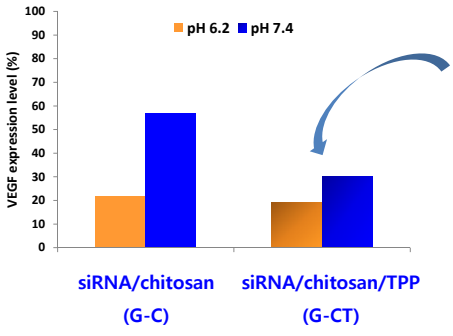

Transfection efficacy in physiological pH

Thiamine Pyrophosphate (TPP)

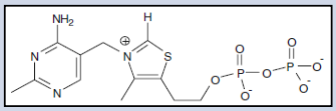

- Active form of thiamine (Vit. B1) in the body

- The positively charged amine group of thiazolium regardless of pH
- Zwitterion interacting between siRNA and chitosan

Biophys J 93 (2007) 952–959
Pharm Res 25 (2008) 2807–2814

Aggregation of Nanoparticle in Blood Stream

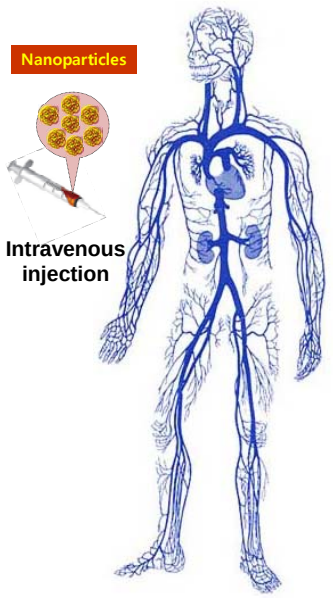

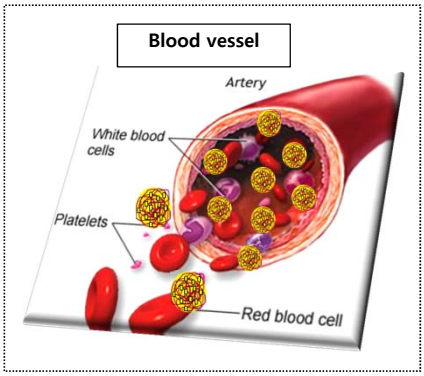

- Serum protein binding
- Aggregation
- Blood clotting
- Hemolysis

Expert Opin Drug Deliv. 8 (2011) 343–357.
Br J Pharmacol 146 (2005) 882–893.
Mol Pharm 5 (2008) 487–495.
Biochim Biophys Acta 1612 (2003) 136– 143

Aggregation of Nanoparticle in Serum

PEI(0.8kD) nanoparticle

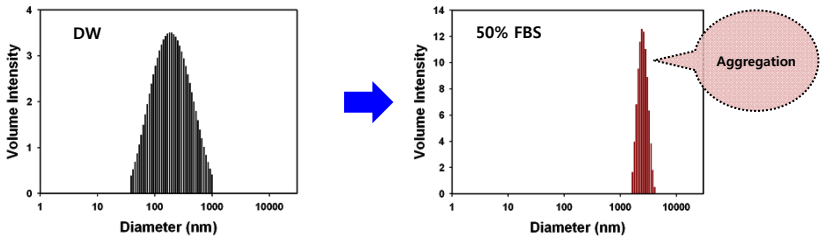

Chitosan nanoparticle (G-C)

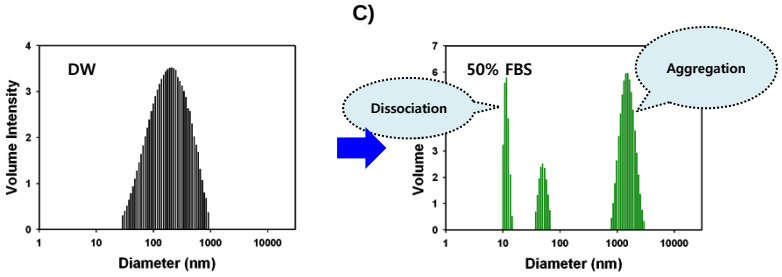

Complexation with Protamine & Lecithin

Protamine Sulfate

- Small, arginine-rich, nuclear protein
- DNA packing and stabilization in sperm
- Sequence of salmon protamine

PRRRRSSSRPVRRRRRPRVSRRRRRRGGRRRR

(Mw. 5.1 kDa)

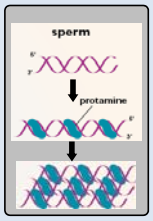

Lecithin

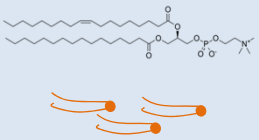

Naked siRNA

siRNA condensation with protamine (GP)

Lecithin incoporation (GP-L)

Eur J Pharm Biopharm. 80 (2012) 257–267.
Eur J Pharm Biopharm 79 (2011) 495–502.
Biomaterials 30 (2009) 6451–6459.

Design of Hybrid Nanocomplex System (GP-L-CT)

	G-C
	G-CT
GP	GP-CT
GP-L	GP-L-CT

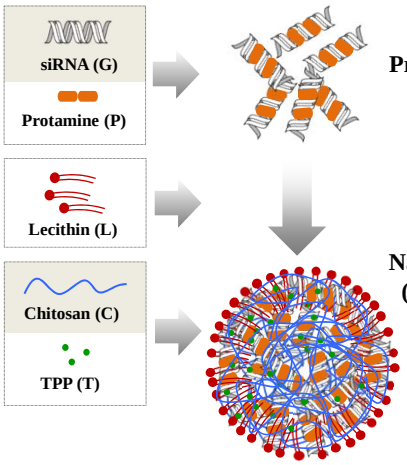

Fig. 1. Schematic illustration of GP-L-CT hybrid nanocomplex preparation

Selection of Chitosan

Table 1. Specifications of the chitosans used in this study.

	Chitosan	Molecular weight (MW: kDa)	Deacetylation degrees (%)
A	Chitosan acetate	100	84
B	Chitosan acetate	300	84
C	Chitosan HCl	50 ~ 150	83
D	Chitosan HCl	150 ~ 400	95

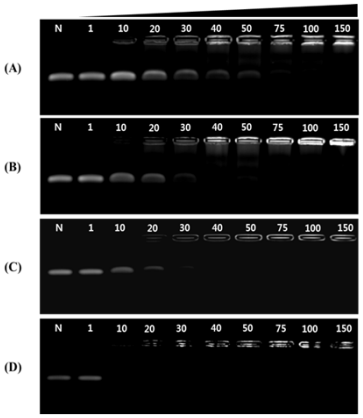

Fig. 2. Gel retardation assays of siRNA with different chitosans; (A) chitosan acetate (MW: 100 kDa), (B) chitosan acetate (MW: 300 kDa), (C) chitosan HCl (MW: 50~150 kDa), and (D) chitosan HCl (MW: 150~400 kDa). Complex formation according to the weight ratios between chitosan and siRNA was investigated by gel electrophoresis in 2.5% agarose gel.

Selection of Chitosan

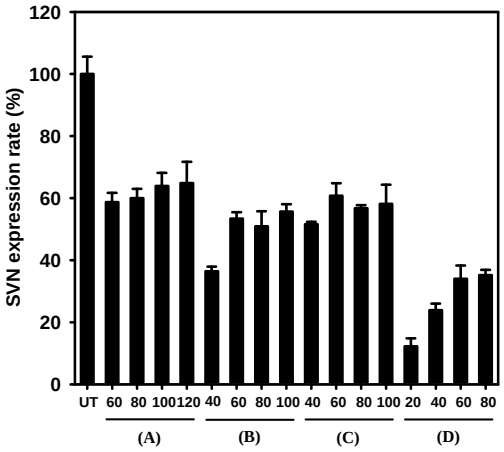

Fig. 3. *In vitro* gene transfection efficiency of different chitosans; (A) chitosan acetate (MW: 100 kDa), (B) chitosan acetate (MW: 300 kDa), (C) chitosan HCl (MW: 50~150 kDa), and (D) chitosan HCl (MW: 150~400 kDa). SVN expression rate (%) was shown after incubating for 48 h with various weight ratios between chitosan and SVN siRNA in PC-3 cells. Each value was presented as the mean ± S.D. (n = 3).

Preparation of Hybrid Nanocomplex

Table 2. Compositions of SVN siRNA-loaded chitosan-based nanocomplexes.

components	G-C	G-CT	GP	GP-CT	GP-L	GP-L-CT
SVN siRNA	1	1	1	1	1	1
Protamine	-	-	0.6	0.6	0.6	0.6
Lecithin	-	-	-	-	8	8
Chitosan	6.8	6.8	-	6.8	-	6.8
TPP	-	1.2	-	1.2	-	1.2

Negative surface charge

Positive surface charge

All values were presented as weight ratios.

Reference

New combination

Particle Size and Zeta Potential Measurements

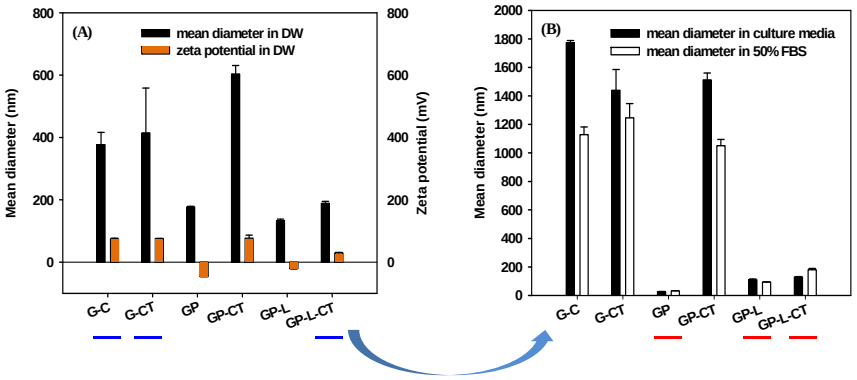

Fig. 4. Characterization of SVN siRNA-loaded hybrid nanocomplex. (A) Particle size and zeta potential values of nanocomplex formulations in DW. (B) Mean diameters of nanocomplexes in cell culture media and FBS. Each value represents the mean ± S.D. (n = 3).

Cryo-Transmission Electron Microscopy

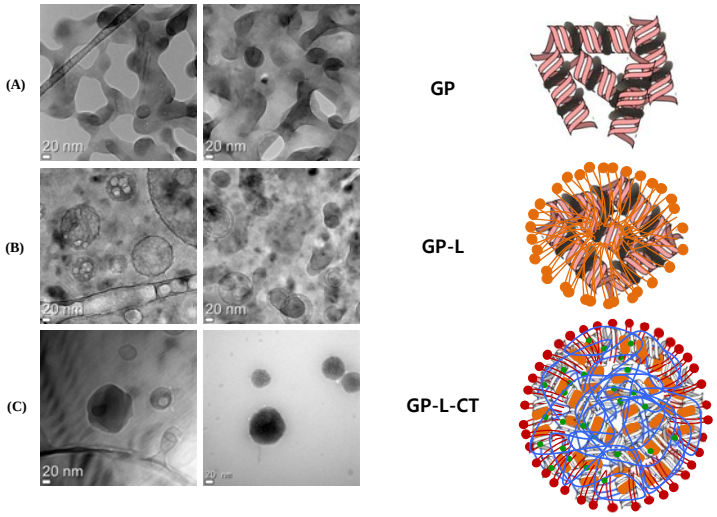

Fig. 5. Morphology of nanocomplex formulations observed by cryo-transmission electron microscopy (cryo-TEM). Images of (A) siRNA/protamine (GP), (B) siRNA/protamine/lecithin complex (GP-L), (C) siRNA/protamine/lecithin/chitosan/TPP complex (GP-L-CT). The length of scale bar is 20 nm.

in vitro Cellular Uptake

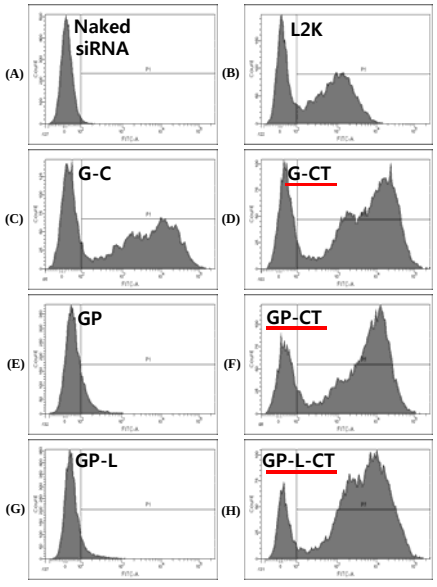

Fig. 6. *In vitro* cellular uptake efficiency of the nanocomplexes in PC-3 cells. Fluorescent siRNA was loaded into various nanocomplex formulations and fluorescence intensity was measured by flow cytometry after incubating for 24 h. Plots, between cell count and fluorescence intensity, of (A) naked siRNA, (B) siRNA/Lipofectamine 2000 (L2K), (C) siRNA/chitosan (G-C), (D) siRNA/chitosan/TPP (G-CT), (E) siRNA/protamine (GP), (F) siRNA/protamine/chitosan/TPP (GP-CT), (G) siRNA/protamine/lecithin (GP-L), and (H) siRNA/protamine/lecithin/chitosan/TPP (GP-L-CT) are presented.

in vitro Transfection Study

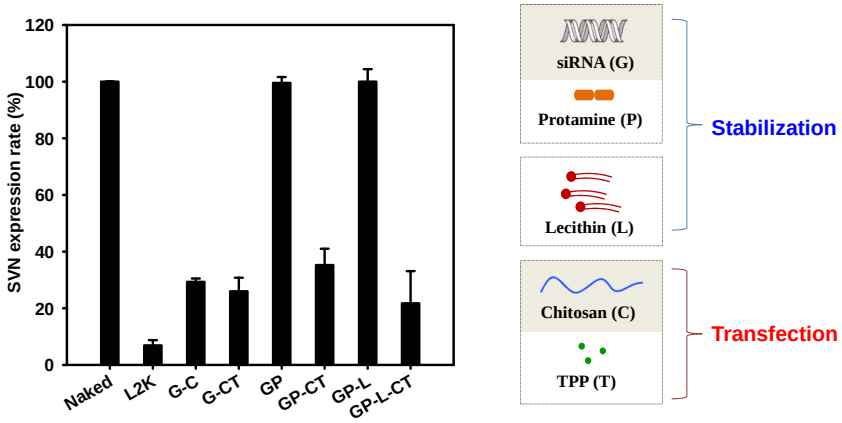

Fig. 7. *In vitro* transfection efficiency of SVN siRNA-loaded nanocomplex formulations in PC-3 cells. SVN expression levels (%) of naked siRNA (naked), siRNA/Lipofectamine 2000 (L2K), siRNA/chitosan (G-C), siRNA/chitosan/TPP (G-CT), siRNA/protamine (GP), siRNA/protamine/chitosan/TPP (GP-CT), siRNA/protamine/lecithin (GP-L), and siRNA/protamine/lecithin/chitosan/TPP (GP-L-CT)-incubated groups (for 48 h) are presented. Each value represents the mean ± S.D. (n = 3).

in vivo Near-infrared Fluorescence (NIRF) Imaging

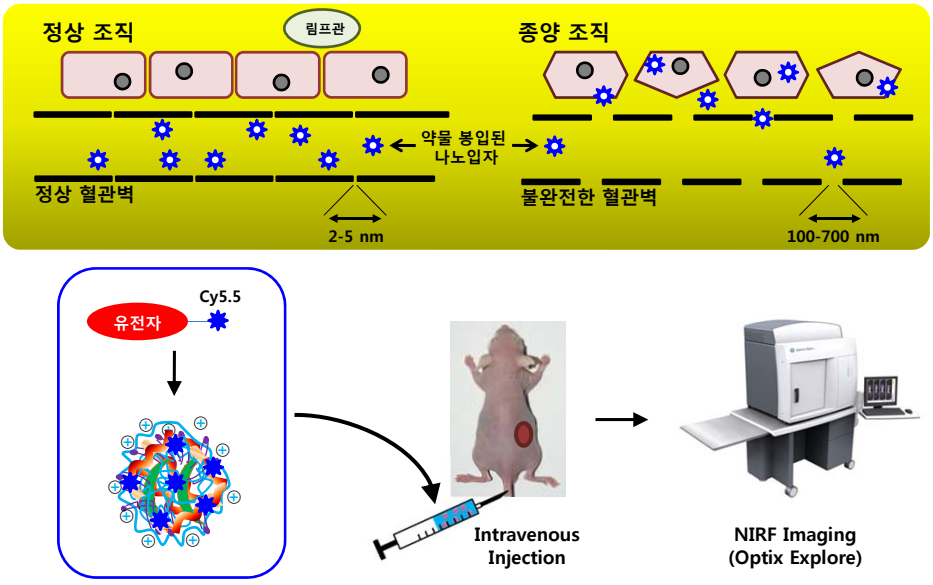

in vivo Near-infrared Fluorescence (NIRF) Imaging

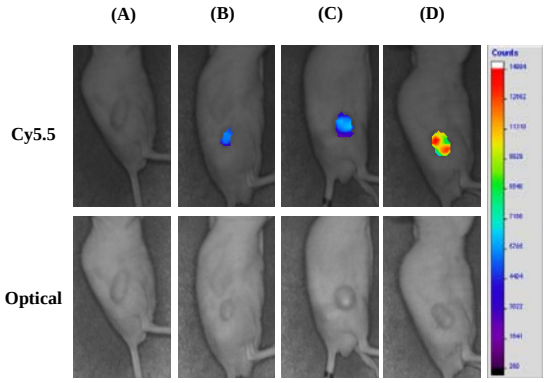

Fig. 8. *In vivo* NIRF images of siRNA-loaded nanocomplex formulations in PC-3 tumor-xenografted mouse model. Cy5.5-filtered and optical images of tumor in (A) control, (B) naked cy5.5-siRNA, (C) cy5.5-siRNA/Lipofectamine 2000 (Cy5.5-siRNA/L2K), (D) cy5.5-siRNA/protamine/lecithin/chitosan/TPP complex (Cy5.5-siRNA/GP-L-CT) groups 2 h post-injection via intravenous route.

in vivo Anti-tumor Efficacy

- **Anti-tumor Efficacy of Survivin-siRNA Nanocomplex**
  - **Animal : BALB/c nu/nu mouse, male (6 weeks)**
  - **Cell : PC-3 cell, human prostate cancer cell line**
    Inoculation= 2 × 10^6 cell/mouse
  - **Formula : Scrambled siRNA/GP-L-CT, SVN siRNA/GP-L-CT**
  - **Treatment : 40 ug / mouse, 6 times for 2 weeks**
  - **Tumor Volume = 0.5 × longest diameter × shortest diameter^2.**

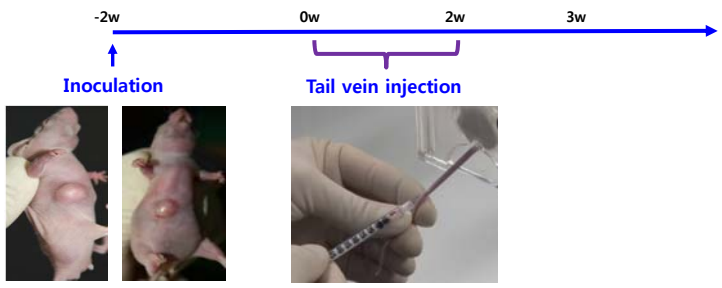

in vivo Anti-tumor Efficacy

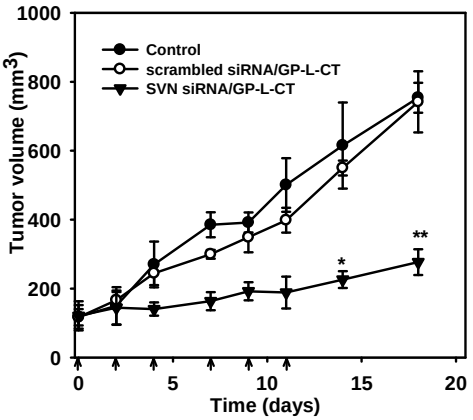

Fig. 9. *In vivo* anti-tumor efficacy test of siRNA-loaded nanocomplex in PC-3 tumor-xenografted mouse model. Tumor volume profiles of control, luciferase-siRNA/protamine/lecithin/chitosan/TPP (scrambled siRNA/GP-L-CT), survivin-siRNA/protamine/lecithin/chitosan/TPP complex (SVN siRNA/GP-L-CT). Nanocomplexes were injected 6 times for 2 weeks via intravenous route. $*P < 0.05$ and $**P < 0.01$ are established between scrambled siRNA/GP-L-CT and SVN siRNA/GP-L-CT. Data represents the mean ± S.D. ($n \geq 3$).

Conclusions

1. **A pre-complex based on siRNA and protamine was formed and lecithin, chitosan, and TPP were added to develop a more stable and efficient hybrid nanocomplex (GP-L-CT) in this study.**

2. **GP-L-CT provided suitable physicochemical properties (< 200 nm mean diameter in serum and positive zeta potential) for intravenous injection of siRNA as well as superior *in vitro* cellular uptake and gene silencing efficiencies.**

3. ***in vivo* tumor targetability and anti-tumor efficacy in tumor xenografted mouse model have been proven. The newly developed theranostic hybrid nanocomplex can therefore be used efficiently for the systemic siRNA delivery in cancer therapy.**

4. **A chitosan-based hybrid nanocomplex could serve as an alternative to the cationic polymeric nanoparticles that are unstable in serum.**

Injectable liquid crystal-forming system for the sustained release of leuprolide

2013년 11월 26일

기 민 효

제약학과 약제과학

Liquid Crystal-forming System (LCFS) for SR Injection

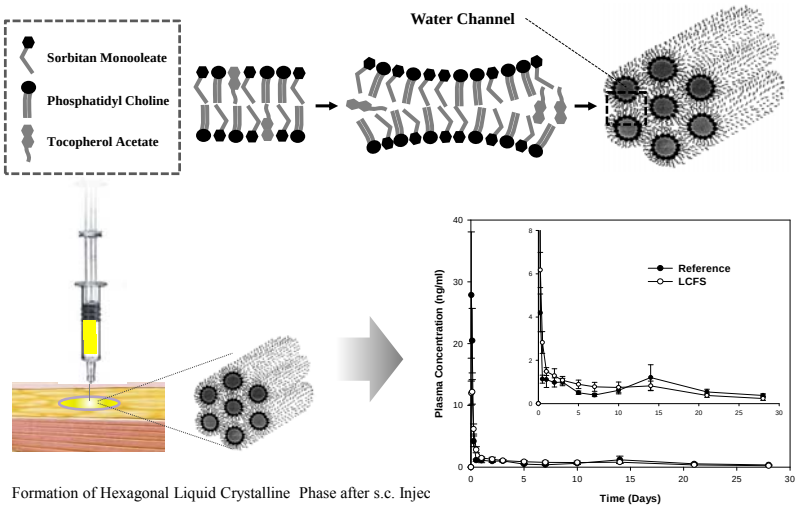

Fig. 1. Schematic illustration about leuprolide acetate-loaded LCFS for the subcutaneous injection.

Liquid Crystal-forming Material (LCFM)

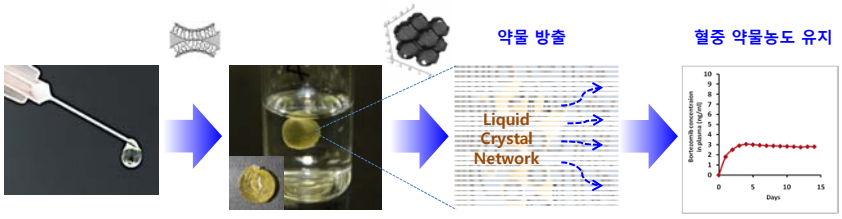

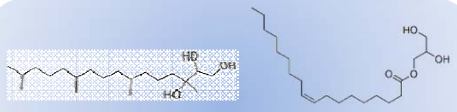

Phytantriol (PT)

Glycerol monooleate (GMO)

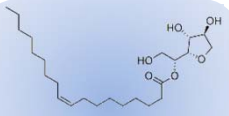

Sorbitan monooleate (Span 80)

J. Liposome Res. 19 (2009) 12-28.
Biomaterials 21 (2000) 223-224.
Int. J. Pharm. 391 (2010) 284-291.
Int. J. Pharm. 309 (2006) 218-226.

Non-injectable **Injectable**

Leuprolide SR (Depot) Injection

Leuprolide SR Injection : Prostatic Cancer, Endometriosis, Precocious Puberty

PLGA SR Injection

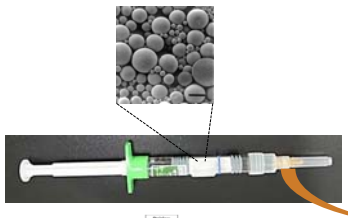

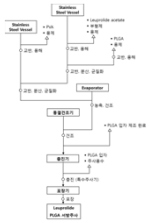

Liquid Crystal Technology

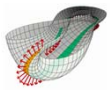

Liquid Crystal SR Injection

Ease of Injection

Productivity

Patient Compliance

Adv. Drug Deliv. Rev. 28 (1997) 43-70.
Pharm. Res. 8 (1991) 713-720.
Int. J. Pharm. 350 (2008) 14-26.